

DEVELOPMENT OF CYCLODEXTRIN-BASED  
PICKERING NANOEMULSION CONTAINING  
AMPHOTERICIN B FOR TREATMENT OF FUNGAL  
KERATITIS



A Thesis Submitted in Partial Fulfillment of the Requirements  
for the Degree of Master of Science in Pharmacy in Pharmaceutics  
Department of Pharmaceutics and Industrial Pharmacy  
Faculty of Pharmaceutical Sciences  
Chulalongkorn University  
Academic Year 2019  
Copyright of Chulalongkorn University

การพัฒนาฟิสิกเกอร์ิงนาโนอิมัลชันที่มีไซโคลเดกซ์ทรินเป็นฐานบรรจุแอมโฟเทอริซินบี สำหรับ  
รักษากระจกตาอักเสบจากเชื้อรา



วิทยานิพนธ์นี้เป็นส่วนหนึ่งของการศึกษาตามหลักสูตรปริญญาเภสัชศาสตรมหาบัณฑิต  
สาขาวิชาเภสัชกรรม ภาควิชาวิทยาการเภสัชกรรมและเภสัชอุตสาหกรรม  
คณะเภสัชศาสตร์ จุฬาลงกรณ์มหาวิทยาลัย  
ปีการศึกษา 2562  
ลิขสิทธิ์ของจุฬาลงกรณ์มหาวิทยาลัย

Thesis Title	DEVELOPMENT OF CYCLODEXTRIN-BASED PICKERING NANOEMULSION CONTAINING AMPHOTERICIN B FOR TREATMENT OF FUNGAL KERATITIS
By	Miss Phyo Darli Maw
Field of Study	Pharmaceutics
Thesis Advisor	Phatsawee Jansook, Ph.D.
Thesis Co Advisor	Varin Titapiwatanakun, Ph.D.

---

Accepted by the Faculty of Pharmaceutical Sciences,  
Chulalongkorn University in Partial Fulfillment of the Requirement for  
the Master of Science in Pharmacy

..... Dean of the Faculty of  
Pharmaceutical Sciences  
(Assistant Professor RUNGPETCH  
SAKULBUMRUNGSIL, Ph.D.)

#### THESIS COMMITTEE

..... Chairman  
(Associate Professor PARKPOOM  
TENGAMNUAY, Ph.D.)

..... Thesis Advisor  
(Phatsawee Jansook, Ph.D.)

..... Thesis Co-Advisor  
(Varin Titapiwatanakun, Ph.D.)

..... Examiner  
(Assistant Professor Dusadee Charnvanich,  
Ph.D.)

..... External Examiner  
(Associate Professor Warisada Sila-on, Ph.D.)

โพ ดาลี มอว์ : การพัฒนาฟิกเกอร์ิงนาโนอิมัลชันที่มีไซโคลเดกซ์ทรินเป็นฐานบรรจุแอมโฟเทอริซินบี สำหรับรักษากระจกตาอักเสบจากเชื้อรา. ( DEVELOPMENT OF CYCLODEXTRIN-BASED PICKERING NANOEMULSION CONTAINING AMPHOTERICIN B FOR TREATMENT OF FUNGAL KERATITIS) อ.ที่ปรึกษาหลัก : อ. ภก. ดร.ภาสวีร์ จันทรสุก, อ.ที่ปรึกษาร่วม : อ. ภญ. ดร.วฤณ จิตาภิวัฒน์กุล

วัตถุประสงค์ในการศึกษานี้เพื่อพัฒนาฟิกเกอร์ิงนาโนอิมัลชันที่มีแอมโฟเทอริซินบีสำหรับรักษาโรคติดเชื้อราที่กระจกตา ศึกษาการละลายของแอมโฟเทอริซินบีในสารละลายไซโคลเดกซ์ทรินความเข้มข้นต่างๆ และศึกษาการละลายของแอมโฟเทอริซินบีในน้ำมันและสารลดแรงตึงผิวชนิดต่างๆ จากการศึกษาเลือกใช้ แกมมาไซโคลเดกซ์ทริน และไฮดรอกซีโพรพิลแกมมาไซโคลเดกซ์ทริน น้ำมันไตรกลีเซอไรด์ชนิดสายโซ่ปานกลาง และฟอสฟาทีลคลอลีน (เลซิทีน) เนื่องจากละลายแอมโฟเทอริซินบีได้สูง ศึกษา NMR ชนิดโปรตอนในสถานะสารละลายพบว่า เกิดสารประกอบเชิงซ้อนของน้ำมันไตรกลีเซอไรด์ชนิดสายโซ่ปานกลางกับแอลฟาไซโคลเดกซ์ทริน แอมโฟเทอริซินบีกับแกมมาไซโคลเดกซ์ทริน และแอมโฟเทอริซินบีกับไฮดรอกซีโพรพิลแกมมาไซโคลเดกซ์ทริน ในสถานะของแข็ง (FT-IR, PXRD และ DSC) พบว่ามีอันตรกิริยาระหว่างกับไซโคลเดกซ์ทริน และการศึกษาแรงตึงระหว่างผิว ณ ชั้นน้ำมัน-น้ำ การวิเคราะห์ปริมาณไซโคลเดกซ์ทริน และการศึกษาลักษณะทางสัณฐานวิทยา ยืนยันความชอบของแอลฟาไซโคลเดกซ์ทรินต่อน้ำมันไตรกลีเซอไรด์ชนิดสายโซ่ปานกลาง ดังนั้นจึงใช้สารประกอบเชิงซ้อนของน้ำมันไตรกลีเซอไรด์ชนิดสายโซ่ปานกลางกับแอลฟาไซโคลเดกซ์ทริน เป็นอนุภาคของแข็งในการเพิ่มความคงตัวของฟิกเกอร์ิงนาโนอิมัลชัน พัฒนาสูตรตำรับฟิกเกอร์ิง และนั่นฟิกเกอร์ิงนาโนอิมัลชันโดยใช้ไฮโมจิโนเซอร์แรงดันสูง ศึกษาคุณสมบัติทางเคมีฟิสิกส์และเคมี ได้แก่ ความเป็น กรด-ด่าง ออสโมลาลิตี ความหนืด ขนาดและการกระจายขนาดอนุภาค ความต่างศักย์ไฟฟ้า ปริมาณยา และประสิทธิภาพการกักเก็บยา พบว่าค่าดังกล่าวอยู่ในช่วงที่ยอมรับได้ สูตรตำรับมีระดับการเกาะกลุ่มและความเป็นพิษต่อเซลล์เม็ดเลือดต่ำกว่าผลิตภัณฑ์ในท้องตลาด Amphotericin-B® การศึกษาการปลดปล่อยโดยวิธีภายนอกร่างกายผ่านเมมเบรนเลือกผ่านชี้ให้เห็นว่าฟิกเกอร์ิงนาโนอิมัลชันปลดปล่อยยาแบบนั้นเนื่องจากยาเกือบทั้งหมดถูกบรรจุใน โครงสร้างชั้นใน สำหรับการศึกษากุทศิยบยั้งเชื้อรา สูตรตำรับแอมโฟเทอริซินบีให้ผลดีกว่าตัวยาเดี่ยว แต่ให้ผลเท่าเทียม และดีกว่า Amphotericin-B® ต่อ *C. albicans* และราสาย ตามลำดับ การศึกษาความคงสภาพในอุณหภูมิสูงและต่ำสลับกัน ในสถานะแข็ง และระยะยาว พบว่าฟิกเกอร์ิงนาโนอิมัลชันที่ใช้ไซโคลเดกซ์ทรินเป็นฐานมีความคงสภาพทั้งทางกายภาพและเคมีต่างกับสูตรเปรียบเทียบกับสูตรตำรับนั้นฟิกเกอร์ิงนาโนอิมัลชัน มีความไม่คงตัวหลังเก็บไว้ 3 เดือน ดังนั้นฟิกเกอร์ิงนาโนอิมัลชันที่ใช้ไซโคลเดกซ์ทรินเป็นฐานบรรจุแอมโฟเทอริซินบี จึงเป็นสูตรตำรับที่มีศักยภาพในการศึกษาต่อไป

สาขาวิชา	เภสัชกรรม	ลายมือชื่อนิติ
ปีการศึกษา	2562	.....
		ลายมือชื่อ อ.ที่ปรึกษาหลัก
		.....
		ลายมือชื่อ อ.ที่ปรึกษาร่วม
		.....

# # 6076127333 : MAJOR PHARMACEUTICS

KEYWORD Amphotericin B/ Cyclodextrin/ Solubilization/ Pickering  
D: nanoemulsions/ Antifungal

Phyo Darli Maw : DEVELOPMENT OF CYCLODEXTRIN-BASED PICKERING NANOEMULSION CONTAINING AMPHOTERICIN B FOR TREATMENT OF FUNGAL KERATITIS. Advisor: Phatsawee Jansook, Ph.D. Co-advisor: Varin Titapiwatanakun, Ph.D.

The purpose of this study was to develop pickering nanoemulsions (NEs) containing amphotericin B (AmB) for fungal keratitis therapy. The phase-solubility profiles of AmB in various aqueous cyclodextrin (CD) solutions were determined. The AmB solubilization in oils and surfactants was also examined. Two CDs i.e.,  $\alpha$ CD and 2-hydroxypropyl- $\beta$ -CD (HP $\beta$ CD), medium-chain triglycerides (MCT oil) and phosphatidylcholine (lecithin) were chosen because of their high solubility increment of AmB. Solution-state by  $^1\text{H-NMR}$  studies demonstrated the formation of MCT oil/ $\alpha$ CD, AmB/ $\alpha$ CD and AmB/HP $\beta$ CD complexes. Some interactions between AmB and CD have been observed by solid-state characterizations (FT-IR, PXRD and DSC). The interfacial tension at oil-water interface, CD analysis and the morphology studies have confirmed the affinity of  $\alpha$ CD to MCT oil. Thus, MCT oil/ $\alpha$ CD complex was used as solid particle to stabilize pickering NEs. The CD-stabilized pickering and non-pickering NEs loaded AmB were developed by using high pressure homogenizer. The physicochemical and chemical properties i.e., pH, osmolality, viscosity, particle size and size distribution, zeta potential, drug content and entrapment efficiency were within the acceptable range. The developed formulations showed less degree of aggregation of AmB and lower hemolytic activity when compared with commercial product, Amphotericin-B<sup>®</sup>. *In vitro* drug release through semipermeable membrane studies revealed that pickering NEs provided the sustained drug release owing to most of drug entrapped in the inner core. For antifungal activity, the AmB formulations were superior to AmB itself but equally and inferior to Amphotericin-B<sup>®</sup> against *C. albicans* and filamentous fungi, respectively. The stability studies i.e., freeze-thaw, accelerated and long-term stability have found that CD-based pickering NEs exhibited good physical and chemical stability in contrast to the respective non-pickering NEs that showed instability after storage for 3 months. Therefore, CD-based AmB pickering NEs had the potential formulations for further studies.

Field of Study: Pharmaceutics

Student's Signature

Academic 2019

.....  
Advisor's Signature

Year:

.....  
Co-advisor's Signature

.....

## ACKNOWLEDGEMENTS

First and most of all, I would like to express the deepest gratitude and profound respect to my advisor, Phatsawee Jansook, Ph.D. for his invaluable guidance, helpfulness, kindness, professional expertise, mentorship, patient and encouragement at all the stages of my thesis work. Moreover, I also would like to say additional thank to him for taking time to read this research work and making corrections and giving suggestions. Moreover, I also would like to thank to my co-advisor, Varin Titapiwatanakun, Ph.D. for her kindness, encouragement and suggestions.

I would like to thank my thesis committee members for their valuable suggestions and encouragements. I would like to express grate appropriation to Chulalongkorn University for the provision of the Scholarship for the International Graduate Students in ASEAN Countries. I would like to special thank to every teachers and staffs in Department of Pharmaceutics and Industrial Pharmacy, Faculty of Pharmaceutical Sciences, Chulalongkorn University. They provided information and grateful supports for laboratory equipment and other facilities for my research work.

Furthermore, I would like to thank Master of Sciences program in cosmetic science in our department for kindly permitted to use Rheometer and Chulalongkorn University Centenary Academic Development Project for providing powder X-ray diffractometer within CU.D.HIP to fulfill my research. I also would like to special thank to Assistant Professor Prompong Pienpinijtham from Faculty of Sciences, Chulalongkorn University for his supporting and guidance to use atomic force microscope. In addition, I would like to express much appreciation to Dr. Patamaporn Pruksakorn

from Medical Life Sciences Institute, Department of Medical Sciences, Ministry of Public Health for her supporting in antifungal activity study for the fulfillment of my study.

I would like to pay my heartfelt thanks to all my lab members for helping me in numerous ways, sharing many lab experiences and encouragement throughout the study years. I also would like to thank all of the teachers from the University of Pharmacy, Mandalay for their teaching in my Bachelor degree.

Finally, I would like to express the deepest thanks to my parents, my grandparents, my uncle, my sisters and my friends for their never-ending support and encouraging talk, which are invaluable and precious for me to complete my research.

Phyo Darli Maw

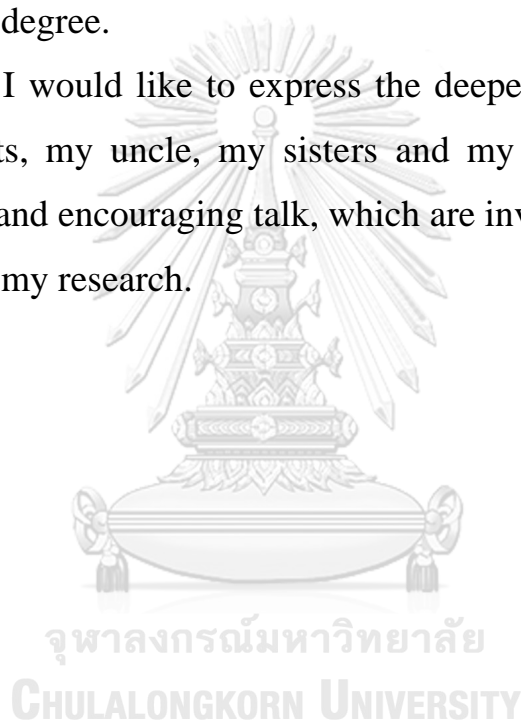


## TABLE OF CONTENTS

	<b>Page</b>
ABSTRACT (THAI) .....	iii
ABSTRACT (ENGLISH).....	iv
ACKNOWLEDGEMENTS.....	v
TABLE OF CONTENTS.....	vii
LISTS OF TABLES.....	xi
LIST OF FIGURES .....	xiii
LIST OF ABBREVIATION .....	1
CHAPTER I INTRODUCTION.....	3
CHAPTER II LITERATURE REVIEWS.....	10
1. Keratitis .....	10
1.1. Fungal keratitis.....	10
2. Amphotericin B .....	12
2.1. Mechanism of action of Amphotericin B.....	13
3. Ocular drug delivery system.....	13
3.1. Anatomy of the eye .....	13
3.2. Barriers for the ocular drug delivery .....	14
3.3. Topical application to the ocular drug delivery system .....	16
4. Cyclodextrin .....	17
4.1. Drug/CD complex formation.....	19
4.2. Classification of CD inclusion complex and drug solubility .....	20
4.3. CD in ocular drug delivery system.....	24
5. Pickering emulsion .....	25
5.1. Role of CDs in pickering emulsions.....	26
CHAPTER III MATERIALS AND METHODS .....	28
Materials .....	28



Equipments .....	29
Methods	31
1. Phase-solubility profile.....	31
2. Solubility determination of AmB in oils and surfactants .....	32
3. Quantitative analysis of AmB .....	32
3.1. Calibration curve of AmB .....	32
3.2. Sample preparation.....	33
3.3. HPLC condition.....	33
4. Characterization of MCT oil/CD inclusion complexes .....	33
4.1. Oil-water interfacial tension measurement.....	33
4.2. Quantitative analysis of CD .....	34
4.3. Morphology of MCT oil/CD inclusion complexes .....	35
4.3.1. Optical microscopic study .....	35
4.3.2. SEM study .....	35
4.4. Fourier-transform infra-red (FT-IR) spectroscopy.....	35
5. Proton nuclear magnetic resonance ( <sup>1</sup> H-NMR) study .....	36
6. Solid-state characterizations of AmB/CD inclusion complexes .....	36
6.1. FT-IR spectroscopy .....	37
6.2. Powder X-ray diffraction (PXRD) studies .....	37
6.3. Differential scanning calorimetry (DSC) .....	37
7. Screening the concentration components for AmB pickering emulsion.....	38
8. Preparation of pickering NEs and non-pickering NEs .....	38
9. Physicochemical and chemical characterizations.....	39
9.1. pH determination.....	39
9.2. Osmolality measurement.....	40
9.3. Viscosity measurement.....	40
9.4. Interfacial tension and contact angle measurement.....	40
9.5. Morphology, particle size and size distribution and zeta potential .....	41
9.6. Determination of drug content and Entrapment Efficiency (%EE) .....	41

10. Stability index study .....	42
11. Degree of AmB aggregation.....	42
11.1. UV-Vis spectroscopy .....	42
11.2. Circular dichroism.....	43
12. <i>In vitro</i> drug release study .....	43
13. Rheological measurement .....	44
14. Surface morphology of AmB NEs .....	44
14.1. SEM analysis.....	44
14.2. Atomic force microscopy (AFM) study .....	45
15. <i>In vitro</i> hemolytic study.....	45
16. <i>In vitro</i> antifungal activity .....	46
17. Physical and chemical stability studies of AmB NEs .....	47
17.1. Freeze-Thaw stability study .....	47
17.2. The stability study .....	48
18. Statistical analysis .....	48
CHAPTER IV     RESULTS AND DISCUSSION.....	49
1. Phase-solubility study.....	49
2. Solubility determination of AmB in oils and surfactants .....	50
3. Characterization of MCT oil/CD inclusion complexes .....	53
3.1. Interfacial tension measurement.....	53
3.2. Quantitative analysis of CD .....	55
3.3. Morphology of MCT oil/CD inclusion complexes .....	56
3.3.1. Optical microscope study .....	56
3.3.2. SEM study .....	57
3.4. FT-IR spectroscopy .....	58
4. <sup>1</sup> H-NMR determination .....	60
5. Solid-state characterizations of AmB/CD complexes .....	64
5.1. FT-IR spectroscopy .....	64
5.2. PXRD analysis .....	65

5.3. DSC analysis .....	67
6. Screening the concentration of components for AmB pickering emulsion.....	69
7. Physicochemical and chemical characterization .....	70
7.1. Appearance, pH, osmolality and viscosity .....	70
7.2. Interfacial tension and contact angle measurement.....	73
7.3. Morphology, particle size and size distribution and zeta potential .....	75
7.4. Drug content and entrapment efficiency .....	78
8. Stability index study .....	79
9. Degree of aggregation behavior .....	80
9.1. UV-Vis spectroscopy .....	80
9.2. Circular dichroism.....	82
10. <i>In vitro</i> drug release study .....	83
11. Rheological study .....	85
12. Surface morphology of AmB NEs .....	88
12.1. SEM analysis.....	88
12.2. AFM study.....	89
13. <i>In vitro</i> hemolytic study.....	90
14. <i>In vitro</i> antifungal activity .....	92
15. Physical and chemical stability studies of AmB NEs .....	94
15.1. Freeze-Thaw stability study .....	94
15.2. The stability study .....	98
CHAPTER V      CONCLUSIONS .....	103
APPENDIX A      PHYSICAL STABILITY .....	106
APPENDIX B      CHEMICAL STABILITY .....	114
REFERENCES .....	118
VITA.....	136

## LISTS OF TABLES

	<b>Page</b>
<i>Table 1 Some physicochemical properties of parent CDs and selected CD derivatives (modified from Ref (85))</i> .....	19
<i>Table 2 The composition of pickering NEs and non-pickering NEs containing AmB</i> .39	39
<i>Table 3 Apparent stability constant values (<math>K_{1:1}</math> and <math>K_{1:2}</math>) and the complexation efficiency (CE) of AmB/CD complexes in pure aqueous CD solutions at <math>25 \pm 1</math> °C</i> ...53	53
<i>Table 4 The <math>^1\text{H}</math>-chemical shifts associated with different hydrogen atoms of free form of the <math>\alpha\text{CD}</math> and of the formed IC (MCT oil/<math>\alpha\text{CD}</math>)</i> .....	61
<i>Table 5 The <math>^1\text{H}</math>-chemical shifts of AmB alone and in the presence of <math>\gamma\text{CD}</math></i> .....62	62
<i>Table 6 The <math>^1\text{H}</math>-chemical shifts of AmB alone and in the presence of HP<math>\gamma\text{CD}</math></i> .....63	63
<i>Table 7 pH value, osmolality and viscosity of the formulations (Mean<math>\pm</math>S.D., n=3)</i> ..71	71
<i>Table 8 The surface tension and contact angle of all formulations (n=3, Mean<math>\pm</math>S.D.)</i> .....	74
<i>Table 9 The mean particle size, size distribution and zeta potential of all formulations (n=3, Mean<math>\pm</math>S.D.)</i> .....	77
<i>Table 10 The total drug content (%) and entrapment efficiency (%EE) of AmB loaded formulations (n=3, Mean<math>\pm</math>S.D.)</i> .....79	79
<i>Table 11 Peak ratio values of AmB solution, Amphotericin-B® and selected formulations (n=3, Mean<math>\pm</math>S.D.)</i> .....82	82
<i>Table 12 In vitro antifungal activities of AmB loaded formulations against various species of fungi (n=3, Mean<math>\pm</math>S.D.)</i> .....	94
<i>Table 13 pH values, average particle size (PS), size distribution (PDI) and zeta potential values of AmB NEs after storage zero to three freeze-thaw cycles (n=3, Mean<math>\pm</math>S.D.)</i> .....	97
<i>Table 14 pH values, average particle size (PS), size distribution (PDI) and zeta potential, AmB NEs storage at accelerated stability condition for 0, 1, 3 and 6 months (n=3, Mean<math>\pm</math>S.D.)</i> .....	100

<i>Table 15</i> pH values, average particle size (PS), size distribution (PDI) and zeta potential, of AmB NEs storage at long-term stability condition for 0, 1, 3 and 6 months (n=3, Mean±S.D.) .....	101
<i>Table 16</i> Total AmB content (%) and %EE of AmB NEs storage at accelerated and long-term stability conditions for 0, 1, 3 and 6 months (n=3, Mean±S.D.) .....	102
<i>Table 17</i> The pH values of AmB NEs storage at accelerated stability condition for 0, 1, 3 and 6 months .....	106
<i>Table 18</i> The pH values of AmB NEs storage at long-term stability condition for 0, 1, 3 and 6 months .....	107
<i>Table 19</i> The average particle size (nm) of AmB NEs storage at accelerated stability condition for 0, 1, 3 and 6 months .....	108
<i>Table 20</i> The average particle size (nm) of AmB NEs storage at long-term stability condition for 0, 1, 3 and 6 months .....	109
<i>Table 21</i> The PDI values of AmB NEs storage at accelerated stability condition for 0, 1, 3 and 6 months .....	110
<i>Table 22</i> The PDI values of AmB NEs storage at long-term stability condition for 0, 1, 3 and 6 months .....	111
<i>Table 23</i> The zeta potential values (mV) of AmB NEs storage at accelerated stability condition for 0, 1, 3 and 6 months (n=3, Mean±S.D.).....	112
<i>Table 24</i> The zeta potential values (mV) of AmB NEs storage at long-term stability condition for 0, 1, 3 and 6 months .....	113
<i>Table 25</i> The total AmB content (%) of AmB NEs storage at accelerated stability condition for 0, 1, 3 and 6 months .....	114
<i>Table 26</i> The total AmB content (%) of AmB NEs storage at long-term stability condition for 0, 1, 3 and 6 months .....	115
<i>Table 27</i> %EE of AmB NEs storage at accelerated stability condition for 0, 1, 3 and 6 months .....	116
<i>Table 28</i> %EE of AmB NEs storage at long-term stability condition for 0, 1, 3 and 6 months .....	117

## LIST OF FIGURES

	Page
<i>Figure 1 Chemical structure of AmB</i> .....	12
<i>Figure 2 Anatomy of the eye</i> .....	14
<i>Figure 3 The main ocular components and barriers (80)</i> .....	16
<i>Figure 4 Schematic presentations of native cyclodextrin (88)</i> .....	18
<i>Figure 5 Graphical representation of A and B-type phase-solubility profiles (25)</i> ...	22
<i>Figure 6 Solid particles stabilized pickering emulsion and surfactant stabilized by classical emulsion (107)</i> .....	26
<i>Figure 7 Phase-solubility profiles of AmB in aqueous CD solutions. (a) <math>\beta</math>CD (■), (b) <math>\alpha</math>CD (◆), <math>\gamma</math>CD (●) and HP<math>\gamma</math>CD (▲)</i> .....	52
<i>Figure 8 Solubility of AmB in various oils and surfactants</i> .....	53
<i>Figure 9 Interfacial tension at MCT oil/water interface as a function of CD concentrations; <math>\alpha</math>CD (◆), <math>\beta</math>CD (●), <math>\gamma</math>CD (■) and HP<math>\gamma</math>CD (▲)</i> .....	55
<i>Figure 10 Observed concentration of dissolved CD from the mixture of MCT oil and CD (1.5% w/v) (column) versus the theoretical value (dotted line)</i> .....	56
<i>Figure 11 Optical micrographs of MCT oil/<math>\alpha</math>CD (a) and MCT oil/<math>\beta</math>CD complexes (b)</i> .....	57
<i>Figure 12 SEM images of MCT oil/<math>\alpha</math>CD (a) and MCT oil/<math>\beta</math>CD complexes (b) at the magnification of x5000</i> .....	58
<i>Figure 13 FT-IR spectra of pure <math>\alpha</math>CD (a), pure MCT (b) and FD MCT/<math>\alpha</math>CD (c)</i> .	59
<i>Figure 14 FT-IR spectra of pure AmB (a), pure <math>\gamma</math>CD (b), pure HP<math>\gamma</math>CD (c), PM AmB/<math>\gamma</math>CD (d), PM AmB/HP<math>\gamma</math>CD (e), FD AmB/<math>\gamma</math>CD (f) and FD AmB/HP<math>\gamma</math>CD (g)</i> .....	65
<i>Figure 15 The PXRD spectra of pure AmB (a), pure <math>\gamma</math>CD (b), pure HP<math>\gamma</math>CD (c), PM AmB/<math>\gamma</math>CD (d), PM AmB/HP<math>\gamma</math>CD (e), FD AmB/<math>\gamma</math>CD (f) and FD AmB/HP<math>\gamma</math>CD (g)</i> ...	67
<i>Figure 16 DSC thermograms of pure AmB (a), pure <math>\gamma</math>CD (b), pure HP<math>\gamma</math>CD (c), PM AmB/<math>\gamma</math>CD (d), PM AmB/HP<math>\gamma</math>CD (e), FD AmB/<math>\gamma</math>CD (f) and FD AmB/HP<math>\gamma</math>CD (f)</i>	68

<i>Figure 17 The phase diagrams of different concentration of <math>\alpha</math>CD, MCT oil and lecithin: 10% of MCT oil (a) and 20% of MCT oil (b), the phase separation (x) and stable emulsion (♦) .....</i>	70
<i>Figure 18 Optical microscopic images of AmB pickering NEs (F1-F8) and AmB non-pickering NEs (F9-F12).....</i>	76
<i>Figure 19 The stability index (%) of AmB NEs.....</i>	80
<i>Figure 20 Circular dichroism of AmB in DMSO:Methanol (1:999 v/v) (a) and selected formulations and Amphotericin-B<sup>®</sup> in STF (b) .....</i>	83
<i>Figure 21 In vitro drug release profiles of AmB NEs and Amphotericin-B<sup>®</sup> within 48 h (a) and AmB NEs within 8 h (b) through the semipermeable membrane with MWCO 12000-14000 Da (n=3, Mean<math>\pm</math>S.D).....</i>	84
<i>Figure 22 Shear rate dependence of viscosity for F2 (■), F6 (♦), F9 (▲) and F11 (●) .....</i>	86
<i>Figure 23 Dynamic frequency sweep of (a) pickering NEs; F2 (■), F6 (♦), and (b) non-pickering NEs; F9 (▲) and F11 (●); filled (G') and opened (G'') .....</i>	87
<i>Figure 24 SEM images of pickering NEs; F2 (a); F6 (b); and non-pickering NEs; F9 (c) and F11(d).....</i>	89
<i>Figure 25 AFM images of pickering NEs; F2 (a) and F6 (b).....</i>	90
<i>Figure 26 In vitro hemolytic study of sheep RBC at the various concentrations of AmB in formulations; F2 (■),F6 (♦),F9 (▲),F11 (●) and Amphotericin-B<sup>®</sup> (x), (n=3, Mean<math>\pm</math>S.D.).....</i>	91
<i>Figure 27 The appearance of AmB NEs after storage zero to three freeze-thaw cycles .....</i>	96
<i>Figure 28 Optical micrographs of AmB NEs after storage zero to three freeze-thaw cycles.....</i>	98

## LIST OF ABBREVIATION

%	percentage
°C	degree Celsius
μg	microgram (s)
αCD	alpha-cyclodextrin
βCD	beta-cyclodextrin
γCD	gamma-cyclodextrin
AFM	atomic force microscope
AmB	amphotericin B
BAC	benzalkonium chloride
CD	cyclodextrin
CE	complexation efficiency
Da	dalton
DMSO	dimethyl sulfoxide
DSC	differential scanning calorimetry
DLS	dynamic light scattering
e.g.	for example
Eq.	equation
FT-IR	Fourier-transform infra-red spectroscopy
FD	freeze dried
HPγCD	2-hydroxypropyl-gamma-cyclodextrin
HPLC	high performance liquid chromatography
<sup>1</sup> H-NMR	proton nuclear magnetic resonance
K	stability constant



M	molarity
mg	milligram (s)
mL	milliliter (s)
mV	millivolts
MWCO	molecular weight cut-off
NEs	nanoemulsions
PM	physical mixture
psi	pound per square inch
PXRD	powder X-ray diffraction
Rpm	revolution per minute
R <sup>2</sup>	coefficient of determination
SEM	scanning electron microscope
STF	simulated tear fluid
SD	standard deviation

## CHAPTER I

### INTRODUCTION

Since fungal keratitis leading to the loss of the vision and cause of corneal blindness, it becomes an important ophthalmic problem all over the world (1). It is most commonly related with ocular trauma that resulted from the vegetative matter or soil-contaminated materials in both developed and developing countries (2-6). The incidence rate can also be elevated by some environmental factors such as temperature, annual rainfall, windy season and harvested period. In the tropical and subtropical regions, the incidence rate of fungal keratitis is higher and much more frequent in developing countries (1).

In developing countries such as India and Thailand, ocular trauma is the major risk factor of fungal keratitis. In these countries, among the microbial keratitis, up to 40% of the cases are caused by fungi. In India, *Aspergillus* is the most contributing species of fungal keratitis and it is found that approximately 113 per 100000 patients (3, 7-10). Conversely, the wearing of contact lens is the major cause of fungal keratitis in the developed countries because it has become more popular. In the United States, 37% of the fungal keratitis rise from the wearing of contact lens whereas only 25% of the patients undergo fungal keratitis from the risk of ocular trauma (2, 11).

The eye is likely to be harmed by microbial infections from local and systemic risk factors that can permeate into the protective mechanism. Two main types of fungi are mostly associated with the fungal keratitis; filamentous fungi such as *Fusarium* and *Aspergillus* and yeast-like fungi such as *Candida* (2, 12). Fungal keratitis has predominantly occurred in the patients with chronic ocular surface

diseases, diabetes mellitus, topical steroid use or the immunosuppressive patients because these conditions can promote the invasion of the pathogen and this can lead to the fungal keratitis (13, 14). The significant signs and symptoms of fungal keratitis are defects of corneal epithelium with the inflammation of the corneal stroma, ocular pain, foreign body sensation and blurred vision (15). Fungal keratitis is serious, and it can lead to loss of the vision, therefore, it necessitates the prompt and adequate treatment. Treatment options include local and systemic antifungal administration according to the underlying cause and severity of the diseases.

Various antifungal agents have been evaluated and including two major categories of antifungal agents: azole family and polyene family (16). Amphotericin B (AmB) has been used for more than 50 years and it remains the drug of choice for the management of severe systemic fungal infections (17, 18). AmB affiliates to the family of polyene macrolide antibiotics and is the first broad-spectrum antifungal agents. In the 1950s, AmB is isolated from *Streptomyces nodosus*. In the 1960s after the approval of FDA, it has become popular due to its prominent efficiency in the treatment of disseminated fungal infections. The mechanism of action is based on the interaction of ergosterol, the steroidal component of the fungal cell membrane, leading to the pore formation through the lipid membrane. Consequently, the change in the cell permeability allows the leakage of ions, leading to cell death (19, 20).

Its chemical structure is designated by a glycolated lactone with an amphiphilic poly-hydroxyl region, conjugated heptenes chromophore and an amphoteric ion pair. AmB has two physicochemical properties: amphiphilic, due to the apolar and polar sides of the lactone

ring and amphoteric due to the presence of the ionizable carboxylic and amine groups. Unfortunately, the development of AmB formulations is retarded because of its poor solubility in aqueous media and that leads to the limited bioavailability (21).

Several methods are used to increase the aqueous solubility of poorly water-soluble drugs. The complexation by cyclodextrins (CDs) as inclusion complex is a promising strategy to enhance the solubility of drugs (22). CDs are cyclic oligosaccharides obtained by the enzymatic degradation of the starch. Natural CDs are composed of six ( $\alpha$ CD), seven ( $\beta$ CD) and eight ( $\gamma$ CD) glucose residues. Since the structures of CDs are hydrophobic inside and hydrophilic outside, they can form inclusion complexes with lipophilic compounds by inserting the lipophilic portion into the CDs cavity. In such a way, the CD complexation can enhance the solubility and increase the bioavailability of such compounds (23). In the aqueous eye drops formulations, CD complexation can increase drug bioavailability by enhancing drug permeation through the aqueous tear film and biomembrane (24-26).

At present, AmB is available in lyophilized form as Fungizone<sup>®</sup>, Abelcet<sup>®</sup>, Ambisome<sup>®</sup> for the intravenous route. It is being used as one of the first-line therapies in the management of fungal keratitis administered at every 30-60 minutes. In the Fungizone<sup>®</sup>, sodium deoxycholate is incorporated to improve the solubility of crystalline AmB. When administered intravenously with Fungizone<sup>®</sup>, approximately 80% of the patients show various acute side effects such as fever, chills, vomiting, headache, nausea (27) and about 30% exhibit the renal malfunctions (28, 29). Moreover, systemic administration of AmB has poor permeability into ocular tissues and does not reach therapeutic levels

in the cornea, aqueous or vitreous humor. These effects discourage the use of AmB in systemic administration for fungal keratitis treatment (30-33). Although it can be administered subconjunctivally, it may render conjunctival necrosis, scleritis and scleral thinning (34, 35). Several approaches have been reported for the ocular delivery of AmB such as using collagen shields (36) and intracameral injection (37, 38). Collagen shields are associated with limitations like lack of individual fit for patients, chances of expulsion and reduction in visual acuity (28). Cataracts are observed in some patients treated with intracameral injections (39).

Topical administration is commonly the first choice for the treatment of fungal keratitis. Presently, in the developing countries, the extemporaneous preparation of AmB is obtained by using the intravenous formulation (Fungizone<sup>®</sup> - Bristol-Meyers Squibb) that was reconstituted with sterile water for injection and properly diluted. It is used at hourly intervals at the beginning of treatment, and then every 4 hours after the therapeutic response is observed (40-43). In the case of lipid-based formulations, (i.e. liposomes) its major drawback is the physical and chemical stability during storage condition (44-46). When it is prepared as eye drop solution, it is not possible to maintain the therapeutic concentration for prolonged time as it is easily washed away by the tear dilution and blinking reflex (28).

Nanoemulsions (NEs) are the potential advantages that are possible for high drug payload in the oil phase and able to increase the residence time on the eye surface. Nevertheless, the drawback of obtained emulsion is destabilized by sedimentation or creaming, Ostwald ripening and coalescence (fusion) of the droplets (47). To overcome these

problems, solid colloidal particles have been used as emulsion stabilizing agents (48). The resulting emulsion is named as pickering emulsion and has been extensively studied in the last decades. It has a significant potential in reducing the coalescence, Ostwald ripening and improving the stability of the emulsion (49-51). The mechanism of stabilizing the pickering emulsion is based on the development of the film-like structure of the solid aggregates around the oil droplets, and it behaves as steric barriers at the oil-water interface. In this way, stability of emulsion is greatly enhanced by preventing coalescence of the droplets and Ostwald ripening (52, 53).

Recently, literature reported that the development of pickering emulsion by using native CDs. The microcrystals of oil/CD inclusion complexes can stabilize the pickering emulsion. They are formed by threading CD from the aqueous phase on oil molecules that can be deposited on the emulsion droplets surface. It may grow further into the microrods and micro platelets depending on the type of CD used. As a result, the coalescence of the emulsion is prevented by the densely packed layer which is formed around the emulsion droplets by the attachment of these microcrystal inclusion complexes (54). The oil/CD inclusion complexes formed at low CD concentration showed surface-activity but stable pickering emulsion cannot be obtained from these complexes. On the other hand, at high CD concentrations, oil/CD complexes can transform into the precipitated complexes and serve as an emulsifier for the formation of stable pickering emulsion (55). The state of the art of this emulsion stabilization mechanism is based on the molecular adsorption on the emulsion droplets i.e. molecularly dissolved CDs

congregated as colloidal solid particles directly adsorb onto the emulsion droplets that lead to the formation of stable pickering emulsion.

According to the literature, when  $\alpha$ CD is incorporated into cycloalkanol/water emulsion system, inclusion complexes of cycloalkanol/ $\alpha$ CD are formed and pickering emulsion is obtained. This may be due to the surface activity character of  $\alpha$ CD (56-58). Cheong et al. (2016) reported the formation of the kenaf seed o/w pickering emulsions stabilized by the synergistic effect between sodium caseinate, Tween 20 and  $\beta$ CD (59). Mathapa et al. (2013) also investigated the self-assembly of CD molecules at the tetradecane-aqueous solution interface through the formation of inclusion complexes. This revealed that pickering emulsion is formed by the formation of microcrystals of inclusion complexes with CD (60). The stabilized o/w emulsion using triglyceride as oily phase had been emulsified with aqueous solutions of  $\alpha$ CD and  $\beta$ CD which had been studied by Shimada et al (1992). The authors have found that the interfacial tension of the oil-water interface decreased with the increase in CD concentration (61). These kinds of pickering emulsion are very promising in many areas such as cosmetics, food, pharmaceuticals, oil recovery and wastewater treatment (62).

It is well known that poor ocular penetration and low residence time are the major problems of the ocular drug delivery system. To overcome these obstacles for ocular drug delivery, pickering NEs has been exploited. It had been evidenced that these platforms can provide remarkable controlled release capability (52), and can increase the ocular retention time, ocular bioavailability and reduce the dosing frequency. The addition of CD can enhance the solubility of AmB in the formulations and consequently obtain its adequate concentration for

ocular mucosa. In this study, the AmB solubility, solution ( $^1\text{H-NMR}$ ) and solid-state (FT-IR, PXRD and DSC) characterizations of AmB/CD complexes were investigated. The oil/CD inclusion complexes were evaluated by the interfacial tension measurement, quantitative analysis of CDs, FT-IR and  $^1\text{H-NMR}$  and the morphology was observed by optical microscope and SEM study. Then, the CD-based pickering NEs containing were developed. These AmB NEs utilized the combined strategies i.e. AmB/CD inclusion complexes and incorporation of AmB in an internal phase of o/w pickering NEs for increasing AmB solubility and stability. The physicochemical and chemical properties of these formulations were determined. In addition, *in vitro* drug release, *in vitro* hemolysis, *in vitro* antifungal activity and the stability studies were evaluated. Thus, the main objectives of this present study are as follows:

1. To study the CD solubilization of AmB
2. To prepare the AmB/CD and oil/CD complexes and evaluate by solution and solid-state characterizations
3. To develop and characterize the CD-based pickering NEs containing AmB for fungal keratitis



## CHAPTER II

### LITERATURE REVIEWS

#### 1. Keratitis

Keratitis is the inflammation of the corneal layers caused by many factors. Microorganisms cannot penetrate the healthy cornea because of the defensive system of the eye. However, environmental factors or pathogens lead to fungal keratitis. Inflammation at the corneal surface epithelial is termed as superficial keratitis whereas inflammation at corneal stroma is known as stromal or interstitial keratitis. There are two types of keratitis; non-infectious keratitis and infectious keratitis (1).

Non-infectious keratitis can be caused by a relatively minor injury, wearing of prolong contact lens or the invasion of foreign things (63). Moreover, there are many factors that can cause eye defects and leading to the inflammation of corneal layers such as eyelid abnormalities and inflammations, tear film disorder, allergies, physical or chemical trauma and facial neuropathy (1).

Infectious keratitis is the most usual form of keratitis and caused by bacteria, virus, fungi and parasites. The invasion of microorganisms caused the innate and adaptive immune-mediated inflammation and consequently, necrosis and destruction of corneal layers were resulted (2). Among the microbial keratitis, fungal keratitis is one of the more virulent and dangerous in some global areas (2, 63).

##### 1.1. Fungal keratitis

Among the microorganisms that caused keratitis, fungi are one of the most distinct and challenging organisms for the diagnosis and

treatment (2). Fungal keratitis comprised 44% to 67% of all microbial keratitis. The most common species of fungi causing keratitis are *Fusarium* spp., *Aspergillus* spp., and *Candida* spp. Fungal keratitis was firstly occurred a patient having the corneal ulcer induced by *Aspergillus* spp. in 1879 in Germany (64). The incidence rate of fungal keratitis depends on the geographical area and season. The higher rate of fungal keratitis is found in tropical and subtropical regions. Moreover, rainfall, windy season, temperature and harvesting time are the significant parameters for the cause of fungal keratitis.

Trauma is the most usual risk factors for fungal keratitis. Corneal infection can be caused by even minor injuries. Wearing of prolong contact lens is the main factor for the minor injuries, consequently, microorganisms in the environment or contaminated lens preservative solution usually lead to the corneal ulcers. In the literature, 36.4% of trauma and 33.7% of contact lens wearing were included in all cases of fungal keratitis (65). Prolonged application of antibiotics and steroids are also predisposing cause of fungal keratitis. After using of these medicines, local immunosuppression and disorder of microbial flora of the eye were emerged and lead the saprophytic fungi to pathogenic (66, 67). Other prevailing factors predisposing individuals to develop fungal keratitis include industrial farming, diabetes, human immunodeficiency virus status, past penetrating keratoplasty, exposure keratitis, previous ocular surgery, and preexisting herpes emulsions simplex virus keratitis (68).

## 2. Amphotericin B

AmB is the polyene antifungal antibiotic and produced from the cultures of *Streptomyces nodosus*, soil actinomycete (69). It has used in the treatment of progressive and life-threatening fungal infections caused by *Aspergillus*, *Candida*, *Blastomyces*, *Coccidioides*, *Cryptococcus* and *Histoplasma* and certain protozoan infections such as *Leishmaniasis* over the past five decades (70). It was discovered in the mid-1950s and remains the drug of choice for the treatment of systemic fungal infections (71). It is a heptane macrolide antibiotic, composed of macrolide ring with seven conjugated double bonds and mycosamine ring connected to the macrolide ring by a glycosidic bond (Figure 1). The name amphotericin B is derived from the amphoteric properties of the drug due to the presence of carboxyl group on the lactone ring and amino group on mycosamine ring (72).

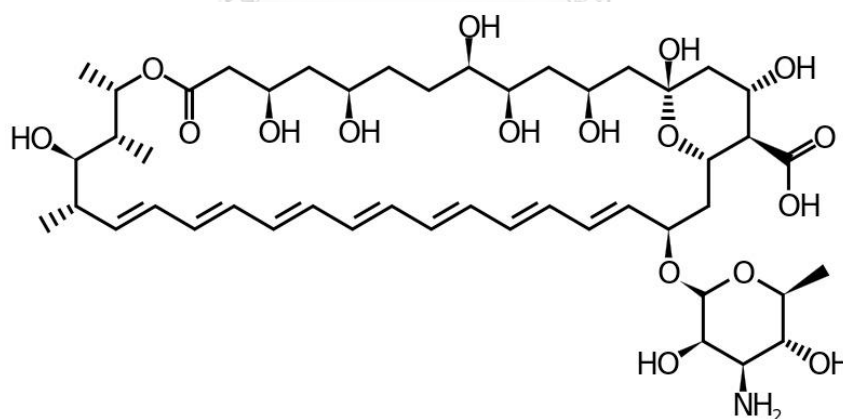


Figure 1 Chemical structure of AmB

(<https://blogs.sciencemag.org>.)

The main obstacle for the use of AmB is its insolubility in water. Its aqueous solubility is less than 1mg/L at physiological pH. The

drug is sparingly soluble in the organic solvents. Because of its poor water solubility, gastrointestinal absorption is very low and oral drug bioavailability is minimal. At a pH below 2 or above 11, AmB is water soluble (about 0.1mg/mL). However, AmB is not stable under these extreme conditions.

### **2.1. Mechanism of action of Amphotericin B**

The polyene region of AmB can bind to the sterol of both fungal and human cell wall. AmB has the higher affinity to ergosterol than cholesterol, therefore, it shows the selective toxicity to fungal cell wall (69). There are two binding sites of AmB to ergosterol or cholesterol. The first binding is related to the formation of hydrogen bonds, which is caused by the hydroxyl groups of sterols and the carboxyl group at C-18 of AmB molecule. This binding is also enhanced by the involvement of the amino group of the mycosamine moiety. The other kind of interaction is based on the whole sterol molecules and the seven conjugated bonds of AmB by Van der Waals forces (73). After binding to the ergosterol, membrane integrity is impaired and leading to the pore formation. Consequently, AmB induced leakage of potassium and other cellular components are occurred and resulted in fungal cell death.

## **3. Ocular drug delivery system**

### **3.1. Anatomy of the eye**

The eye is a complex organ with the distinct anatomy and physiology. There are two main parts of the eye: anterior portion and posterior portion (Figure 2). Approximately one-third of the eye is included in the anterior part and the rest two-third builds up the posterior

segment. The anterior segment composed of tissues such as cornea, conjunctiva, aqueous humor, iris, ciliary body and lens. Whereas, sclera, choroid, retinal pigment epithelium, neural retina, optic nerve and vitreous humor make up the posterior segment of the eye (74).

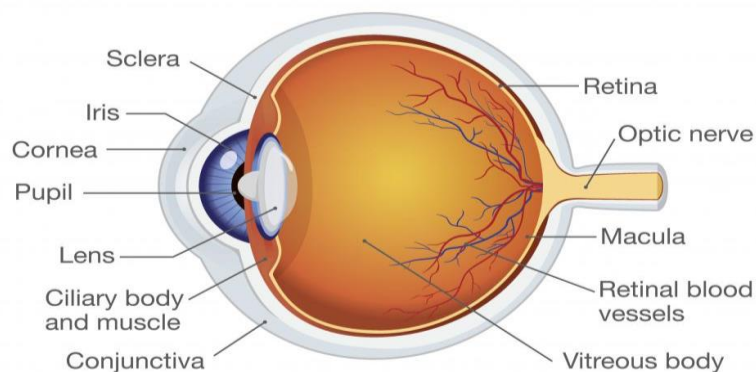


*Figure 2 Anatomy of the eye*  
(<https://www.medicinenet.com>)

### **3.2. Barriers for the ocular drug delivery**

The cornea is the major barrier, which impedes the absorption of the drug into the eye (Figure 3) It is mainly composed of three layers i.e. epithelium, stroma and endothelium tissues. Corneal epithelium is the lipid nature which limits the permeation of hydrophilic drugs. Moreover, ribbon-liked tight junctions of corneal epithelium also inhibit the paracellular permeation from the tear film into the intracellular corneal epithelium. (75, 76). The corneal stroma is consisted of an extracellular matrix and lamellar arrangement of collagen fibrils. Because of the highly hydrophilic nature of corneal stroma, it becomes the important barrier for the permeation of lipophilic compounds (77). Endothelium is the inner most layer of cornea and composed of monolayer of hexagonal-shaped

cells. Although it is the separating barrier, the corneal endothelial junctions help the passage of macromolecules due to their selected carrier-mediated transport. Therefore, the epithelial layer and stroma are the important barriers and the compound should have appropriate hydrophilic and lipophilic properties to cross through these barriers (78).

Conjunctival tissue acts as a permeability barrier to eye drop solutions. Due to the presence of conjunctival blood capillaries and lymphatics, there is a significant drug loss into systemic absorption and result in low ocular bioavailability. Although the paracellular route of drug administration via conjunctiva is the major pathway, the absorption of the hydrophilic molecules can be restricted owing to the conjunctival epithelial tight junctions (79).

The other important barrier for the ocular drug delivery system is the blood-ocular barriers and classified into two barriers: blood-aqueous barrier and blood-retinal barrier for anterior segment and posterior segment, respectively. Blood-aqueous barrier locates in the endothelium of iris, ciliary blood vessels and epithelium. It composes of two distinct cell layers and retards the passage of compounds from the plasma to the aqueous humor by tight junctions (77). Whereas, blood-retinal barrier limits the absorption of therapeutic agents form the blood into the posterior segment. The retinal capillary endothelial cells and retinal pigment epithelium cells (RPE) are included in the blood-retinal barrier. The tight junctions of the RPE prevent the entry of drugs from the choroid into the retina (74).

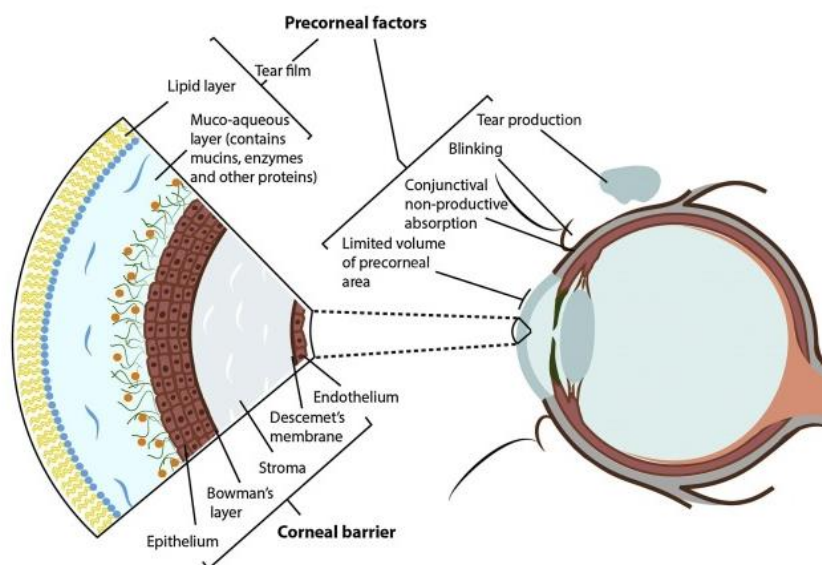


Figure 3 The main ocular components and barriers (80)

### 3.3. Topical application to the ocular drug delivery system

In comparison of invasive ocular route of administration, topical administration is mostly preferred to the systemic administration for the treatment of anterior segment diseases. There are various sites of action for the topically applied drugs: cornea, conjunctiva, sclera and tissues of anterior segment (iris and ciliary body). About 90% of the marketed products are conventional dosage forms such as solutions, suspensions and ointments, which delivery to the anterior segment of the eye via topical administration. However, topically applied drugs have the poor ocular bioavailability, this is mainly due to the precorneal factors and anatomical barriers. These factors involve the solution drainage, blinking, tear film, tear turnover and lacrimation and become a challenge and restrict the ocular penetration. Because of the drug loss by tear turn over, tear film is the foremost barrier for the topically administered drugs. The human tear volume is about 7-9  $\mu\text{L}$  with the turnover rate of 0.5-2.2

$\mu\text{L}/\text{min}$ . These precorneal factors lead to low contact time with ocular membrane and result in poor ocular bioavailability, less than 5% of the administered dose reach to the intraocular tissues. During the topical administration, the eye can accept volume of 30  $\mu\text{L}$  of the administered drugs and excess volume drains into the systemic circulation by nasolacrimal duct and resulted in systemic side effects (81). This can be overcome by prolonging the contact time of drugs to the ocular surface. Presently, cyclodextrins (CDs) are becoming popular in topical ocular drug delivery because of their unique properties, increasing in solubility and permeability of the drugs. CDs behave as the potential drug carrier by protecting the drug in solution and distributing towards the ocular surface (82). The CD micro- and nanoparticles are beneficial in increasing the corneal contact time for sustained drug release in ophthalmic drug delivery (83).

#### 4. Cyclodextrin

CDs, the cyclic oligosaccharides, are obtained from the starch by glycotransferase enzyme-induced degradation. The mostly found three parent CDs are  $\alpha\text{CD}$ ,  $\beta\text{CD}$  and  $\gamma\text{CD}$  with different glucopyranose units: 6, 7 and 8, respectively (Figure 4) (84, 85). It has truncated cone, bucket, or torus shape with unique chemical structure of outer hydrophilic portion and inner lipophilic cavity. The hydroxyl (OH) functions are located to the cone exterior and the primary OH groups at narrow side of the cone and the secondary OH groups at broader side. The lipophilic nature of central activity is obtained by linking of skeletal carbons with ethereal oxygen of the glucose units. CDs have the very negative Log P values because of their outer hydrophilic region and increase sites for hydrogen



bond donors and acceptors (86). The three parent CDs have been involved in the list of “Generally Recognized As Safe” (GRAS) in US Food and Drug Administration. The monographs of  $\alpha$ CD,  $\beta$ CD,  $\gamma$ CD, HP $\beta$ CD, SBE $\beta$ CD and HP $\gamma$ CD are presented in USP/NF.  $\alpha$ CD,  $\beta$ CD,  $\gamma$ CD are well tolerated and non-toxic when given orally but the toxicity was detected after parenteral administration in case of  $\alpha$ CD and  $\beta$ CD (82, 87).  $\gamma$ CD did not show embryotoxic or teratogenic effect in animal studies and can probably be used in the parenteral preparations (82). Table 1 shows the physicochemical properties of parent CDs and selected CD derivatives.

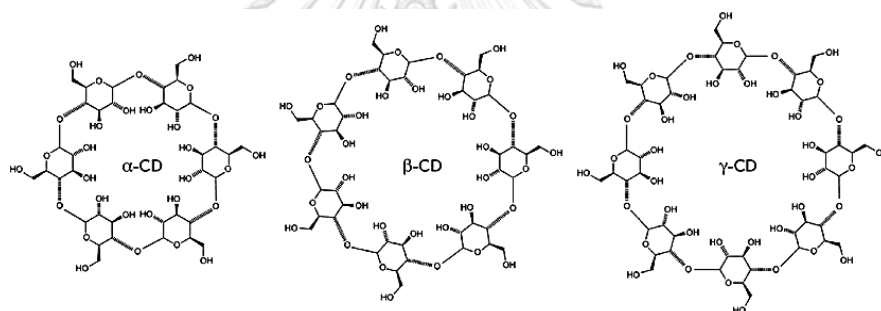


Figure 4 Schematic presentations of native cyclodextrin (88)

*Table 1 Some physicochemical properties of parent CDs and selected CD derivatives (modified from Ref (85))*

Cyclodextrin	Substitution <sup>a</sup>	Molecular weight (Da)	Solubility in water <sup>b</sup> (mg/mL)
$\alpha$ -cyclodextrin ( $\alpha$ CD)	-	972	145
$\beta$ -cyclodextrin ( $\beta$ CD)	-	1135	18.5
$\gamma$ -cyclodextrin ( $\gamma$ CD)	-	1297	232
2-hydroxylpropyl- $\beta$ CD (HP $\beta$ CD)	0.65	1400	>600
Sulfobutylether- $\beta$ CD (SBE $\beta$ CD)	0.9	2163	>500
2-hydroxylpropyl- $\gamma$ CD (HP $\gamma$ CD)	0.6	1576	>500

<sup>a</sup>average number of substituents by glucopyranose per repeat unit

<sup>b</sup>solubility in pure water at about 25 °C

#### 4.1. Drug/CD complex formation

CD in the aqueous solution can form the inclusion complex with various compounds especially with the lipophilic character by inserting the hydrophobic portion into its central cavity. During the inclusion complex formation, no covalent bonds are formed or broken and drug/CD complexes are in equilibrium with the free molecules in the aqueous solution (25). There are several factors that influence the formation of CD inclusion complexes. The appropriate size of CD to the size of guest molecules or major functional groups of the active

ingredients is the main parameter for the formation of inclusion complexes. According to the dimension of CDs,  $\alpha$ CD can couple with compounds with aliphatic side chain or low molecular weight compounds.  $\beta$ CD has the appropriate size to form the inclusion complexes with the aromatic or heterocyclic compounds whereas  $\gamma$ CD can complex with the larger compounds: macrocycles and steroids. The other important factor for inclusion complexes is the thermodynamic interaction. Because of the distinct chemical structure of CD; the narrow and wide openings with OH groups and inner hydrophobic cavity create the thermodynamic reactions that are needed for inclusion complex formation. The major interactions for the inclusion complexes formation are removal of polar water molecules from the hydrophobic CD cavity, hydrogen bond formation, electrostatic interaction, Van der Waals' forces, reduction of repulsive forces between the lipophilic guest and the aqueous surrounding and increase in the hydrophobic interaction by entering of guest molecule itself into CD cavity (25). The formation of inclusion complex has various advantages; enhancement of aqueous solubility, stability and bioavailability of the drugs, reducing the ocular and gastrointestinal irritation and masking of unpleasant odor and taste.

#### **4.2. Classification of CD inclusion complex and drug solubility**

Phase-solubility determination is mostly used for the investigation of effect of CD on the solubility of guest molecules, stability or binding constants and guest/CD stoichiometry at equilibrium (25). Types of drug/CD inclusion complex and the stability or binding constants are obtained by plotting the solubility of drug against the concentration of CD from the phase-solubility technique. Higuchi and

Connors categorized into A-type and B-type phase solubility profiles by investigating the influence of CD concentration on the solubility of the drug (Figure 5) (89). Generally, A-type phase-solubility profiles are formed by the water-soluble CDs whereas B-type phase-solubility profiles are obtained from the poor water-soluble parent CDs. When the solubility of the drug is enhanced with the rise of CD concentration, A-type profiles are resulted. A-type profiles can be classified into three kinds. The linear increase in the solubility of drug with increasing CD concentration is defined as  $A_L$  type.  $A_P$ -type is the positive deviation from the linearity of solubility, this means that solubilizing effect is more prominent at higher concentration of CD whereas in  $A_N$ -type, solubility of drug is less effective at higher CD concentration and shows the negative deviation from the linearity (90). B-type phase-solubility profiles present the inclusion complex formation with retarded aqueous solubility and are further classified into  $B_S$  and  $B_I$  types. However, phase-solubility profiles are unable to verify the inclusion complexes, and represent only the influence of CD concentration on the solubility of drug (91).

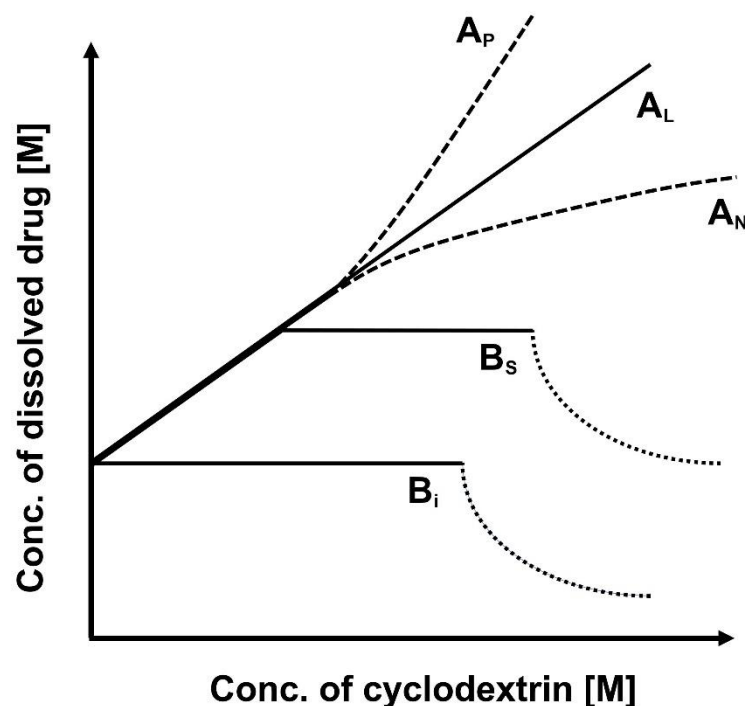
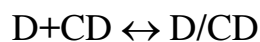


Figure 5 Graphical representation of A and B-type phase-solubility profiles (25)

The stability constant ( $K_{1:1}$ ), in which one molecule can complex with one molecule of CD, is the most usual form of CD complex. This can be characterized by following equation:

$$K_{1:1}$$



According to this condition, A<sub>L</sub>-type phase solubility was observed with the slope of less than one and the stability constant can be determined from the slope of the phase-solubility graph and the intrinsic solubility of the drug in aqueous media.

$$K_{1:1} = \frac{\text{slope}}{S_0(1 - \text{slope})}$$

$K_{1:1}$  can be applied for the comparison of the affinity of drugs for the different CDs or CDs derivatives. For 1:1 D/CD complexes, the complexation efficiency (CE) values can be calculated from the slope of the phase-solubility profile (92). It is more reliable to compare CE values than  $K_{1:1}$  for the selection of CD or complexation condition.

$$CE = \frac{\text{slope}}{(1 - \text{slope})} = K_{1:1} \cdot S_0$$

For the higher order of D/CD complexation,  $K_{1:2}$  is the most common stoichiometry and resulting in  $A_P$ -type phase-solubility profile. The continuing complexation is pretended in which the 1:2 complex is resulted when one additional CD molecules will complex with an existing 1:1 complex:



$K_{1:1}$  and  $K_{1:2}$  values can be obtained by curve fitting of the diagram with a quadratic model:

$$[S_t] - [S_0] = K_{1:1}[S_0][CD] + K_{1:1} K_{1:2}[S_0][CD]^2$$

[CD] means the total concentration of free CD and it is essential to plot the total amount of dissolved drug ( $S_t$ ) against the total CD concentration in solution [ $CD_t$ ] assuming that the extent of complexation is low (i.e.  $[CD] \sim [CD_t]$ ) (85).

Besides the phase-solubility profiles determination of drug/CD complexation, UV/Visible spectroscopy (93), fluorescence spectroscopy (94), pH-potentiometric titration (95), nuclear magnetic resonance

(NMR) (96) and permeation studies (97) are the alternative analytical techniques.

### 4.3. CD in ocular drug delivery system

Generally, the use of CDs in ocular drug delivery is mainly related to the enhancement of drug or drug/CD complex solubility, improvement the stability of the drug, reduction in ocular irritation and or increment of permeability of drug through the ocular surface (98). The literatures have been reported the reduction of ocular irritation in eye drop formulations containing CDs (99, 100). The increase concentration of CD is required to solubilize the hydrophobic drugs. The relevant concentration of CDs for the ocular preparations should be less than 15%. Since the eye drops are kept in the multidose container, the suitable preservatives should be included. Due to complex formation, CDs can reduce the efficiency of the preservatives, therefore, increased amount of preservatives are necessary for the achievement of optimal activity of preservative in the presence of CDs in formulations. It can be seen that benzalkonium chloride (0.02% w/v) is the potential preservative for CD containing eye drop solutions (82).

CDs can hardly permeate through the biological membrane because of their large molecular weight with outer hydrophilic part. CDs are generally known as the true permeation enhancers by keeping the lipophilic compounds in the solution and distributing them to the ocular membranes (101-103). The relatively lipophilic membrane has low affinity for hydrophilic CDs and thus they remain in the aqueous solution or tear fluid. The *in vivo* studies in rabbits and human of dorzolamide and dexamethasone eye drops containing CD showed that the significant of

drugs reached to the ocular tissues and provided the higher extent of bioavailability (104). CDs are the potential excipients for the development of eye drops in ocular drug delivery.

## **5. Pickering emulsion**

Emulsions are the most extensively applicable dosage form in various fields such as cosmetics, food industry, pharmaceuticals and drug delivery, etc. Emulsions are the thermodynamically binary dispersion system composed of two immiscible liquid phases stabilized by surfactants (105).

In recent years, solid colloidal particles have been accepted as the emulsion stabilizers in place of surfactants. The emulsions which are stabilized by the solid particles by adsorbing at oil-water interface are defined as the pickering emulsions. Pickering emulsions were firstly recognized in 1990s; however, a great development rose from many research works and become popular over twenty years (106). Pickering emulsions have the higher extent of protection from the coalescence and Ostwald ripening of emulsions and show the improvement of the stability. The emulsion droplets are stable because the kinetic collision energy will not be enough to separate the particles, which attached at o/w interface (49, 107, 108). It has been manifested that many kinds of organic and inorganic particles are capable to stabilize pickering emulsions including silica, clay, hydroxyapatite, carbon nanotubes, CD, wax and so on.

The stabilizing phenomenon for pickering emulsions is depended on dual wettability of solid particles to both liquid phases. This permits the continuous accumulation of particles and consequently, the



formation of steric boundary by the adsorption of particles at o/w interface stabilized against the coalescence (109). These particles have ability to irreversibly anchor to o/w interface and result in more powerful stability than conventional emulsions (Figure 6). The wettability of the solid particles is the useful tool for the evaluation of type of emulsions (50). If one of the liquid phases is more wetted by solid particles, this liquid phase is the continuous phase and the other liquid phase is the dispersed phase. The type of pickering emulsions can be classified by the value of contact angle ( $\theta$ ). If  $\theta$  is smaller than  $90^\circ$ , o/w pickering emulsions will form whereas w/o pickering emulsions will result when  $\theta$  is higher than  $90^\circ$  (50, 110).

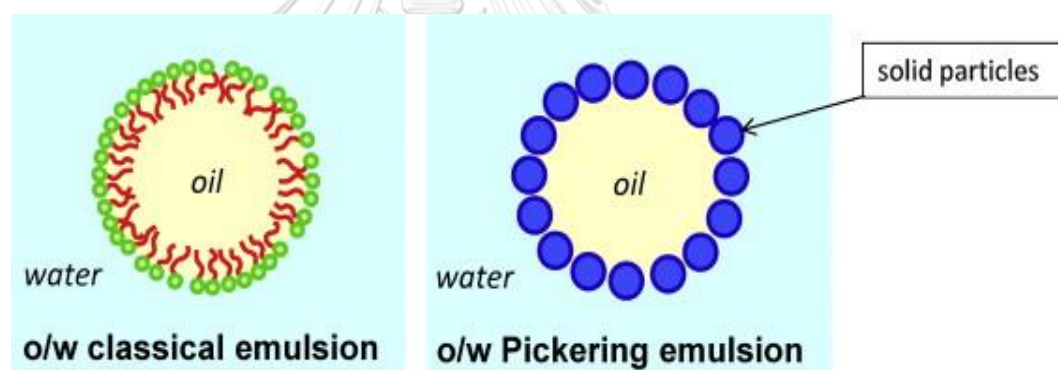


Figure 6 Solid particles stabilized pickering emulsion and surfactant stabilized by classical emulsion (107)

### 5.1. Role of CDs in pickering emulsions

CDs can be used as alternative emulsion stabilizers because the surface active oil/CD complexes can be obtained at o/w interface (48, 54). Literatures have been reported that the microcrystals of oil/CD inclusion complexes can stabilize the pickering emulsions by reducing the interfacial tension (111). Shimada et al. (1992) investigated the effect

of  $\alpha$ CD and  $\beta$ CD on the stabilization of o/w pickering emulsions (61). They found that the interfacial tension at o/w interface reduced with the increasing of CD concentrations. This is probably due to the production of oil/CD inclusion complexes by one of the fatty acids inserted into CD cavity with CD directed towards aqueous phase. At the same time, the other two fatty acids favored to the oily phase.  $\alpha$ CD and  $\beta$ CD-based pickering emulsions by using different oils containing bupivacaine were developed by Hu et al. (2008) (52). It was found that pickering emulsions exhibited the controlled drug release. Leclercq et al. (2016) demonstrated that econazole pickering emulsions using parent CDs as stabilizer was stable. The stabilizing mechanism was based on the formation of oil/CD inclusion complexes and these complexes led to the formation of nanoparticles when CD concentrations were increased (111).

## CHAPTER III

### MATERIALS AND METHODS

#### Materials

The following materials were used as

- Acetonitrile HPLC grade (Burdisk & Jackson, Korea)
- Alpha-cyclodextrin (Wacker Chemie AG, Germany)
- Alpha-tocopherol (Srichand United Dispensary, Co.Ltd, Thailand)
- Amphotericin B (Fagron Inc., United States)
- Beta-cyclodextrin (Wacker Chemie AG, Germany)
- Benzalkonium chloride (Sigma-Aldrich, USA)
- Dimethyl sulfoxide (Merck-Schuchardt, Germany)
- Ethylenediamine tetra-acetic acid disodium salt (Ajax Finechem Pty Ltd, Australia)
- Gamma-cyclodextrin (Wacker Chemie AG, Germany)
- Glycerol (Srichand United Dispensary, Co.Ltd, Thailand)
- Hydroxypropyl gamma-cyclodextrin (Wacker Chemie AG, Germany)
- Medium-chain triglycerides oil (Evansville, Indiana, USA)
- Phosphatidylcholine lecithin (Calbiochem, EMD Chemicals, Merck KGaA, Germany)
- Potassium dihydrogen phosphate (Ajax Finechem Pty Ltd, Australia)
- Sabouraud dextrose agar (SDA) media (S3181, Sigma-Aldrich)
- Semipermeable membrane (MWCO 12-14 kD, Spectra/Por molecularporous membrane, Spectrum Labs, United Kingdom)
- Sodium chloride (Ajax Finechem Pty Ltd, Australia)

## Equipments

- Analytical balance (MettlerToledo AG285, Germany)
- Atomic force microscope (Navi controller SPA-400, Seiko instrument SII, Tokyo, Japan)
- Centrifuge (Thermo Fisher Scientific Model X3, USA)
- Differential scanning calorimetry (MettlerToledo, model DSC822 °STAR System, Germany)
- Dynamic contact angle meter and tensiometer (DCAT 21, Dataphysics instrument, Germany)
- Fourier transform infrared spectroscopy (Thermo Scientific, model Nicolet iS10, USA)
- Franz diffusion cell (NK Laboratories Co. Ltd., Bangkok, Thailand)
- Freeze dryer (Labconco Lyophilizer, MO, USA)
- Haake MARS III rotational rheometer (Thermo Fisher Scientific, Schwerte, Germany)
- High performance liquid chromatography (HPLC) instrument equipped with
  - Liquid chromatography pump (quaternary pump, Agilent 1260 Infinity II, G7111A)
  - UV-VIS detector (Agilent 1260 Infinity II, G7115A)
  - Auto sampler (Agilent 1260 Infinity II, G7129A)
  - C18 column (Shiseido™ Capcell Pack, 5µm, 150×4.5 mm ID reverse phase column)
- High pressure homogenizer (Microfluidics LM20, Westwood, MA)
- Microplate reader (Multilabel plate reader, Perkin Elmer VICTOR 3™)

- Nanosizer (Zetasizer, Nano-ZS with software version 7.11, Malvern, UK)
- Optical microscope (Nikon Ts2 inverted microscope, Japan)
- pH meter (MettlerToledo, sevenCompact, Germany)
- Proton nuclear magnetic resonance spectroscopy ( $^1\text{H-NMR}$ , BRUKER, model AVANCE III HD, USA)
- Scanning electron microscope (JEOL, JSM-IT500, Japan)
- Shaking incubator (Shaking incubator, N-Biotek NB2015, Korea)
- Spectropolarimeter (Jasco J-810 spectropolarimeter, Japan Spectroscopic, Tokyo, Japan)
- Thermostat circulating water bath (Grant W28/ZD, England)
- Ultrasonic bath (GT sonic, China)
- UV-Visible spectrophotometer (Agilent Cary 60, UV-Vis spectrophotometer)
- Viscometer (Brookfield, LVDV-II+, USA)

## Methods

### 1. Phase-solubility profile

The solubility of the AmB was determined by the heating method (112). Excess amount of the AmB was added to the aqueous solution containing various concentrations of  $\alpha$ CD (0-12% w/v),  $\beta$ CD (0-1.5% w/v),  $\gamma$ CD and HP $\gamma$ CD (0-20% w/v). The drug suspensions were heated by sonication and controlled the temperature at 60 °C for 30 min and then allowed to cool to room temperature. Then, small amount of the solid drug was added to promote the drug precipitation. The obtained suspension was allowed to equilibrate at 25±1 °C for 7 days under constant agitation. After equilibrium was attained, the suspensions were filtered through 0.45  $\mu$ m nylon membrane filter, the filtrates were then diluted with the mixture of methanol and water (50:50 v/v) and analyzed by high-performance liquid chromatography (HPLC). The phase-solubility diagrams were constructed by plotting the total dissolved AmB concentration (mM) against the CD concentration (mM). The apparent stability constants of AmB/CD ( $K_{1:1}$  and/or  $K_{1:2}$ ) were determined by Eq.1 and Eq.2 according to the phase-solubility method of Higuchi and Connors (89). The complexation efficiency (CE) was calculated by using Eq.3 (92).

$$K_{1:1} = \frac{\text{slope}}{S_0(1-\text{slope})} \quad \text{Eq.1}$$

$$[S_t] - [S^0] = K_{1:1}[S^0][CD] + K_{1:1} \cdot K_{1:2} \cdot S_0[CD]^2 \quad \text{Eq.2}$$

$$CE = \frac{\text{slope}}{(1-\text{slope})} = K_{1:1} \cdot S_0 \quad \text{Eq.3}$$

where  $S_0$  is the intrinsic solubility of AmB and  $S_t$  is the total amount of dissolved AmB

## **2. Solubility determination of AmB in oils and surfactants**

The solubility of AmB in various oils and surfactants was determined. Various long-chain triglycerides (LCTs: castor oil, olive oil, and oleic acid) and medium-chain triglycerides (MCTs: MCT oil, isopropyl myristate and miglyol) were used. Surfactants were chosen that based on their ionic classification; non-ionic surfactants (tween 80, poloxamer 407 and labrasol) and amphoteric surfactant (phosphatidylcholine, lecithin). The individual surfactant was prepared at the concentration of 0.1% w/v. Briefly, an excess amount of AmB was added into each screw-capped glass vial of various oils or aqueous solutions of surfactants. After vortex mixing, the mixtures were equilibrated at 100 rpm,  $25 \pm 1$  °C for 7 days. The equilibrated samples were centrifuged at 4000 rpm for 30 min to remove undissolved AmB. The supernatants were withdrawn and properly diluted with methanol. The amount of AmB in methanolic solutions were analyzed by HPLC.

## **3. Quantitative analysis of AmB**

### **3.1. Calibration curve of AmB**

Accurate amount of AmB (10.0 mg) was weighed and dissolved with the solvent mixture of DMSO:methanol (1:999 v/v) in 100-mL volumetric flask and diluted to final concentration of 100  $\mu\text{g/mL}$ . The solution was further diluted to give a concentration range of 1-20  $\mu\text{g/mL}$ . Each concentration was subjected to HPLC analysis in triplicate. Peak area was recorded for all concentration and the equation was calculated

from the linear relationship between peak area of AmB and their concentrations.

### **3.2. Sample preparation**

The sample was diluted with the methanol:water (50:50 v/v). A portion of the sample was filtered through 0.45  $\mu\text{m}$  nylon membrane filter and subjected to HPLC analysis. The AmB content in the sample was calculated from the AmB calibration curve.

### **3.3. HPLC condition**

Quantitative determination of AmB was performed by a reversed-phase HPLC component system from Agilent 1260 Infinity II consisting of Liquid chromatography pump (quaternary pump, G7111A), UV-Vis detector (G7115A), autosampler (G7129A) with Chem Station software C.01.08. and Shiseido™ Capcell Pack C18 MG II S-5, C18, 150x4.5 mm ID with C18 guard cartridge column MGII 5  $\mu\text{m}$ , 4x10 mm. The HPLC condition was as follows; mobile phase: acetonitrile: 0.025 mM EDTA (40:60 v/v); flow rate: 0.8 mL/min; oven temperature: ambient; UV detector wavelength: 407 nm; injection volume: 20  $\mu\text{L}$ ; and run time: 7 min.

## **4. Characterization of MCT oil/CD inclusion complexes**

### **4.1. Oil-water interfacial tension measurement**

To evaluate the affinity of CD complexation of MCT oil, the oil/water interfacial tension of the MCT oil/water interface was performed with dynamic contact angle meter and tensiometer (DCAT 21, Dataphysics instrument, Germany) by using Wilhelmy plate. A series of



aqueous solutions of CDs i.e.,  $\alpha$ CD,  $\beta$ CD,  $\gamma$ CD and HP $\gamma$ CD (15mL), at the concentration range of 0-1.5% w/v were transferred into the glass vessels and the equal volume of MCT oil was added into each CD solution and thoroughly mixed. MCT oil itself (i.e., the absence of CD) was also determined. The system was calibrated by measuring the surface tension of Milli-Q water ( $72.00\pm 0.01$  mNm<sup>-1</sup>) prior to study. The experiment was conducted at  $25\pm 1$  °C during study.

#### 4.2. Quantitative analysis of CD

MCT oil/CD complexes i.e.,  $\alpha$ CD,  $\beta$ CD,  $\gamma$ CD and HP $\gamma$ CD obtained from the interfacial tension measurement at the concentration of 1.5% w/v were centrifuged at 10000 rpm for 45 min (Thermo Fisher Scientific Model X3, MA, USA). The supernatant was withdrawn and determined the CD content by HPLC. Quantitative determination of CDs was performed by a reversed-phase HPLC component system from Agilent 1260 Infinity II consisting of Liquid chromatography pump (quaternary pump, G7111A), refractive index detector (G71162B), autosampler (G7129A) with Chem Station software C.01.08. and Phenomenex Luna NH<sub>2</sub> column, 10  $\mu$ m, 250x4.6 mm ID with analytical guard cartridge system KJ10-4282. The HPLC condition was as follows; mobile phase: acetonitrile: water (67:33 v/v); flow rate: 1.2 mL/min; column temperature: 40 °C; injection volume: 20  $\mu$ L; and run time: 12 min. The retention time of  $\alpha$ CD,  $\beta$ CD,  $\gamma$ CD and HP $\gamma$ CD were 6.1 min, 8.2 min, 9.3 min and 9.5 min, respectively.

### **4.3. Morphology of MCT oil/CD inclusion complexes**

The crystalline MCT oil/ $\alpha$ CD and MCT oil/ $\beta$ CD samples (the solid fraction after centrifugation) obtained from the section of 4.1 was subjected to the optical microscopic study and scanning electron microscope (SEM) analysis.

#### **4.3.1. Optical microscopic study**

A drop of the sample was placed on the microscope slide, covered with glass cover slip and then observed under optical microscope (Nikon Eclipse Ts2 inverted microscope, Japan) with the magnification of  $\times 40$ .

#### **4.3.2. SEM study**

Briefly, the samples were placed in each concentration of ethanol i.e., 70% v/v and 95% v/v for three times. After that, the samples were put in absolute ethanol and dried with acetone. The samples were then gold sputter-coated under vacuum. The gold coated sample was then mounted on a SEM sample stub and observed with a SEM (JEOL, JSM IT-300, Japan).

### **4.4. Fourier-transform infra-red (FT-IR) spectroscopy**

The mixture of  $\alpha$ CD (0.75 g) and MCT oil (1 g) was mixed and equilibrated at  $25 \pm 1$  °C under agitation for 24 h. Then, the obtained sample was centrifuged at 10000 rpm for 45 min (Thermo Fisher Scientific Model X3, MA, USA). The supernatant was pipetted off, collected the crystalline pellet, frozen at -80 °C for 2h and then lyophilized for 48 h in a freeze-dryer (Labconco Lyophilizer, MO, USA). The samples i.e., intact  $\alpha$ CD, MCT oil, and then the freeze-dried samples

were measured by using FT-IR spectrometer (Thermo Fisher model Nicolet iS10, USA) using the Attenuated Total Reflectance (ATR) technique. The data were obtained in the range of 400-4000  $\text{cm}^{-1}$ . The analysis was performed at room temperature.

### 5. Proton nuclear magnetic resonance ( $^1\text{H-NMR}$ ) study

The pure compounds of AmB,  $\alpha\text{CD}$ ,  $\gamma\text{CD}$ ,  $\text{HP}\gamma\text{CD}$ , and MCT oil as well as AmB/ $\gamma\text{CD}$ , AmB/ $\text{HP}\gamma\text{CD}$  and MCT oil/ $\alpha\text{CD}$  complexes were dissolved in  $\text{DMSO-}d_6$ , and equilibrated at  $25\pm 1$   $^\circ\text{C}$  for 24 h.  $^1\text{H-NMR}$  measurements were performed by using a 500 MHz  $^1\text{H-NMR}$  spectrometer (BRUKER model AVANCE III HD, USA). The spectrum and chemical shift values were recorded.  $^1\text{H-NMR}$  chemical shifts were referred to DMSO (2.5000 ppm) as internal standard and calculated according to the formula:

$$\Delta\delta^* = (\delta_{\text{complex}} - \delta_{\text{free}}) \quad \text{Eq.4}$$

### 6. Solid-state characterizations of AmB/CD inclusion complexes

#### *Sample preparations*

Aqueous solutions containing 1:1 molar ratio of AmB and  $\gamma\text{CD}$  or  $\text{HP}\gamma\text{CD}$  mixtures were prepared by the heating in the sonicator for 30 min. The samples were equilibrated at  $25\pm 1$   $^\circ\text{C}$  for 7 days under constant agitation. After centrifugation (Thermo Fisher Scientific, Model X3,MA, USA) at 10000 rpm for 45 min, the supernatant was withdrawn, frozen at  $-80$   $^\circ\text{C}$  for 2 h and then lyophilized for 48 h in a freeze-dryer (Labconco Lyophilizer, MO, USA), yielding a solid complex powder

(FD). The obtained FD samples were collected and stored in the desiccator. Identical physical mixtures (PM) were prepared by careful blending of AmB and  $\gamma$ CD or HP $\gamma$ CD with the same molar ratio in a mortar with pestle. The samples were characterized in solid-state as follows: intact, PM and FD of AmB/ $\gamma$ CD and AmB/HP $\gamma$ CD complexes.

### **6.1. FT-IR spectroscopy**

The samples were measured by using FT-IR spectrometer (Thermo Scientific model Nicolet iS10, USA) using the Attenuated Total Reflectance (ATR) technique. The data were obtained in the range of 400–4000  $\text{cm}^{-1}$ . The analysis was performed at room temperature.

### **6.2. Powder X-ray diffraction (PXRD) studies**

The proper amount of sample was placed onto the glass plate containing the rectangular window. After firmly pressing it down by using another piece of a glass plate, any surplus of the sample was removed. The sample was mounted on the sample holder. The PXRD patterns were recorded using Powder X-ray diffractometer (Rigaku model MiniFlex II, Japan) and operated at a voltage of 30 kV and a current of 15 mA. The samples were scanned with the diffraction angle increasing from  $3^\circ$  to  $45^\circ$ ,  $2\theta$  angle, with step-angle of  $0.04^\circ$  and scan speed of  $2^\circ$  per min (113).

### **6.3. Differential scanning calorimetry (DSC)**

DSC thermograms were determined by using differential scanning calorimeter (Mettler Toledo, DSC822 STAR<sup>e</sup> System, Germany). The samples (3-5 mg) were heated ( $10^\circ\text{C}/\text{min}$ ) in sealed

aluminium pans under nitrogen. The temperature range was from 0 to 300 °C. An empty aluminium pan was used as a reference.

## **7. Screening the concentration components for AmB pickering emulsion**

Various concentration of components (i.e., lecithin: 1-5 % w/v, MCT oil: 10-20% w/v and  $\alpha$ CD: 5-10% w/v) were chosen for the development of AmB pickering emulsion.  $\alpha$ CD was dissolved in Milli-Q water and then was added into the MCT oil as the oily phase. Then, the lecithin solution which was preheated at 50 °C for 10 min was added into the oily phase. The resulted mixture was adjusted with Milli-Q water and thoroughly mixed by vortex mixer for 10 min. Finally, the appearance of the resulted emulsion was visually observed and recorded.

## **8. Preparation of pickering NEs and non-pickering NEs**

Firstly, two-third of the amount of AmB was dissolved in the aqueous phase containing  $\gamma$ CD or HP $\gamma$ CD. Lecithin was heated at 50 °C for 10 min. The resulted lecithin and benzalkonium chloride (BAC) were then added and mixed. The rest of AmB was added into another vial with MCT oil and  $\alpha$ -tocopherol as the oily phase. In the case of pickering NEs,  $\alpha$ CD was employed in the oil phase in order to form MCT oil/ $\alpha$ CD complexes. Then, the NEs were prepared by mixing the oil phase into the aqueous phase and the resulted mixture was pre-homogenized with probe sonicator for 3 min to form coarse emulsions. After that, the tonicity of the formulations was adjusted with glycerol. Finally, the obtained coarse emulsions were passed through high pressure homogenizer (Microfluider LM 20, Westwood, MA) at 20000 psi with 20 cycles to obtain AmB NEs.

The composition of pickering NEs and non-pickering NEs containing different AmB concentrations is shown in Table 2.

*Table 2 The composition of pickering NEs and non-pickering NEs containing AmB*

Ingredients	Pickering NEs								Non-pickering NEs			
	F1	F2	F3	F4	F5	F6	F7	F8	F9	F10	F11	F12
AmB	0.075	0.12	0.12	0.18	0.075	0.12	0.12	0.18	0.12	0.18	0.12	0.18
$\gamma$ CD	5	7.5	5	7.5	-	-	-	-	7.5	7.5	-	-
HP $\gamma$ CD	-	-	-	-	5	7.5	5	7.5	-	-	7.5	7.5
$\alpha$ CD	10	7.5	10	7.5	10	7.5	10	7.5	-	-	-	-
MCT	10	10	10	10	10	10	10	10	10	10	10	10
Lecithin	1	1	3	3	1	1	3	3	1	3	1	3
Glycerol	2.25	2.25	1	1	1.5	1.5	1	1	2.5	1.5	2.5	1.5

All AmB NEs contained 0.02% w/v of BAC, 0.01% w/v of  $\alpha$ -tocopherol and adjusted the formulation with Milli-Q water to 100 mL

## 9. Physicochemical and chemical characterizations

### 9.1. pH determination

The pH value of formulations was measured with pH meter (Mettler Toledo, Seven Compact, Germany). The equipment was

calibrated at pH 4, 7 and 11 using standard buffer solutions before measurement. All measurement samples were performed in triplicate.

### **9.2. Osmolality measurement**

The osmolality of formulations was assessed by Osmometer (Gonotec, OSMOMAT 3000 basic, Germany) at room temperature using freezing point depression principle. The instrument was calibrated with 300 mOsmol/kg of standard solution. The sample volume of 50  $\mu$ L was measured as value for osmolality concentration in mOsmol/kg. Each sample was measured in triplicate.

### **9.3. Viscosity measurement**

The viscosity measurement of each formulation was conducted by using the viscometer (Brookfield LVDV-II+, USA) at 25 °C and 34 °C equipped with the thermostat circulating water bath (Grant W28/ZD, England). All measurement samples in triplicate were performed.

### **9.4. Interfacial tension and contact angle measurement**

The measurement of interfacial tension and contact angle were evaluated by using dynamic contact angle meter and tensiometer (DCAT 21, Dataphysics instrument, Germany) equipped with Wilhelmy plate at 25 °C. The machine was calibrated with water before measurement. The data of the interfacial tension and contact angle were expressed as millinewton per meter (mN/m) and degree (°), respectively.

### **9.5. Morphology, particle size and size distribution and zeta potential**

The morphology of the pickering NEs and non-pickering NEs was visualized by using an optical microscope (Nikon Eclipse Ts2 inverted microscope, Japan). A drop of the sample was spread on microscope slide, covered with glass cover slip and then observed under total magnification of  $\times 40$  at room temperature.

The particle size and size distribution, and zeta potential were measured with dynamic light scattering (DLS) technique (Zetasizer™ Nano-ZS with software version 7.11, Malvern, UK) by using quartz glass cuvette. Measurements were carried out at 25 °C, 180 degrees scattering angle. All measurements were determined in triplicate.

### **9.6. Determination of drug content and Entrapment Efficiency (%EE)**

Total AmB content was determined by diluting 100  $\mu$ L of sample with mixture of methanol:water (80:20 v/v), and further diluted to appropriate AmB concentration. Then, the sample was analyzed by HPLC.

For the determination of the percent entrapment efficiency (%EE), the sample was centrifuged (Thermo Fisher Scientific, Model X3, MA, USA) at 25 °C, 10000 rpm for 45 min. The dissolved AmB content in the supernatant was diluted with methanol:water (80:20 v/v) and analyzed by HPLC. All the experiments were done in triplicate. %EE was calculated by using the following equation:



$$\%EE = \frac{(Dt-Ds)}{Dt} \times 100 \quad \text{Eq.5}$$

Where Dt is total drug content and Ds is drug content in supernatant.

## 10. Stability index study

The stability index can provide indirect information to estimate the extent of droplet coalescence in the NEs (59). The formulations (10 mL) were transferred into the cylinder, tightly sealed and then stored at room temperature. The NEs stability index was calculated by taking the ratio between the volume of the NEs at the time of assessment (six weeks) and the total initial volume of the mixture.

$$\text{Stability index (\%)} = \frac{\text{Volume of resulted NEs}}{\text{Total initial volume of NEs}} \times 100 \quad \text{Eq.6}$$

## 11. Degree of AmB aggregation

To access the toxicity of AmB, degree of AmB aggregation was determined by Ultraviolet-Visible (UV-Vis) spectroscopy and circular dichroism.

### 11.1. UV-Vis spectroscopy

Initially, AmB was solubilized in DMSO:methanol (1:999 v/v) to obtain AmB solution. The commercial product, Amphotericin-B<sup>®</sup>, was reconstituted with sterile water for injection. Then, the obtained AmB solution, Amphotericin-B<sup>®</sup> and the selected formulations were further diluted with simulated tear fluid (STF), pH 7.4 to reach AmB concentrations of 20 µg/mL. UV-Vis spectra of AmB preparations were recorded by using UV-Vis spectrophotometer (Model UV-1601, Shimadzu, Japan) within the range of 300 nm to 500 nm. The ratio of the

absorbance at 348 nm (peak I) and the absorbance at 409 nm (peak IV) of AmB was calculated to assess the degree of aggregation of AmB in STF, pH 7.4.

### 11.2. Circular dichroism

To confirm the AmB aggregation, the CD spectra was recorded within the range of 250-450 nm with a Jasco J-810 spectropolarimeter (Japan Spectroscopic, Tokyo, Japan) and expressed as the differential molar absorption dichroic coefficient ( $\Delta\epsilon$ ,  $M^{-1}cm^{-1}$ ). The formulations were diluted as described in the section 11.1 to obtain the final concentration of 20  $\mu g/mL$ . This measurement was investigated at room temperature to evaluate the aggregation state of AmB in different formulations.

## 12. *In vitro* drug release study

The *in vitro* release of Amphotericin-B<sup>®</sup>, AmB pickering NEs and non-pickering NEs through semipermeable membrane (MWCO 12000-14,000 Da) was performed by modified Franz diffusion cell apparatus consisting of donor and receptor compartments (NK Laboratories Co.Ltd., Bangkok, Thailand). These two compartments were separated by the semipermeable membrane. The receptor phase was consisted of 2.0 % w/v  $\gamma$ CD in the phosphate buffer saline, pH 7.4 to allow the sink condition. Prior to perform the experiment, the receptor medium was sonicated to remove dissolved air and the membrane was soaked overnight in the receptor medium. The sample (1.5 mL) of each formulation was placed in the donor phase. The receptor phase was continuously stirred at 150 rpm throughout the experiment and

temperature was controlled at  $34\pm 0.5$  °C by using the thermostat circulating water bath (Grant W28/ZD, England). A 150  $\mu$ L aliquot of the receptor medium was withdrawn at time interval and replaced immediately by an equal volume of fresh receptor medium. The AmB content in the receptor medium was determined by HPLC and the amount of cumulative drug release was calculated. Each formulation was done in triplicate.

### **13. Rheological measurement**

The flow sweep and the oscillation experiments were carried out by using a HAAKE RheoScope Module (RheoStress 600, GmbH, Germany) equipped with parallel plate rheometry at 25 °C. The sample was poured onto the plate and two different gaps were fixed. The flow sweep experiments were measured as follows; the frequency was 1 Hz, the shear rate ranged from 0 to 100  $s^{-1}$ . For the determination of the linear viscoelastic region in the oscillatory study, the oscillation strain sweep experiment was firstly measured. The oscillation strain was ranged from 0.01 to 10 % at the fixed frequency of 1 Hz at room temperature. After that, the frequency sweep was performed at 0-10 Hz at fixed strain 0.05%. The dynamic mechanical spectra were obtained in term of the storage modulus ( $G'$ ) and loss modulus ( $G''$ ) as a function of the frequency.

### **14. Surface morphology of AmB NEs**

#### **14.1. SEM analysis**

The morphology of the AmB pickering NEs and non-pickering NEs was observed by SEM. The samples were dropped onto

the cover slip and placed into the container containing 2% Osmium tetroxide for 1-2 h. Then, the samples were placed into absolute ethanol three times, each time was 5 min. The samples were dried with the critical point dryer (Leica model EM CPD 300, Australia). Finally, the samples were coated with gold by sputter coater (Bazlers model SCD 040, Germany) and examined under SEM (JEOL, JSM-IT500, Japan).

#### **14.2. Atomic force microscopy (AFM) study**

Morphology of AmB pickering NEs was investigated by AFM equipped with a Navi controller (SPA-400) Seiko Instruments Inc (SII) operating in non-contact mode. The scanning area in all samples was 5  $\mu\text{m}^2$ . The image correction was applied by flattening during image analysis (Spisel 32). Briefly, several drops of diluted sample solutions were dropped onto freshly pre-cleaned cover glass, and then the samples were dried and stored at ambient temperature before imaging (114).

#### **15. *In vitro* hemolytic study**

Sheep blood was collected and centrifuged for 10 min at 3000 rpm. Then, supernatant was pipetted off. Red blood cells (RBCs) was washed 3 times and resuspended with PBS, pH 7.4 to yield the initial volume. After proper dilution, RBCs were determined by counting with hemocytometer. The commercial product (Amphotericin-B<sup>®</sup>) and selected AmB formulations were added to the suspended RBCs. Then, the obtained suspensions were diluted with PBS to give the final concentrations in the range of 1-100  $\mu\text{g}/\text{mL}$ . The resulted samples were incubated in the shaking incubator (Shaking incubator, N-Biotek NB2015, Korea) at 100 rpm, 37 °C for 30 min and then placed in ice bath

to stop hemolysis. The unlyzed RBCs were removed by centrifugation (Thermo Fisher Scientific, Model X3, MA, USA) at 3000 rpm for 5 min. Then the supernatant was transferred into 96 well-plate and hemoglobin was analyzed by microplate reader (Multilabel plate reader, Perkin Elmer VICTOR 3™) at 576 nm (115). The percentage of hemolyzed RBC was determined by the following equation.

$$\% \text{ Hemolysis} = 100 \times \frac{(\text{Abs} - \text{Abs}_0)}{(\text{Abs}_{100} - \text{Abs}_0)} \quad \text{Eq. 7}$$

Where Abs, Abs<sub>0</sub> and Abs<sub>100</sub> are the absorbances for the sample, control without AmB in PBS and control of distilled water, respectively.

### 16. *In vitro* antifungal activity

The methods for antifungal susceptibility testing was modified according to the National Committee on Clinical Laboratory Standards (NCCLS). Three isolates fungal organisms i.e. *Candida albicans*, *Aspergillus flavus* and *Fusarium solani* were tested by broth microdilution assay. Briefly, the isolated organisms were subcultured onto sabouraud dextrose agar (SDA) slants and stored as suspensions at 2-8 °C. The suspensions of tested organisms were diluted with 0.85% saline to the density of 1x10<sup>6</sup> - 5x10<sup>6</sup> cells/mL. The tests were conducted in 96-well culture plates. Each well was inoculated with 50 µL of two-fold dilution inoculum suspension. An aliquot of 50 µL of test samples was placed in separate wells in triplicate after appropriate dilution with distilled water. DMSO and the AmB-free medium were included as a growth control. The plates were incubated at 35 °C for 24 h *Candida albicans* and for 96-120 h *Aspergillus flavus* and *Fusarium solani*. Minimum inhibitory concentrations (MICs) was read and defined as the

lowest AmB concentration at which no growth could be observed. After MIC readings, 10  $\mu$ L aliquots was removed from each growth-negative well and was spread on SDA petri dishes. The plates were incubated in 35 °C, and the fungal colonies grown was counted after 2 days and approximately 4-7 days of incubation for yeast and filamentous fungi, respectively. The minimum fungicidal concentrations (MFCs) was defined as the lowest drug concentration from which no colonies were visible on the agar plate.

## **17. Physical and chemical stability studies of AmB NEs**

### **17.1. Freeze-Thaw stability study**

Each freeze-thaw cycle was consisted of a freezing phase and a thawing phase (116). In the freezing process, the selected AmB NEs in flat bottomed glass vials were isothermally stored in a freezer for 24 h at -20 °C. Then, the frozen samples were transferred to an oven with a temperature set at 30 °C for 6 h allowing all the frozen oil and aqueous phases were completely thawed. The freeze-thawed samples were continued for determination of three cycles of freeze-thaw treatment. Between each cycle, the freeze-thawed samples were characterized in term of pH, particle size and size distribution and the zeta potential. The physical instability i.e. flocculation, coalescence, creaming and phase separation were evaluated under visual observation and AmB NEs droplet appearance was also observed under the optical microscope (Nikon Eclipse Ts2 inverted microscope, Japan).

### 17.2. The stability study

The stability of the final AmB formulations was evaluated following ICH guidelines (117). The NEs were stored in the tightly closed glass vials at long-term ( $30\pm 2$  °C,  $75 \pm 5\%$  RH) and accelerated ( $40\pm 2$  °C,  $75 \pm 5\%$  RH) conditions. The samples were withdrawn and analyzed at time interval of 0, 1, 3 and 6 months. The samples were subjected to determine pH, particle size, size distribution, zeta potential and the drug content and %EE.

### 18. Statistical analysis

All quantitative data was presented as means  $\pm$  standard deviation (S.D.). Data was statistically calculated using a Student's *t* test or one-way ANOVA with Tukey test. The *p*-value,  $p < 0.05$  was considered as statistical significance.

## CHAPTER IV

### RESULTS AND DISCUSSION

#### 1. Phase-solubility study

AmB is very poor water-soluble compound and its aqueous solubility is less than 1mg/L (118). CDs can increase the solubility of hydrophobic compounds via the formation of inclusion complexes. The phase-solubility diagrams of AmB with  $\alpha$ CD,  $\beta$ CD,  $\gamma$ CD or HP $\gamma$ CD aqueous solutions are shown in Figure 7. In case of  $\alpha$ CD and  $\beta$ CD, there were slightly increased in the solubility of AmB. This result was in accordance with the previous report (119). The solubility of AmB increased with increasing concentrations of  $\gamma$ CD and HP $\gamma$ CD and showed the positive deviation from linearity that represented as A<sub>P</sub>-type profile. It indicated that the formation of higher order water-soluble complexes i.e. 1:2 AmB/CD complexes were obtained at high concentrations of  $\gamma$ CD and HP $\gamma$ CD (120). It is well-known that low molecular weight compounds or compounds with aliphatic chain and aromatic compounds can form the inclusion complexes with  $\alpha$ CD and  $\beta$ CD, respectively. In contrast, the cavity of  $\gamma$ CD may fit in with larger macromolecules (121). Since AmB is a large molecule, it may not fit with the small cavities of  $\alpha$ CD and  $\beta$ CD. The literature revealed that the increase in solubility of AmB in the presence of  $\gamma$ CD and HP $\gamma$ CD was mainly due to the hydrophobic part of the AmB favor to the relatively hydrophobic cavity of CD and by the formation of water-soluble drug/CD inclusion complexes (119). Table 3 shows the stability constant ( $K_{1:1}$  and  $K_{1:2}$ ) and CE values of AmB/CD complexes in pure aqueous CD solutions. The stability constant value ( $K_{1:1}$ ) can be used to compare the affinity of drugs



for different CDs or CDs derivatives. The CE values can be used to compare the solubilization effect of various CDs on the drug (112). The CD ranking regarded with  $K_{1:1}$  and CE values are as follow  $\gamma\text{CD} > \text{HP}\gamma\text{CD} > \alpha\text{CD} \sim \beta\text{CD}$ . This result indicated that AmB has the highest affinity to  $\gamma\text{CD}$  with the CE increment of 70 and 35 times to  $\beta\text{CD}$  and  $\alpha\text{CD}$ , respectively. According to the previous study, the  $K_{1:1}$  values of AmB/ $\gamma\text{CD}$  and AmB/HP $\gamma\text{CD}$  had been reported were lower than that of presently obtained data (120). This might be due to the presence of 0.02% w/v of benzalkonium chloride in the complexation medium could compete the affinity of CD to the inclusion complex formation. Owing to the stability constant and CE values,  $\gamma\text{CD}$  and HP $\gamma\text{CD}$  were selected to further studies.

## 2. Solubility determination of AmB in oils and surfactants

The solubility of AmB in various oils and surfactants is shown in Figure 8. The oils and surfactants that used in this study were selected based on the criteria that can be used for the ophthalmic preparations. The solubility of AmB was highest in MCT oil, followed by castor oil, oleic acid, olive oil, isopropyl myristate and miglyol. Due to that MCT oil mainly composed of a short chain length (C8-C10) of fatty acid, it showed the highest solubilizing capacity. Mostly MCTs showed the superior to drug solubilization than LCTs (122-125). It was also observed that the solubility of paclitaxel increased with the decreasing the chain length of fatty acid (126). Moreover, the solubilizing ability decrease with the increasing the degree of unsaturation (127). MCT oil composed of with three saturated free fatty acid but the other tested oils composed of unsaturated fatty acid. In case of LCTs, castor oil showed higher

solubilization efficiency of AmB than the other two LCTs. This is possible due to the presence of hydroxyl group on the alkyl side chain of the castor oil, this hydroxyl group may form the hydrogen bonding with AmB and resulted in increased solubility. From this study, we have found and concluded that the chain length and degree of unsaturation of the oils had the significantly influenced on the AmB solubilizing capacity.

Amphoteric surfactants and non-ionic surfactants are widely used in ophthalmic preparations because of their compatibility and lower toxicity than ionic surfactants (128). Lecithin displayed the significantly higher solubility of AmB than other tested surfactants. It plays the role of solubilization of AmB, amphiphilic drug by the formation of micellar dispersions (129). Poloxamer, block copolymer, is also formed polymeric micelles with AmB but the solubilization capacity of AmB was lower than that of lecithin. This might be due to the additional effect of charge-charge interaction on the AmB solubilization. The presence of cationic and anionic charge in lecithin provided the strong electrostatic interaction with the amphoteric ion pair of AmB resulted in enhanced AmB solubility (130). For the non-ionic surfactants (i.e., labrasol and tween 80), there was a little interaction of their hydrophobic head groups with AmB consequently lower extent of solubilization of AmB. Regarding to the screening of oils and surfactants for AmB solubility determination, MCT oil and lecithin were selected to further studies.

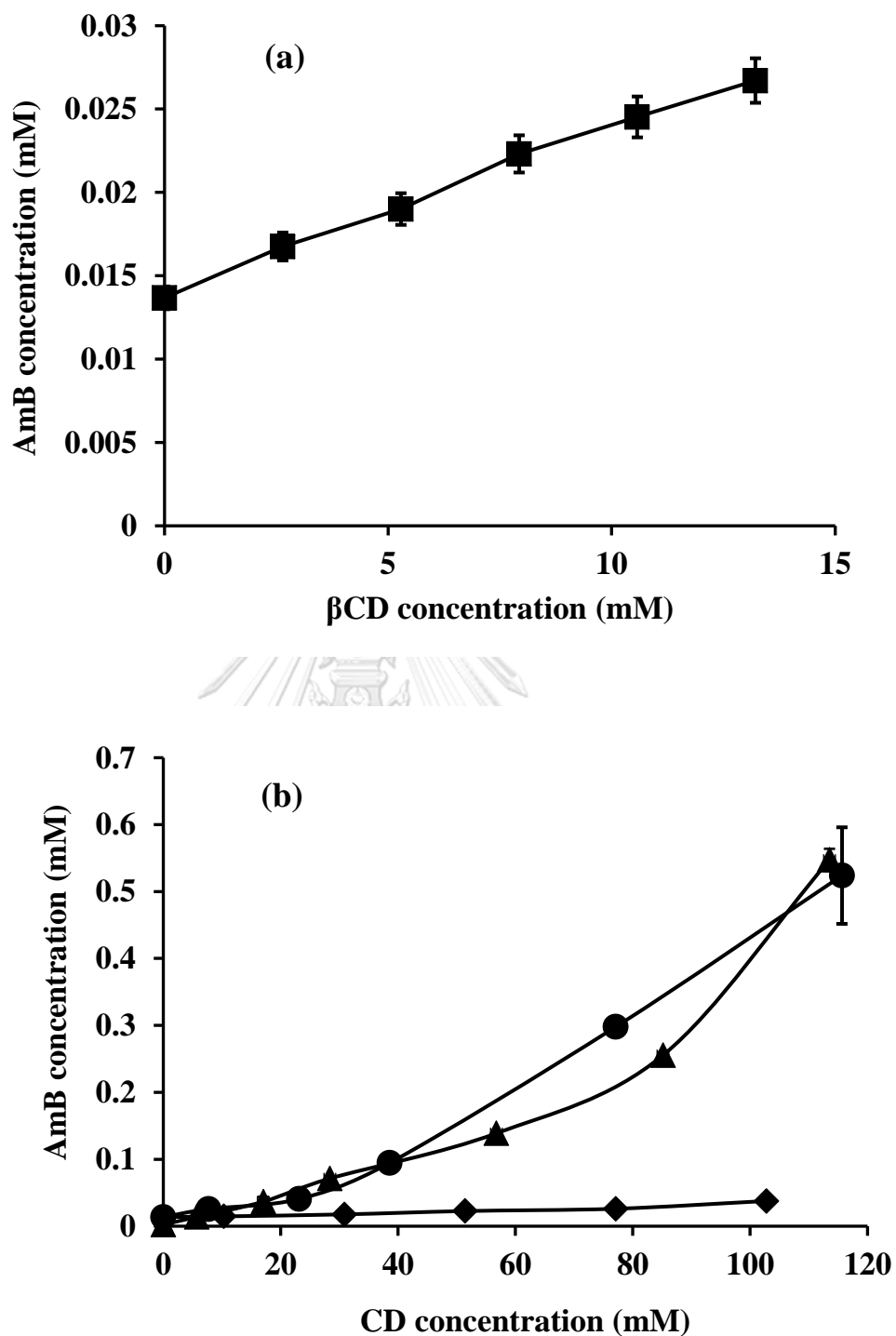
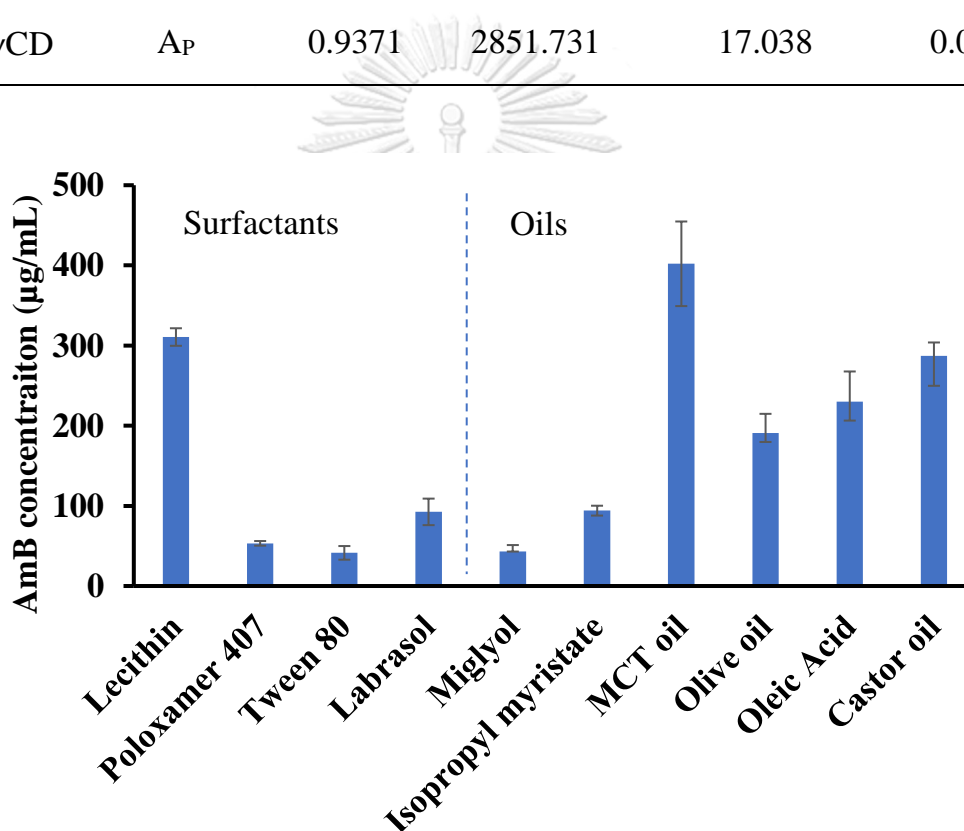


Figure 7 Phase-solubility profiles of AmB in aqueous CD solutions. (a)  $\beta$ CD ( $\blacksquare$ ), (b)  $\alpha$ CD ( $\blacklozenge$ ),  $\gamma$ CD ( $\bullet$ ) and HP $\gamma$ CD ( $\blacktriangle$ )

*Table 3 Apparent stability constant values ( $K_{1:1}$  and  $K_{1:2}$ ) and the complexation efficiency (CE) of AmB/CD complexes in pure aqueous CD solutions at  $25 \pm 1$  °C*

Cyclodextrin	Type	R <sup>2</sup>	K <sub>1:1</sub> (M <sup>-1</sup> )	K <sub>1:2</sub> (M <sup>-1</sup> )	CE
αCD	A <sub>L</sub>	0.9840	145.951	-	0.002
βCD	A <sub>L</sub>	0.9955	72.048	-	0.001
γCD	A <sub>P</sub>	0.9619	4972.248	14.118	0.069
HPγCD	A <sub>P</sub>	0.9371	2851.731	17.038	0.039



*Figure 8 Solubility of AmB in various oils and surfactants*

### 3. Characterization of MCT oil/CD inclusion complexes

#### 3.1. Interfacial tension measurement

It is well-known that CDs have the surface activity by forming the inclusion complexes with oil and adsorbing at oil-water

interface (52). Figure 9 shows the relationship between the interfacial tension of MCT oil/water and CD concentrations. It was observed that the presence of CDs in the aqueous phase caused the reduction of the interfacial tension of MCT oil. This observation indicated that the surface active MCT oil/CD complexes were formed at o/w interface. The interfacial tension was decreased with the increasing of CD concentrations. At the same CD concentration, the ranking order of decreasing the surface tension was  $\alpha\text{CD} > \beta\text{CD} > \gamma\text{CD} \sim \text{HP}\gamma\text{CD}$ . It is believed that MCT oil, composed of aliphatic side chain, mostly accommodated with the cavity of  $\alpha\text{CD}$ . The more MCT oil/ $\alpha\text{CD}$  inclusion complexes were formed at the oil-water interface, the more reduction of interfacial tension was observed. Manthapa et al. (2013) reported that oil-water interfacial tension at the tetradecane/water interface was lower in the presence of  $\alpha\text{CD}$  compared to that of  $\beta\text{CD}$  (60). The similar observations was confirmed by the investigation of Shimada et al. (1992) (61). However, our data showed insignificantly different between two those CDs for lowering o/w interfacial tension.

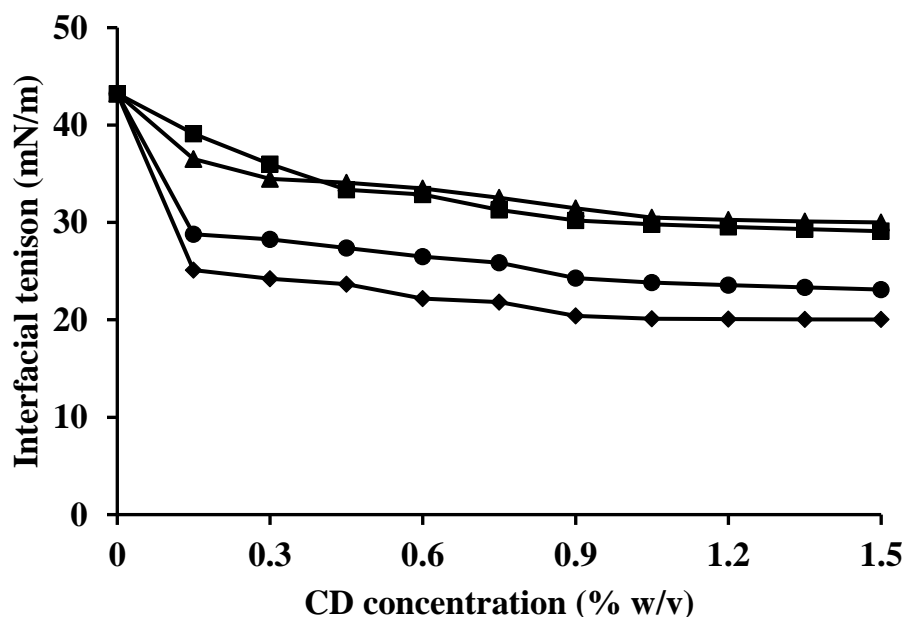


Figure 9 Interfacial tension at MCT oil/water interface as a function of CD concentrations;  $\alpha$ CD (♦),  $\beta$ CD (●),  $\gamma$ CD (■) and HP $\gamma$ CD (▲)

### 3.2. Quantitative analysis of CD

Figure 10 shows the observed concentration of CD in aqueous solutions containing MCT oil. In case of  $\gamma$ CD and HP $\gamma$ CD, the observed amount of dissolved CD was slightly lower than the theoretical concentrations (1.5% w/v). This indicated that most of the CD molecules were existed as dissolved CD and less precipitated solid MCT oil/ $\gamma$ CD or MCT oil/HP $\gamma$ CD complexes were formed. Interestingly, the observed concentration of dissolved CD was shown about a half and one-third fractions for  $\beta$ CD and  $\alpha$ CD, respectively when compared with the theoretical concentration. On the other hand, approximately 50% of  $\beta$ CD and 66% of  $\alpha$ CD content was presumably formed solid MCT oil/CD complexes which were markedly precipitated. To further evaluation of these two complexes formation (i.e., MCT oil/ $\alpha$ CD and MCT oil/ $\beta$ CD),

the morphology studies were performed by optical microscopic and SEM studies.

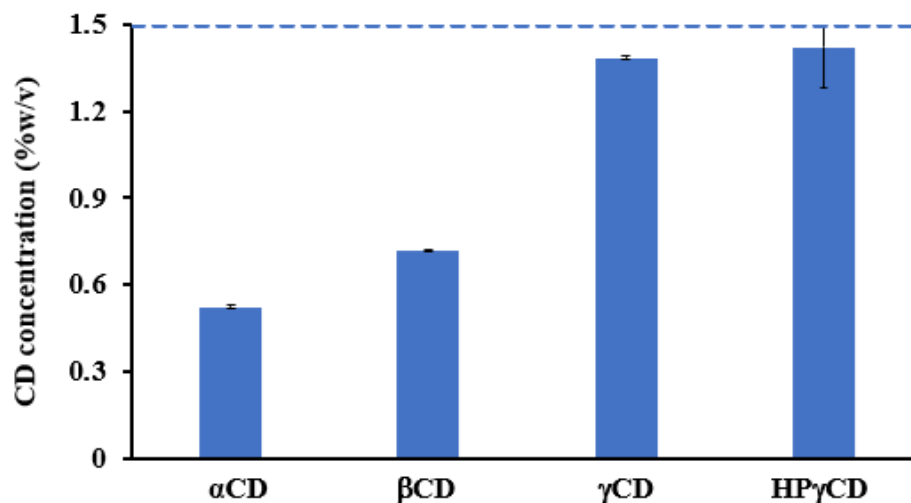


Figure 10 Observed concentration of dissolved CD from the mixture of MCT oil and CD (1.5% w/v) (column) versus the theoretical value (dotted line)

### 3.3. Morphology of MCT oil/CD inclusion complexes

#### 3.3.1. Optical microscope study

The optical micrographs of MCT oil/ $\alpha$ CD and MCT oil/ $\beta$ CD complexes are displayed in Figure 11. The micrograph of MCT oil/ $\alpha$ CD complexes showed that the droplet was covered by the denser and thicker layer of particles than that of MCT oil/ $\beta$ CD complexes (Figures 11a and 11b, respectively). Also, the large number of solid  $\alpha$ CD were continuous surrounded on the oil droplets. It was supported data that  $\alpha$ CD formed more solid complexes with MCT oil than that of  $\beta$ CD.

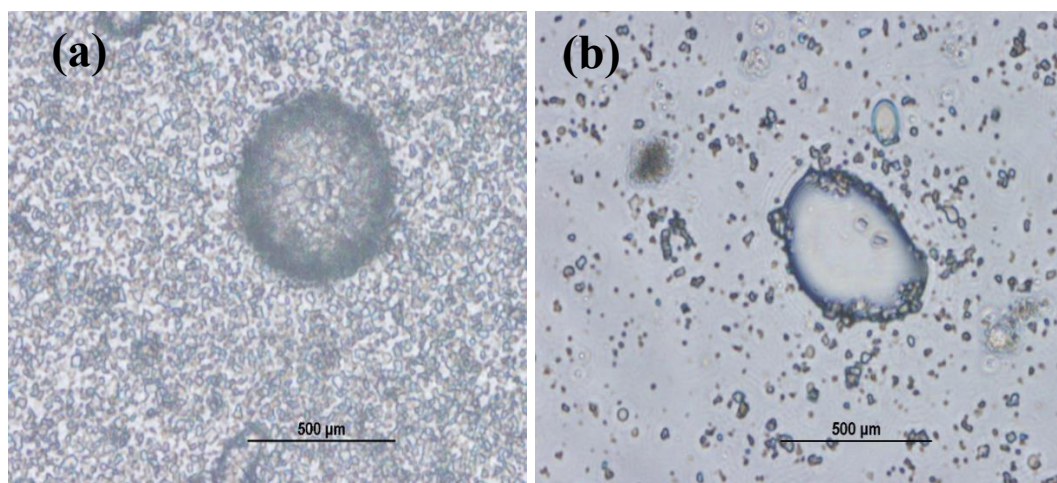


Figure 11 Optical micrographs of MCT oil/ $\alpha$ CD (a) and MCT oil/ $\beta$ CD complexes (b)

### 3.3.2. SEM study

Figure 12 exhibits the SEM images of MCT oil/ $\alpha$ CD and MCT oil/ $\beta$ CD complexes. The microcrystals of MCT oil/ $\alpha$ CD were dominantly in the spherical shape with particle size 0.5-2  $\mu$ m whereas rectangle-like microcrystals were found in MCT oil/ $\beta$ CD complexes with the larger particle size (up to 5  $\mu$ m). The larger amounts of microcrystals were observed in the MCT oil/ $\alpha$ CD than MCT oil/ $\beta$ CD complexes and it emphasized that more MCT oil/ $\alpha$ CD inclusion complexes were formed. These images could provide the supportive data for interfacial tension measurement. The more MCT oil/ $\alpha$ CD microcrystals were obtained, the more interfacial tension was reduced. The literature also revealed that more microcrystals were detected in the tetradecane/ $\alpha$ CD inclusion complexes than that of  $\beta$ CD complexes (60). Nevertheless, the findings of their morphological structure differed from our study. This was possible due to the different sample preparation by using ethanol and



acetone led to the dehydration of the sample which affected the morphological shape of the inclusion complexes (131).

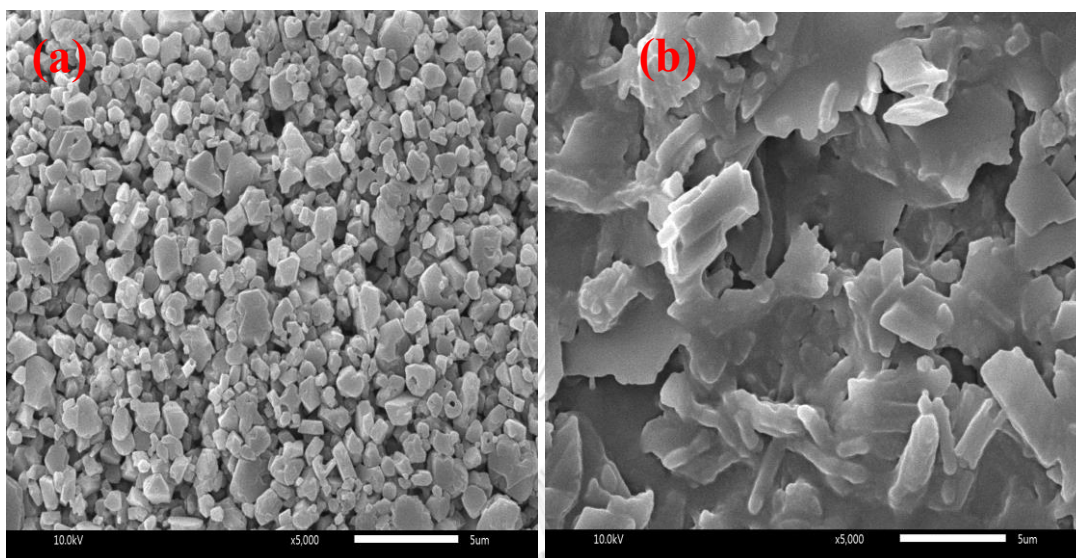


*Figure 12 SEM images of MCT oil/ $\alpha$ CD (a) and MCT oil/ $\beta$ CD complexes (b) at the magnification of x5000*

### 3.4. FT-IR spectroscopy

FT-IR method is useful for analysis and identification of the compounds by the vibrational and rotational transitions of the molecules. The important information related with the inclusion complexes formation can be obtained by the changes in the IR absorption peaks of the compounds.

The most predominant features of MCT oil were C-H stretching vibration at  $2856\text{ cm}^{-1}$ ,  $2925\text{ cm}^{-1}$  and  $2955\text{ cm}^{-1}$ . Moreover, the further distinct peaks were C=O stretching in esters at  $1741\text{ cm}^{-1}$ ,  $\text{CH}_2$  bending at  $1458\text{ cm}^{-1}$  and C-O ester linkage vibration at the region of  $1090\text{--}1120\text{ cm}^{-1}$  (Figure 13a) (132).  $\alpha$ CD was characterized by a large band at  $3312\text{ cm}^{-1}$  due to O-H stretching, the cyclic ether group was

identified by the C-O-C stretching at  $1153\text{ cm}^{-1}$  and A sharp band peak was observed at  $1023\text{ cm}^{-1}$  due to the -OH bending vibration (Figure 13b) (133). Changes in the FT-IR spectra were observed in the FD sample.  $\text{CH}_2$  bending and C-O-C stretching of MCT oil were disappeared and lowering of C-H stretching of MCT oil was observed in the FD sample (Figure 13c). It was suggested that there was the presence of some interactions between MCT oil and  $\alpha\text{CD}$  and/or the moiety of MCT oil molecules were included into the  $\alpha\text{CD}$  cavities. In addition, there was also found that the band peak around  $3312\text{ cm}^{-1}$  which was attributed to primary and secondary OH groups of  $\alpha\text{CD}$  was shifted to a higher frequency ( $3360\text{ cm}^{-1}$ ) in the solid MCT oil/ $\alpha\text{CD}$  complexes. It was probably due to the presence of strong hydrogen bonding. Rakmai et al. (2018) investigated FT-IR studies of black pepper oil and  $\text{HP}\beta\text{CD}$  and concluded that all bands of black pepper oil spectrum were totally masked through inclusion complex (134).

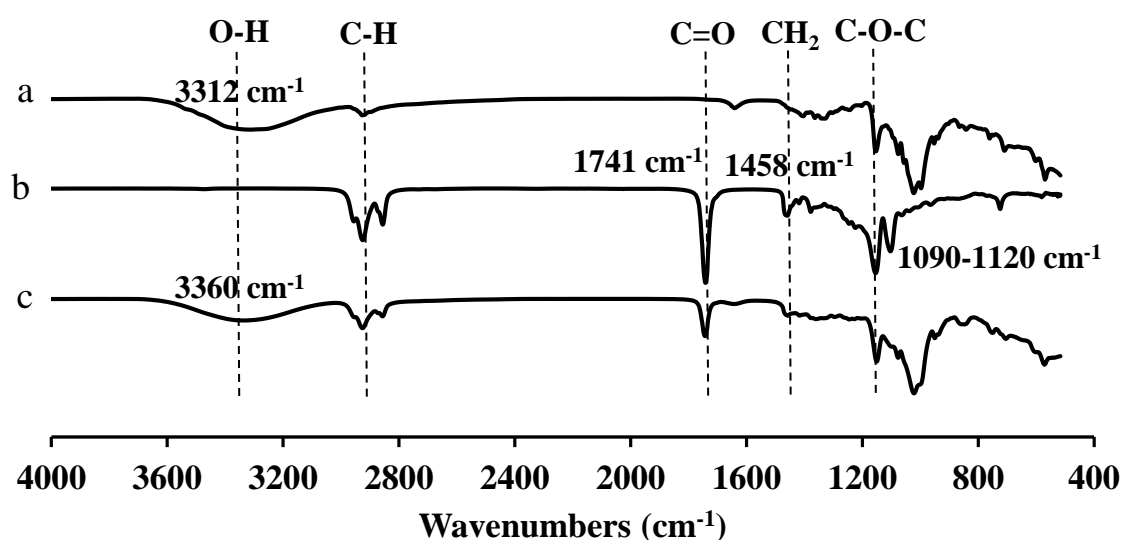


Figure 13 FT-IR spectra of pure  $\alpha\text{CD}$  (a), pure MCT (b) and FD MCT/ $\alpha\text{CD}$  (c)

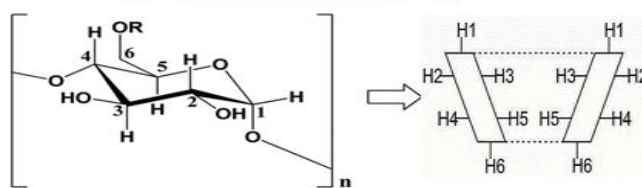
#### 4. $^1\text{H}$ -NMR determination

The information obtained from  $^1\text{H}$ -NMR spectroscopy could be used to establish the inclusion complex modes of guest molecule into CD cavity. The  $^1\text{H}$  chemical shifts of free  $\alpha\text{CD}$  and complex of MCT oil/ $\alpha\text{CD}$  are shown in Table 4. It is well-known that H-3 and H-5 protons of CD are located in the inner cavity of CDs and prominent chemical shifts of H-3 and H-5 are important for the possible complex formation between drug and CD (96). The upfield shift of H-3 and H-5 of  $\alpha\text{CD}$  were -0.004 and -0.013, respectively. The upfield shift of H-5 was moderately higher than that of H-3, it might be suggested that MCT oils preferentially included at the narrow sided of  $\alpha\text{CD}$ . These observed shifts may be due to the insertion of fatty acid of MCT oil into the  $\alpha\text{CD}$  cavity by the hydrophobic interaction (135, 136).

The  $^1\text{H}$  chemical shift of AmB/ $\gamma\text{CD}$  and AmB/HP $\gamma\text{CD}$  complexes are summarized in Tables 5 and 6, respectively. For AmB/ $\gamma\text{CD}$  complexes, the upfield shifts of H-3 and H-5 in  $\gamma\text{CD}$  cavity were -0.003 ppm and -0.048 ppm, respectively. In case of AmB/HP $\gamma\text{CD}$  complexes, the downfield shift of H-3 was +0.040 ppm and upfield shift of H-5 was -0.002 ppm. From the results,  $\Delta\delta^*$  value of H-5 proton is larger than that of H-3 proton in AmB/ $\gamma\text{CD}$  complexes, which indicated that the drug molecule was deeply inserted at the narrow rim of the hydrophobic  $\gamma\text{CD}$  cavity. Conversely, AmB molecule was partially inserted at the wide edge of HP $\gamma\text{CD}$  cavity due to the larger of  $\Delta\delta^*$  value of H-3 proton.

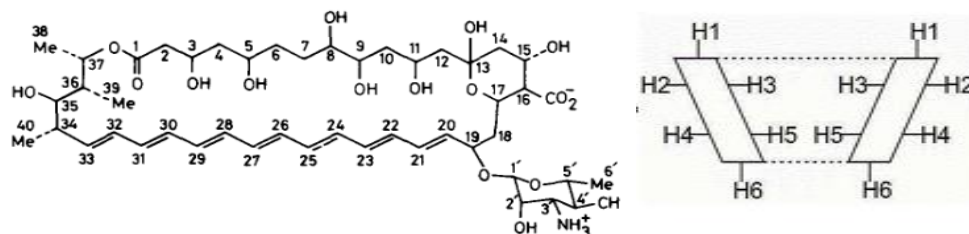
Regarding to  $\Delta\delta^*$  of H-3, H-11, H-19 and H-37 protons of AmB, the significant chemical shifts were observed in both AmB/ $\gamma$ CD and AmB/HP $\gamma$ CD complexes. In addition,  $\Delta\delta^*$  of H-1', H-11, H-17 and H-19 of protons of AmB in AmB/ $\gamma$ CD was significantly shifted. In most cases, the higher chemical shifted of those specified proton values were found in AmB/ $\gamma$ CD complexes. It demonstrated that  $\gamma$ CD has more affinity to AmB molecules than that of HP $\gamma$ CD. This data was supported the strong binding constant of AmB in aqueous solution containing  $\gamma$ CD (Table 3). The significantly chemical shifted of protons are at mycosamine ring and hydrophilic stretch of AmB. It corresponded to the obtained data from phase-solubility profiles that AmB/ $\gamma$ CD and AmB/HP $\gamma$ CD displayed Ap-type diagrams (i.e., stoichiometry 1:1 and 1:2 inclusion complexes).

Table 4 The  $^1\text{H}$ -chemical shifts associated with different hydrogen atoms of free form of the  $\alpha$ CD and of the formed IC (MCT oil/ $\alpha$ CD)



$\alpha$ CD, n=6, R=H

$^1\text{H}$	$\delta_{\text{free}}$	$\delta_{\text{complex}}$	$\Delta\delta^* = (\delta_{\text{complex}} - \delta_{\text{free}})$
<i><math>\alpha</math>CD</i>			
H-1	4.784	4.785	+0.001
H-2	3.374	3.375	+0.001
H-3	3.760	3.756	-0.004
H-4	3.277	3.277	0
H-5	3.585	3.572	-0.013
H-6	3.634	3.634	0

Table 5 The  $^1\text{H}$ -chemical shifts of AmB alone and in the presence of  $\gamma\text{CD}$ 

Amphotericin-B

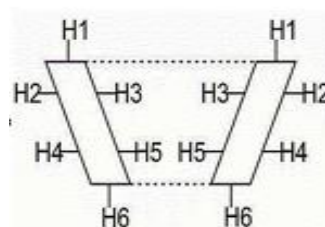
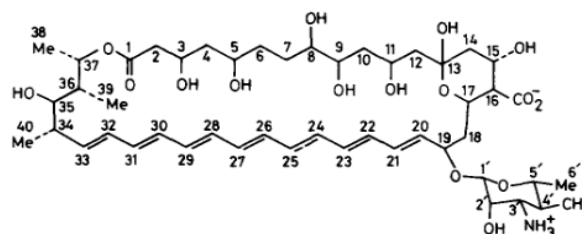
Cyclodextrin

 $\gamma\text{CD}$ , n=8, R=H

$^1\text{H}$	$\delta_{\text{free}}$	$\delta_{\text{complex}}$	$\Delta\delta^* = (\delta_{\text{complex}} - \delta_{\text{free}})$
<i>AmB</i>			
H-32	6.150	6.141	-0.009
H-21	6.083	6.078	-0.005
H-33	5.425	5.421	-0.004
H-37	5.202	5.191	-0.011
H-1'	4.453	4.465	+0.012
H-19	4.391	4.406	+0.015
H-11	4.218	4.191	-0.027
H-17	4.049	4.037	-0.012
H-3	3.986	3.968	-0.018
H-34	2.269	2.264	-0.005
18b	2.162	2.155	-0.007
2b	2.150	2.144	-0.006
6'	1.164	1.162	-0.002
14a	1.092	1.088	-0.004
CH <sub>3</sub> -38	1.105	1.100	-0.005
CH <sub>3</sub> -40	1.026	1.022	-0.004
CH <sub>3</sub> -39	0.902	0.898	-0.004
<i><math>\gamma\text{CD}</math></i>			
H-1	4.872	4.870	-0.002
H-2	3.355	<sub>a</sub>	<sub>a</sub>
H-3	3.611	3.608	-0.003
H-4	3.509	<sub>a</sub>	<sub>a</sub>
H-5	3.566	3.518	-0.048
H-6	3.584	3.574	-0.01

<sup>a</sup>overlapping of chemical shifts

Table 6 The  $^1\text{H}$ -chemical shifts of AmB alone and in the presence of HP $\gamma$ CD



Amphotericin-B

Cyclodextrin

HP $\gamma$ CD, n=8, R=CH<sub>2</sub>(CHOH)CH<sub>3</sub>

$^1\text{H}$	$\delta_{\text{free}}$	$\delta_{\text{complex}}$	$\Delta\delta^* = (\delta_{\text{complex}} - \delta_{\text{free}})$
<i>AmB</i>			
H-32	6.150	6.147	-0.003
H-21	6.083	6.080	-0.003
H-33	5.425	5.422	-0.003
H-37	5.202	5.182	-0.020
H-1'	4.453	4.455	+0.002
H-19	4.391	4.401	+0.010
H-11	4.218	4.225	+0.007
H-17	4.049	4.047	-0.002
H-3	3.986	3.965	-0.021
H-34	2.269	2.267	-0.002
18b	2.162	2.159	-0.003
2b	2.150	2.147	-0.003
6'	1.164	1.162	-0.002
14a	1.092	1.090	-0.002
CH <sub>3</sub> -38	1.105	1.102	-0.003
CH <sub>3</sub> -40	1.026	- <sup>a</sup>	- <sup>a</sup>
CH <sub>3</sub> -39	0.902	0.901	-0.001
<i>HP<math>\gamma</math>CD</i>			
H-1	4.868	4.867	-0.001
H-2	3.523	3.522	-0.001
H-3	4.531	4.571	+0.040
H-4	3.231	- <sup>a</sup>	- <sup>a</sup>
H-5	3.617	3.619	-0.002
H-6	3.742	3.741	-0.001

<sup>a</sup>overlapping of chemical shifts

## 5. Solid-state characterizations of AmB/CD complexes

### 5.1. FT-IR spectroscopy

Figure 14 displays the FT-IR spectra of pure AmB,  $\gamma$ CD, HP $\gamma$ CD, their PM and FD samples. The typical absorption bands of AmB showed a sharp C=O stretching vibration at  $1691\text{ cm}^{-1}$  and C=C stretching band at  $1556\text{ cm}^{-1}$  and O-H stretching at  $3366\text{ cm}^{-1}$  (Figure 14a). In addition, it was also observed that C-H banding and stretching regions of AmB at  $2916\text{ cm}^{-1}$  and C-O-C stretching at  $1368\text{ cm}^{-1}$ . These IR characteristic peaks were in accordance with the previous reports (137-141).  $\gamma$ CD and HP $\gamma$ CD were characterized by broad absorption band at  $3281\text{ cm}^{-1}$  and  $3343\text{ cm}^{-1}$ , respectively due to symmetric and asymmetric O-H stretching and C-H stretching mode at  $2926\text{ cm}^{-1}$  and  $2927\text{ cm}^{-1}$ , respectively (Figures 14b and 14c) (142). The FT-IR spectra of AmB in PM sample showed that C=C and C=O stretching bands of AmB were remained in PM AmB/ $\gamma$ CD whereas these two peaks were slightly masked in PM AmB/HP $\gamma$ CD (Figures 14d and 14e). In addition, the lowering of the C-O-C bands at  $1368\text{ cm}^{-1}$  was observed in both PM samples (139). These observations indicated that there was less interaction between AmB and CD in the PM samples. For the FD samples, two specific peaks of AmB at C=O and C=C stretching bands were disappeared. Likewise, the C-O-C bands of AmB were also disappeared in both FD samples (Figures 14f and 14g). These results possible suggested that there was some interaction of functional groups of AmB (C=C and C=O) and the functional groups of CDs during inclusion complex formation. These findings were consistent with the study of Kim

et al. (2010) and Ruiz et al. (2014) in which they reported that FT-IR spectra of the characteristic peaks of AmB were disappeared in the FD samples (137, 139).

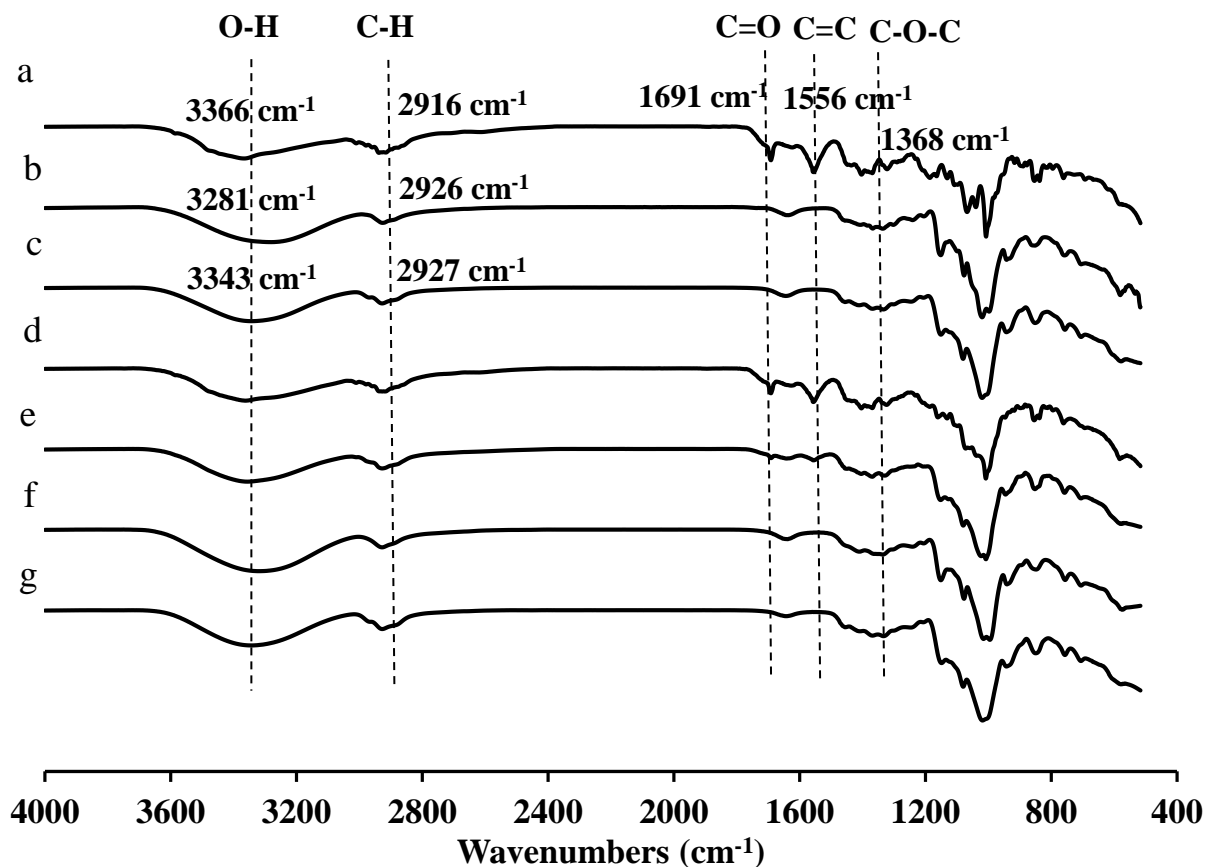


Figure 14 FT-IR spectra of pure AmB (a), pure  $\gamma$ CD (b), pure HP $\gamma$ CD (c), PM AmB/ $\gamma$ CD (d), PM AmB/HP $\gamma$ CD (e), FD AmB/ $\gamma$ CD (f) and FD AmB/HP $\gamma$ CD (g)

## 5.2. PXRD analysis

PXRD is a useful method for the detection of CD complexation of compound in the powder or crystalline states (143). Figure 15 shows the PXRD patterns of intact AmB,  $\gamma$ CD, HP $\gamma$ CD, their PM and FD samples. The diffractogram of AmB displayed the sharp



intense peak at 9.7, 12.32, 13.5, 14.2, 15.8, 18.0, 19.1, 21.6, 23.7 and 27.3° which representing the crystallinity of the drug (Figure 15a) (144). The  $\gamma$ CD represented the crystalline characteristic peaks at 5.1, 6.1, 9.4, 10.2, 11.1, 12.3, 13.8, 15.3, 16.4, 17.7, 18.7, 19.8, 20.4, 21.7, 22.8, 24.6 and 25.3° (Figure 15b) (145). For HP $\gamma$ CD, it presented the halo pattern and did not show any sharp peak (Figure 15c) (146). The distinct peaks of AmB were detectable in PM samples of both AmB/ $\gamma$ CD and AmB/HP $\gamma$ CD complexes (Figures 15d and 15e). This indicated that there was no interaction between AmB and respective CDs. In case of FD samples, the intense peaks of AmB were completely disappeared and showed the broad pattern (Figures 15f and 15g). This finding indicated that crystalline nature of AmB was converted into the amorphous form which possible due to the formation of inclusion complex between the components. Kim. et al. (2010) reported that the disappearance of the distinct peaks; in other word, the halo pattern of AmB represented to the inclusion complex formation of AmB/HP $\gamma$ CD (137).

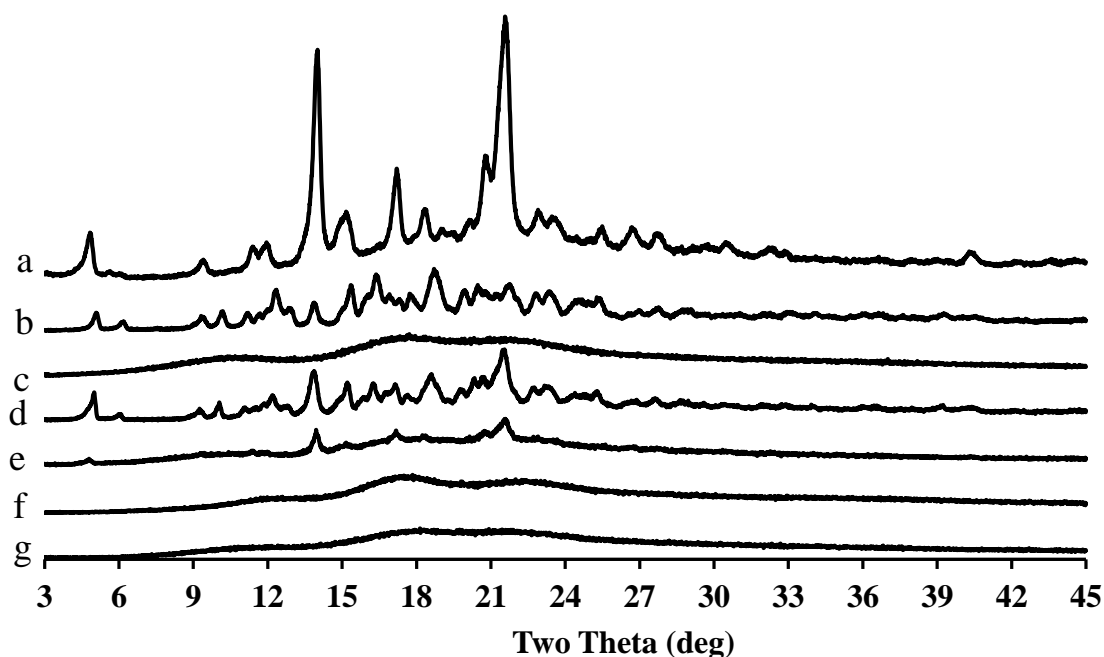


Figure 15 The PXRD spectra of pure AmB (a), pure  $\gamma$ CD (b), pure HP $\gamma$ CD (c), PM AmB/ $\gamma$ CD (d), PM AmB/HP $\gamma$ CD (e), FD AmB/ $\gamma$ CD (f) and FD AmB/HP $\gamma$ CD (g)

### 5.3. DSC analysis

The formation of CD complexation can be confirmed with DSC thermograms. Figure 16 shows the thermal behavior of intact AmB,  $\gamma$ CD, HP $\gamma$ CD, and their PM and FD samples. The thermogram of pure AmB showed the broad endotherms at 127 °C and 205 °C during DSC experiment (Figure 16a). It was observed that the DSC thermogram of AmB showed the same pattern corresponding to previous literature (113). The thermal profile of  $\gamma$ CD and HP $\gamma$ CD exhibited the broad endothermal peak at 106.5 °C and 87.2 °C, respectively, (Figures 16b and 16c) which indicated the dehydration associated with the loss of water from solid

CDs (142). In case of PM, the endothermic peak of AmB at 205 °C was retained in both PM of AmB/ $\gamma$ CD and AmB/HP $\gamma$ CD (Figures 16d and 16e). However, the endothermic peak of AmB at 127 °C was fused with peak of  $\gamma$ CD in PM AmB/ $\gamma$ CD and shifted to lower temperature of about 100 °C in PM AmB/HP $\gamma$ CD. This observation may be attributed to the presence of weak or no interaction between the components. It is possible that the heating process during DSC analysis could promote the interaction between pure AmB and CDs (147). For FD samples, the endothermic peaks of AmB were absent in both FD AmB/ $\gamma$ CD and AmB/HP $\gamma$ CD (Figures 16f and 16g). The disappearance of endothermic peak indicated the transformation of amorphous nature or inclusion complex formation (137).

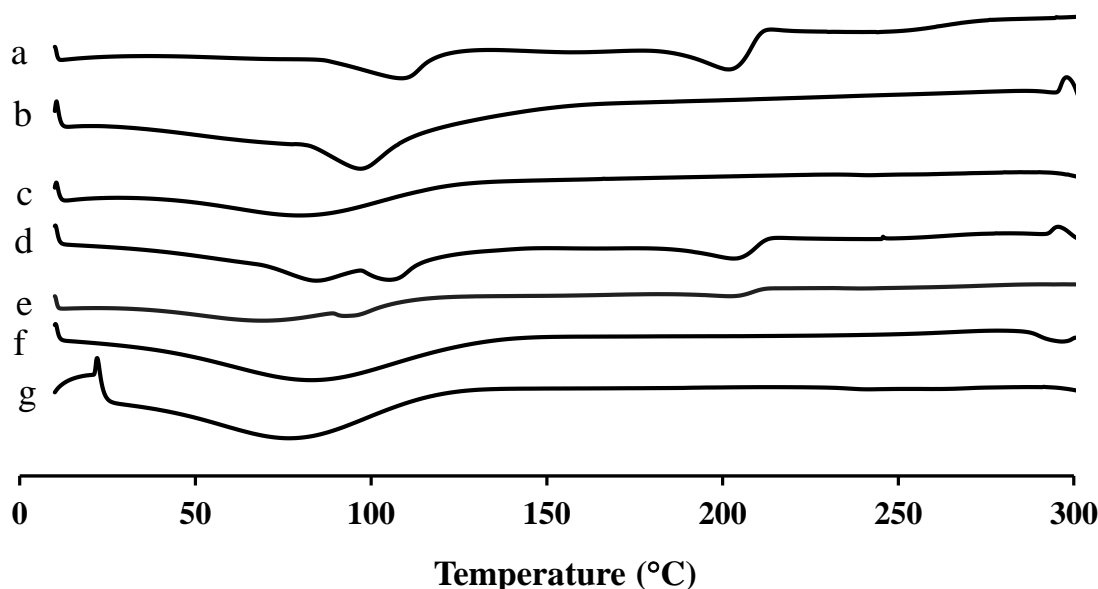


Figure 16 DSC thermograms of pure AmB (a), pure  $\gamma$ CD (b), pure HP $\gamma$ CD (c), PM AmB/ $\gamma$ CD (d), PM AmB/HP $\gamma$ CD (e), FD AmB/ $\gamma$ CD (f) and FD AmB/HP $\gamma$ CD (g)

## **6. Screening the concentration of components for AmB pickering emulsion**

For screening the concentration range of ingredients in formulation development of the pickering emulsion, the phase diagrams were plotted under the visual inspection of the compositions that are shown in Figure 17.  $\alpha$ CD at the concentration of 5% w/v was not enough while 5% w/v of lecithin was too high to provide the stable pickering emulsion for both concentrations of MCT oil (i.e., 10% and 20% w/v). In the study of Inoue et al. (2009), they reported that the inclusion complexes of n-alkane/CD formed at low CD concentration had the surface activity, but were not able to stabilize the pickering emulsion (55). For the composition containing 10% of MCT oil and either lecithin 1% or 3% w/v, the higher  $\alpha$ CD concentrations (7.5% and 10% w/v) showed good appearance and physical stability (Figure 17a). In case of the composition comprised of 20% of MCT oil with the same concentrations of lecithin, the stable pickering emulsion was obtained only when  $\alpha$ CD used up to 10% w/v (Figure 17b). It was observed that the more amount of  $\alpha$ CD was required when MCT oil concentrations was increased. This may be probably due to solid MCT oil/ $\alpha$ CD complexes were not sufficient to stabilize pickering emulsions resulted in formulation instability.

One of the crucial factors to develop the stability of emulsion is the oil concentration. It has been reported that smaller particle size of the emulsion droplet was obtained when the concentration of oil was decreased. It consequently resulted in the emulsion stability (148). Thus, 10% (w/v) MCT oil including 7.5-10% w/v of  $\alpha$ CD concentrations and

lecithin (1-3% w/v) were selected for the formulation development of AmB pickering NEs.

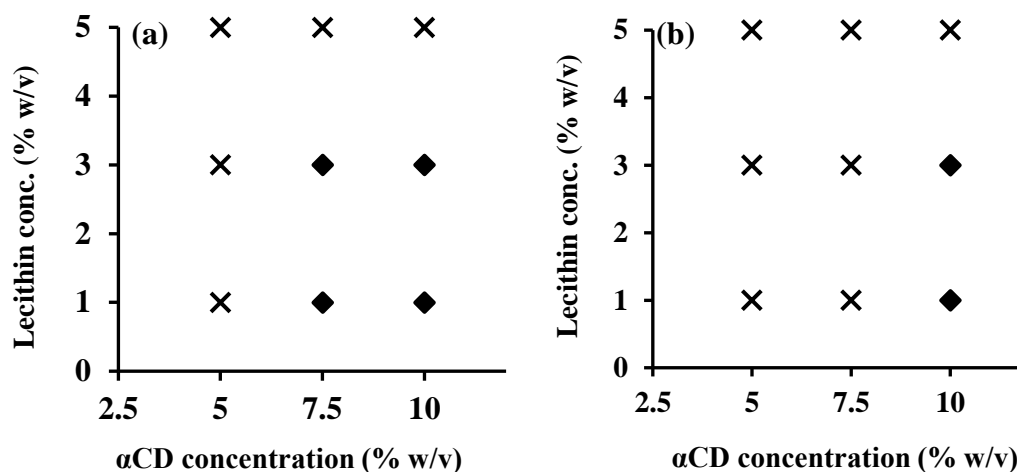


Figure 17 The phase diagrams of different concentration of  $\alpha$ CD, MCT oil and lecithin: 10% of MCT oil (a) and 20% of MCT oil (b), the phase separation (x) and stable emulsion (♦)

## 7. Physicochemical and chemical characterization

### 7.1. Appearance, pH, osmolality and viscosity

AmB loaded pickering NEs (F1-F8) showed pale yellow-colored while non-pickering NEs (F9-F12) displayed the intense yellow-colored in appearance. The pH, osmolality and viscosity of each formulation are shown in Table 7.

*Table 7 pH value, osmolality and viscosity of the formulations (Mean±S.D., n=3)*

Formulations	pH	Osmolality (mOsmol/kg)	Viscosity (cPs)	
			25 °C	34 °C
F1	4.34±0.02	292.10±5.80	3.44±0.35	3.07±0.63
F2	4.91±0.02	302.17±7.12	7.50±0.54	7.25±0.52
F3	4.69±0.09	307.30±9.37	3.57±0.52	2.95±0.35
F4	4.41±0.10	301.20±5.17	28.88±1.19	26.91±2.61
F5	5.02±0.05	296.33±8.50	3.56±0.18	2.83±0.17
F6	4.55±0.03	303.27±5.60	6.51±0.18	5.41±0.67
F7	4.60±0.03	306.00±7.55	6.02±0.42	5.04±0.17
F8	4.70±0.14	303.67±9.07	25.19±0.87	23.24±1.56
F9	4.88±0.04	291.33±4.73	2.58±0.26	2.37±0.12
F10	4.90±0.07	296.90±7.66	20.64±1.04	19.66±0.70
F11	4.67±0.06	292.33±10.79	2.34±0.17	2.09±0.18
F12	4.82±0.07	307.20±6.14	3.07±0.28	2.58±0.52

The pH values of all formulations were in the range of 4.34 - 5.02. Although the ideal pH of lachrymal fluid is 7.4, the eye can tolerate a wide range of pH, 3.5-8.5 due to its natural buffering system (149). It has been well-known that the tonicity is important for ophthalmic preparations. The ideal osmolality for the eye drops is 300 mOsmol/kg. Normally, sodium chloride is used for the isotonicity adjustment but it is physically incompatible with AmB and it can cause precipitation of AmB (150). Glycerol is an alternative choice and often recommended as isotonic agent which mostly found in parenteral formulations. The osmolality is based on the colligative properties of formulation. The formulation is isotonic if it has the same amount of colligative properties

to the physiological fluids. According to the osmolality of each component of the formulation, the concentration of tonicity adjusting agent can be calculated (151). In this study, different amount of glycerol was required to obtain the isotonicity in each formulation. Owing to the absence of  $\alpha$ CD in non-pickering NEs, more amount of glycerol was necessitated compared with their respective pickering NEs. The formulations containing higher lecithin (i.e., 3% w/v) required less glycerol content to achieve the desired osmolality. After adjusting with glycerol, the osmolality of all formulations was in the range of 291-307 mOsmol/kg which was in the acceptable range (260-320 mOsmol/kg) (151).

The viscosities of the formulations were in the range of 2.34-7.50 cPs at 25 °C except F4, F8 and F10. Because of the increasing the temperature resulted in the decrease in viscosity, the viscosity that measured at 34 °C was slightly lower than that measured at 25 °C (152). At low lecithin concentration (i.e., 1% w/v), the viscosities of formulations were no significant difference. However, at high lecithin concentration (3% w/v), the pickering NEs containing high AmB loading and high CD concentration (F4 and F8) showed significantly higher viscosity than those of other pickering NEs. It might be due to the formation of self-assembled or multicomponent of AmB/MCT oil/CD complexes that elevated the viscosity of the formulations. In case of non-pickering NEs, the formulation utilized high  $\gamma$ CD content (F10) also gave high viscosity value. This may be possible that  $\gamma$ CD has the ability to form poly (pseudo)rotaxanes with amphiphilic polymer. Consequently, the high viscosity was derived from the gel-like structure of the supramolecular lecithin/ $\gamma$ CD complexes. (153, 154). Generally, the

viscosity range of ophthalmic preparations is between 12 and 20 cPs for the optimal bioavailability and prolong the corneal contact time. When the viscosity was higher than 20 cPs, there was no further improved and it could lead to the remaining of residue on the eyelid (155, 156).

## **7.2. Interfacial tension and contact angle measurement**

The interfacial tension and contact angle of all formulations are shown in Table 8. It was observed that the interfacial tension of pickering NEs (F1-F8) was significantly lower than those of non-pickering NEs (F9-F12). It represented that the presence of  $\alpha$ CD in the formulations resulted in lower surface tension at the oil-water interface in pickering NEs. It was assumed the formation of surface active MCT oil/ $\alpha$ CD complexes at oil/water interface by the interaction of  $\alpha$ CD with one fatty acid chain of MCT oil. The other two fatty acid of MCT oils were shifted to the oil phase and  $\alpha$ CD was directed to the aqueous phase. Consequently, the interfacial tension was reduced by the adsorption of MCT oil/ $\alpha$ CD complexes at oil/water interface. This finding was in consistent with the investigations by Li et al. (2014) and Manthapa et al. (2013) (48, 60). They revealed that oil/ $\alpha$ CD inclusion complexes could decrease the interfacial tension at the tetradecane and water phase. In addition, the interfacial tension of formulations containing higher  $\alpha$ CD concentration (i.e., 10% w/v) (F1, F3, F5 and F7) was lower than those of formulations consisting of lower  $\alpha$ CD ones (F2, F4, F6 and F8). Hashizaki et al. (2014) reported that the increasing of  $\alpha$ CD concentration resulted in lowering of interfacial tension of n-alkanol/water pickering emulsion (58).



*Table 8 The surface tension and contact angle of all formulations (n=3, Mean±S.D.)*

Formulations	Surface Tension (mN/m)	Contact angle (°)
F1	31.37±0.47	61.63±4.29
F2	35.20±0.49	67.27±6.66
F3	30.89±0.35	60.36±1.35
F4	35.03±0.27	68.18±0.86
F5	31.62±0.51	68.93±0.57
F6	36.63±0.58	69.42±0.86
F7	31.03±0.27	62.97±0.13
F8	36.20±0.35	64.31±0.36
F9	50.63±0.47	63.05±2.20
F10	48.50±2.35	61.69±0.12
F11	51.07±0.14	61.81±0.23
F12	48.18±3.07	63.99±0.19

The wettability of solid particles by a liquid can be characterized by the three-phase contact angle ( $\theta$ ). The relationship between the contact angle and the type of emulsion was reported by Finkle et al. (1923) and Schulman et al. (1954) for the pickering emulsion (157, 158). When  $\theta$  is smaller than  $90^\circ$ , the emulsion was favored to o/w emulsion type whereas  $\theta$  larger than  $90^\circ$  leads to the formation of w/o emulsion type. The contact angle of all formulations was in the range of  $60$ - $69^\circ$  and resulted in o/w emulsion type. It was described that the contact angle of pickering NEs showed the slightly higher values than that of corresponding non-pickering NEs. This indicated that pickering NEs had lower wetting ability than non-pickering NEs. It means the emulsion droplet surrounded by solid MCT oil/ $\alpha$ CD complexes was less

spread out resulted in the decrease tendency of the instability of formulations i.e., flocculation or coalescence. However, the CD-based pickering NEs have dual wettability provided the emulsion droplets homogeneously distributed (107).

### **7.3. Morphology, particle size and size distribution and zeta potential**

The optical microscopic images of AmB loaded NEs are shown in Figure 18. In case of pickering NEs (F1-F8), the emulsion droplets were coated with dense mono-layered film and uniformly distributed in the aqueous phase. It was reported that the stable pickering emulsion was obtained by the formation of dense film around the oil droplets by the adsorption of CD (59, 159-161). Starch-based and silica-based pickering emulsion were also demonstrated a densely packed around the oil droplets (162, 163). For the non-pickering NEs (F9-F12), spherical shaped oil globules were dispersed in the aqueous phase and no layer was found around the oil globules.

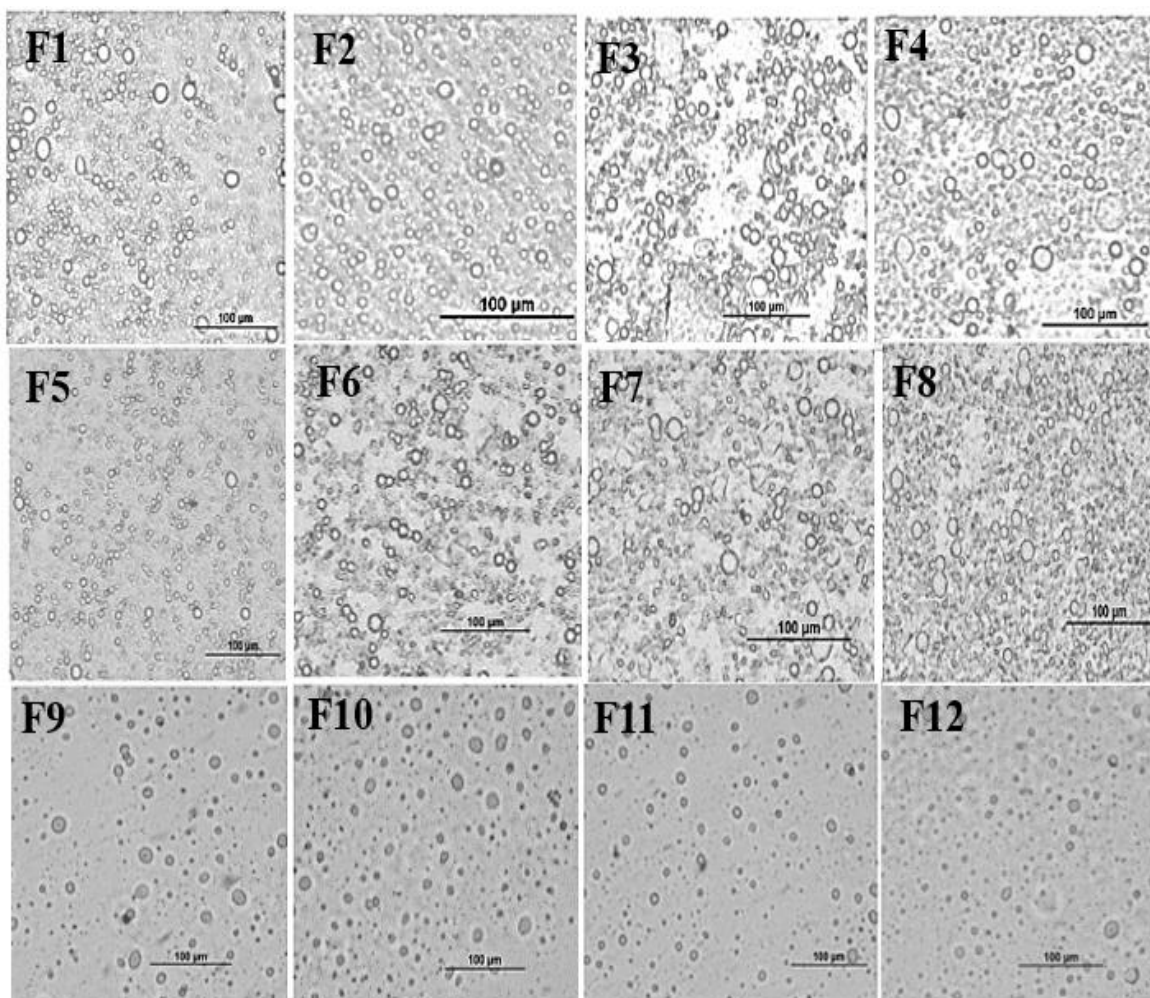


*Figure 18 Optical microscopic images of AmB pickering NEs (F1-F8) and AmB non-pickering NEs (F9-F12)*

Table 9 displays mean particle size and size distribution and zeta potential of AmB NEs determined by DLS technique. All AmB formulations exhibited the trimodal populations (data not shown) and the mean diameter was in the nanometer range of 135-425 nm based on the intensity distribution and PDI values were in the range of 0.39 to 0.77. PDI values of all formulations except F4 were lower than 0.7. It indicated that the formulations had narrow particle size distribution (164).

*Table 9 The mean particle size, size distribution and zeta potential of all formulations (n=3, Mean±S.D.)*

Formulation	Mean particle size (nm)	PDI	Zeta Potential
F1	135.93±0.65	0.39±0.02	+30.33±0.61
F2	289.51±6.86	0.53±0.01	+32.53±1.31
F3	172.62±1.73	0.48±0.01	+31.96±0.38
F4	387.87±13.63	0.77±0.08	+36.66±0.67
F5	186.92±24.76	0.63±0.14	+30.27±0.47
F6	286.63±10.90	0.53±0.01	+31.5±0.52
F7	246.90±1.88	0.63±0.01	+30.63±0.61
F8	324.03±11.75	0.68±0.16	+31.5±0.79
F9	181.03±1.98	0.48±0.01	+31.03±0.83
F10	425.60±4.92	0.65±0.05	+31.37±0.31
F11	159.37±3.33	0.44±0.02	+30.27±0.74
F12	301.95±8.08	0.57±0.03	+32.67±0.21

It was found that the particle size of the formulations increased when increasing of  $\gamma$ CD or HP $\gamma$ CD concentration. This may be due to the AmB solubility enhancement through the formation of AmB/CD complex aggregates at high  $\gamma$ CD or HP $\gamma$ CD concentration (120). Among the formulations, F4, F8, and F10 showed larger mean particle size. Of these formulations composed of the highest concentration of AmB and the excipients. At their high concentration, the multicomponent such as AmB and/or lecithin/CD complexes, self-assembled of CDs could be observed and formed larger particle size. This result data supported that the large particle diameter with the broad size distributions (PDI  $\geq$  0.7) plays the role for high viscosity of these formulations.

Regarding to the zeta potential values, all formulation exhibited high positive zeta potential values (+30 mV to +36 mV). The formulations with high zeta potential above  $\pm 30$  mV is the good condition for the stability of the formulations (165). The zeta potential of the nanoemulsion depends on the ionization of the emulsifier (166). The positive value may be due to the protonation of lecithin in acidic pH. Thus, these formulations had high positive zeta potential are able to prohibit the aggregation of particles.

#### **7.4. Drug content and entrapment efficiency**

The total AmB content and %EE of all formulations are shown in Table 10. It can be detectable that the total drug content was in the range of 96-99%. This indicated that there was no drug loss or degradation during the preparation process. %EE of AmB in pickering NEs (F1-F8) was significantly higher than that of their respective non-pickering NEs (F9-F12) ( $p < 0.05$ ). It was possibly due to that the network formation of MCT oil/ $\alpha$ CD inclusion complexes surrounded on the droplets of the pickering NEs are the additional site of drug entrapment. The increasing concentration of lecithin to the formulation gave lower %EE. The proposed mechanism may be explained that lecithin could form micelle or liposome-like with AmB and localized in the continuous phase. Thakkar et al. (2005) and Dhakar (2012) demonstrated the influence of stabilizer concentration on the %EE of the microspheres. It indicated that increasing the concentration of the stabilizer resulted in decreasing the entrapment efficiency of the microspheres in some extent (167, 168). Furthermore, the higher  $\gamma$ CD or HP $\gamma$ CD concentrations in the pickering NEs, the higher %EE was

obtained. It could be concluded that AmB/CD inclusion complexes were predominately located inner core of the emulsion droplets.

*Table 10 The total drug content (%) and entrapment efficiency (%EE) of AmB loaded formulations (n=3, Mean±S.D.)*

Formulation	Total Drug Content (%)	Entrapment Efficiency (%EE)
F1	96.59±2.70	90.65±0.43
F2	97.37±1.84	93.24±0.39
F3	99.00±1.33	84.50±0.12
F4	99.08±0.69	89.41±1.28
F5	97.71±0.84	90.16±0.79
F6	96.10±2.05	92.59±0.61
F7	97.46±1.87	84.63±1.28
F8	99.32±0.51	86.47±0.78
F9	97.47±1.39	80.07±4.01
F10	97.63±0.86	76.73±6.12
F11	97.70±0.43	78.77±4.31
F12	98.77±0.85	75.68±4.70

## 8. Stability index study

The stability index of AmB NEs at various time interval is presented in Figure 19. At first week, there was no significant change in the stability of all formulations. After that and throughout the study period, low emulsion stability index was observed in F4, F8 and F10. This result may be caused by the presence of large particles in F4, F8 and F10 than that of other formulations, that could lead to some coalescence of large particles and resulted in low stability index. The literature reported that emulsion with larger particle size was less stable than with

smaller particle size (169). Due to the disadvantages i.e., highly viscous preparations, large droplet size trend to form coalescence and low stability index of F4, F8 and F10, they were excluded from further studies. Despite F1 and F5 showed good physicochemical properties and the stability index, they were also excluded because of their low drug loading (Table 2).

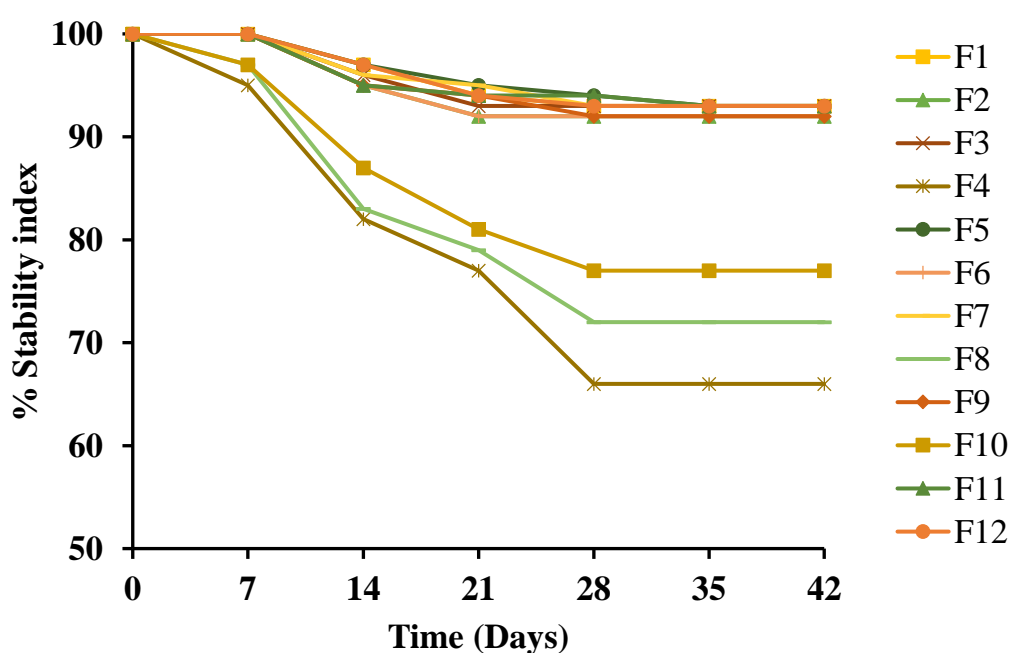


Figure 19 The stability index (%) of AmB NEs

## 9. Degree of aggregation behavior

### 9.1. UV-Vis spectroscopy

In the aqueous solution, AmB can self-associate to the formation of macromolecular aggregation due to its amphoteric and amphiphilic nature. The toxicity of AmB is associated with the aggregated nature and monomeric forms are beneficial for the antifungal activity (21, 170). Because of the presence of conjugated bonds in the

polyene region, the absorption spectra of AmB are characterized by four bands and these are distinct in the wavelength range of 300-500 nm (171, 172). The changes of absorption spectra of AmB depends on the nature of monomer or aggregates. The degree of aggregation of AmB can be assessed by the ratio of peak I to peak IV. The monomeric form is dominant when the value of resulting ratio is less than 0.25, however, if the value is as high as 2.0, the aggregate formation is observed (173).

The peak I/IV ratio values of AmB solution, Amphotericin-B<sup>®</sup> and the selected formulations are shown in Table 11. In this study, the value of peak I/IV ratio of AmB in DMSO:methanol (1:999 v/v) presented as monomeric form while Amphotericin-B<sup>®</sup> showed the highly aggregated nature. The peak I/IV ratio values of AmB in all formulations were in the range of 0.919 to 1.146, indicated the moderate degree of aggregated form (dimers). In comparison with Amphotericin-B<sup>®</sup>, it can be observed that the presence of  $\gamma$ CD or HP $\gamma$ CD could prevent the formation of multimolecular aggregates of AmB. This study was the first investigation of aggregation of behavior of AmB in the presence of  $\gamma$ CD. There was no significant change in the aggregation of AmB in both pickering NEs and non-pickering NEs. In aqueous media, AmB firstly dimerized with apolar heptane and polyol regions and consequently, several thousands of helical forms of aggregates were obtained by heaping of dimers (174). Kajtar et al. (1989) investigated the aggregation state of AmB in the presence of  $\gamma$ CD. They reported that AmB would only associated to the dimers and not to the polymeric aggregates form in the presence of  $\gamma$ CD (175).



*Table 11 Peak ratio values of AmB solution, Amphotericin-B® and selected formulations (n=3, Mean±S.D.)*

Formulations	Diluent	Peak I/IV Ratio
Pure AmB	DMSO:methanol (1:999 v/v)	0.25±0.01
F2	STF	1.00±0.01
F3		0.92±0.02
F6		1.03±0.01
F7		1.15±0.03
F9		1.07±0.02
F11		1.05±0.02
F12		1.07±0.03
Amphotericin-B®		3.87±0.04

## 9.2. Circular dichroism

The circular dichroic spectra of AmB in DMSO:methanol (1;999 v/v), Amphotericin-B® and selected AmB NEs are displayed in Figure 20. The monomeric form of AmB is related with the CD spectra of positive bands at 410, 385 and 365 nm (Figure 20a) (175). In this study, all formulations showed the doublet dichroic pattern centered at the wavelength of 344 nm with related to the aggregated AmB (Figure 20b). The literature reported that the dimer of AmB presented the doublet at the center of 344 nm and positive band at about 290 nm (176). The CD spectra of Amphotericin-B® was observed as stronger doublet at center of 330 nm. The dichroic pattern of super-aggregated AmB was characterized by the center doublet from 337 to 327 nm (177). Therefore, this study can provide the supporting data for the UV-Vis spectroscopic study that AmB

in formulations was exhibited AmB molecules as dimer form but not in super-aggregated form.

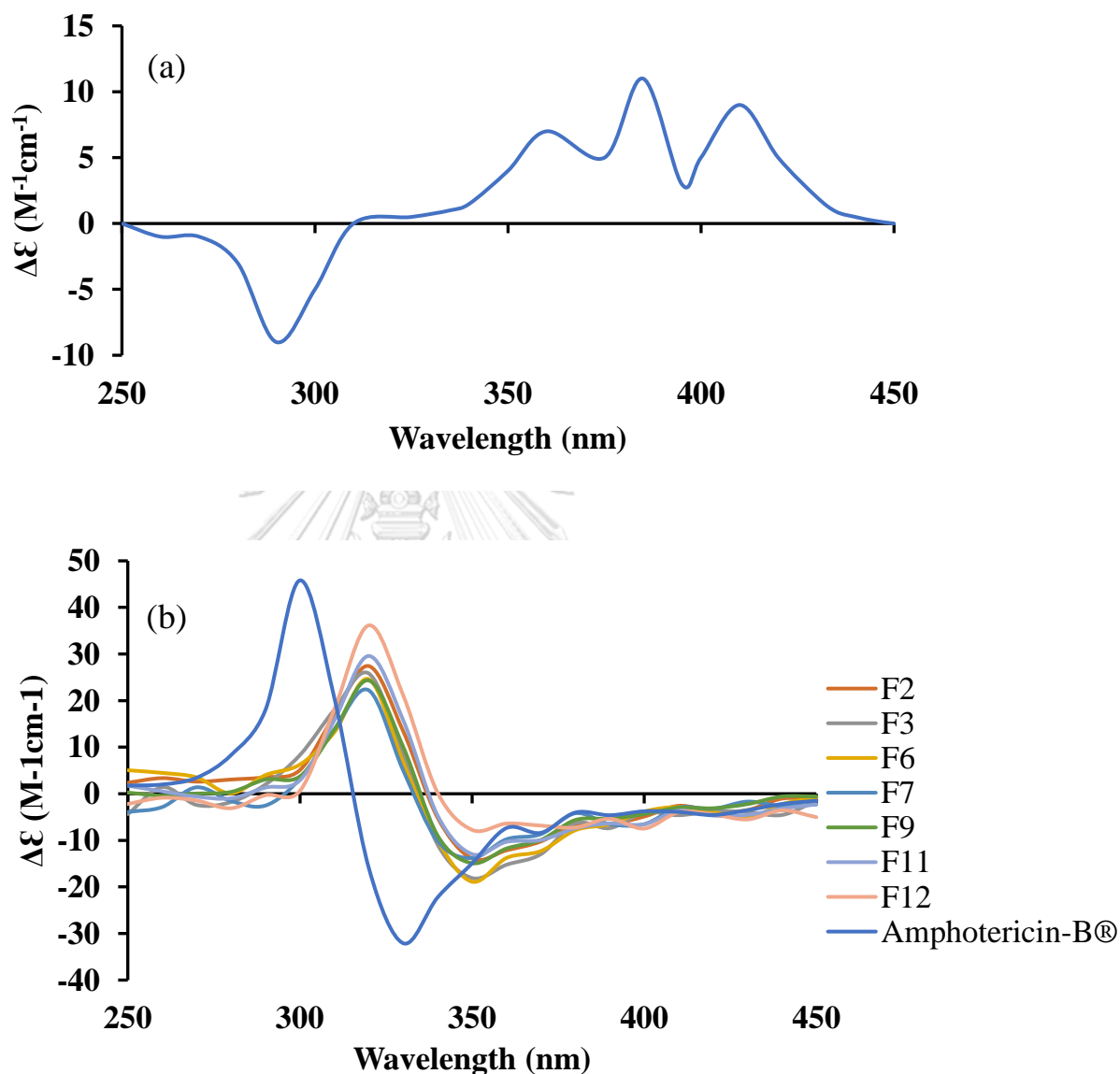


Figure 20 Circular dichroism of AmB in DMSO:Methanol (1:999 v/v) (a) and selected formulations and Amphotericin-B® in STF (b)

## 10. *In vitro* drug release study

The cumulative drug release profiles of Amphotericin-B® and selected AmB NEs are shown in Figure 21. Amphotericin-B® displayed

fast release rate with cumulative release of 93% within 48 h. The release profiles represented that the pickering NEs (F2, F3, F6 and F7) showed slower drug release rate than the non-pickering NEs (F9, F11 and F12). In case of pickering NEs, 28-40% of drug was released while 49-59% of drug was released in non-pickering NEs within 48 h. This result might be attributed to the drug entrapment. The drug entrapment efficiency of pickering NEs was higher than that of non-pickering NEs (Table 10). On the other hand, most of the drug were entrapped in case of pickering NEs. Therefore, drugs were gradually released from the inner core of emulsion droplet in the pickering NEs.

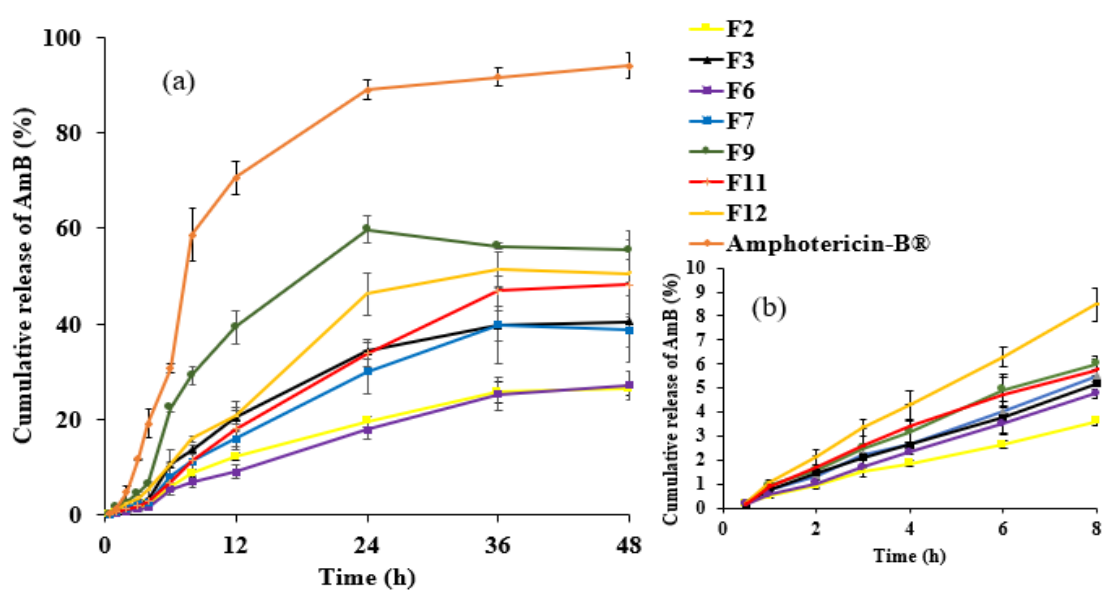


Figure 21 *In vitro* drug release profiles of AmB NEs and Amphotericin-B® within 48 h (a) and AmB NEs within 8 h (b) through the semipermeable membrane with MWCO 12000-14000 Da ( $n=3$ , Mean $\pm$ S.D)

In the literature, it can be observed that the pickering emulsions provided the controlled drug release. The CD-based bupivacaine loaded pickering emulsions showed the remarkable

controlled release of drug (12.2-23.1%) within 48 h (52). Frelichowska et al. (2009) compared the release profile of caffeine loaded pickering emulsion and conventional emulsion stabilized by silica and abil wax, respectively (178). It was found that the release of caffeine from pickering emulsion was slower than that of non-pickering emulsion. They suggested that this result might be due to the dense shell of silica particles around the emulsion droplets, acted as the boundary for the drug release resulting in controlled release was observed (178). Time required to release of 50% of the drug ( $T_{50\%}$  in min) was determined.  $T_{50\%}$  of F2 and F6 were 60 and 80 min, respectively while those of other formulations were in the range of 17-45 min. From this value, F2 and F6 demonstrated the drug release in controlled manner. In addition, because of higher viscosity and larger particle size of F2 and F6 (Tables 7 and 9), they played the important role to retard the release of drug. The slow and sustained release of AmB is beneficial for the drug delivery system and reduced the possibility of toxicity caused by the exposure of aggregated AmB. Therefore, F2 and F6 are the good candidate for further studies. F9 and F11 were also selected as non-pickering NEs to compared with F2 and F6.

## 11. Rheological study

Figure 22 displays the flow behavior of pickering NEs and non-pickering NEs. All formulations showed the typical non-Newtonian behavior (shear thinning) at the shear rate of 0-100  $s^{-1}$ . It was observed that the viscosities of AmB NEs were high at the low shear rate and then decreased with the increased shear rate. This similar pseudoplastic flow property was also observed in the case of o/w pickering emulsions

stabilized by hydrophobic starch particles and phytoglycogen nanoparticles (162, 179). The observed shear thinning behavior may be due to either a disruption of the particle network within the continuous phase (180, 181) or the structural changes of the particles due to the shear rate (182). The viscosities of pickering NEs (F2 and F6) were higher than non-pickering NEs (F9 and F11) throughout the studied shear rate. This means that non-pickering NEs required less shear stress than pickering NEs. This result might be the relationship of shear viscosity and the structure of the precipitated inclusion complexes. The presence of the stronger three-dimensional network in the pickering NEs could increase the shear viscosity than the non-pickering NEs (111). In the literature, it can also be found that the higher shear viscosity in the pickering emulsion of econazole stabilized by CD than the commercial conventional emulsion was observed (111). The formulations containing  $\gamma$ CD (F2 and F9) resulted the higher shear viscosity than their respective of HP $\gamma$ CD contained formulations (F6 and F11). This might be due to the stronger tendency of  $\gamma$ CD to form the complex aggregates than HP $\gamma$ CD (183).

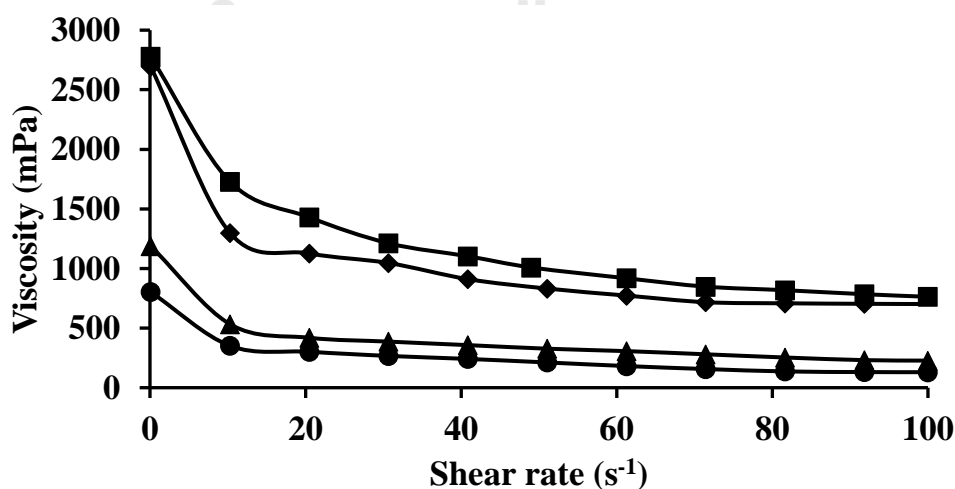


Figure 22 Shear rate dependence of viscosity for F2 (■), F6 (◆), F9 (▲) and F11 (●)

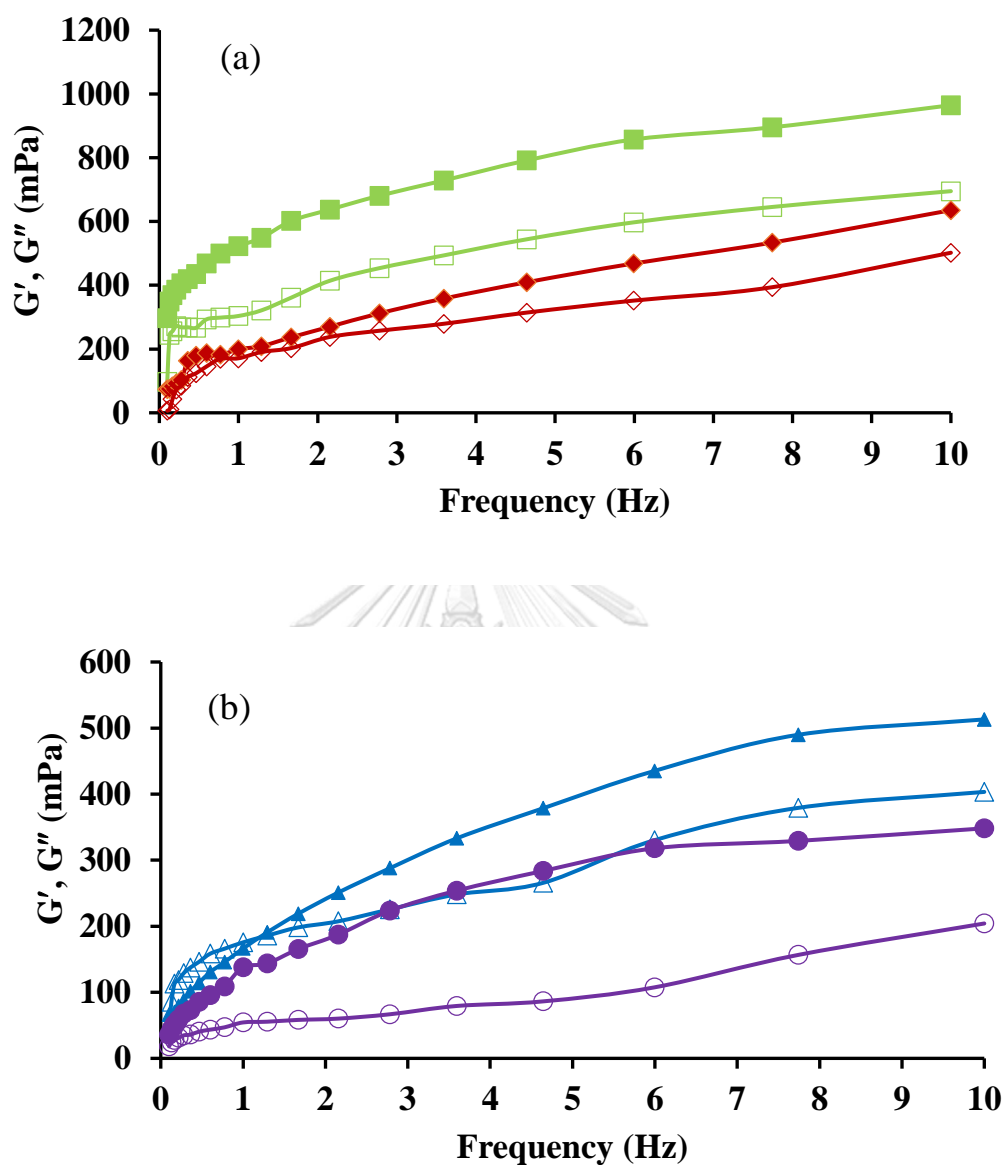


Figure 23 Dynamic frequency sweep of (a) pickering NEs; F2 (■), F6 (◆), and (b) non-pickering NEs; F9 (▲) and F11 (●); filled ( $G'$ ) and opened ( $G''$ )

The dynamic viscoelastic behaviors of formulations are shown in Figure 23. It was evaluated by measuring the linear viscoelastic range with the fixed strain of 0.05%. The  $G'$  expresses the magnitude of the energy that is stored in the material and recoverable per cycle of

deformation whereas  $G''$  is the measure of energy that is lost as viscous drainage per cycle of deformation (184). Since  $G'$  was higher than  $G''$  at high frequency range, AmB NEs had the typical elastic behavior. It indicated that the behavior of the emulsion was predominantly elastic and there was a solid-like network in the emulsions (185). The greater value of  $G'$  means the formation of stronger network of solid particles at the emulsion droplets. Consequently, it resulted in better stability because of prevention the coalescence of emulsion droplets by this solid-like network (186). In the literature,  $\beta$ CD stabilized pickering emulsions displayed the stronger solid-like behavior and high stability of the colloidal structure than the non-pickering emulsions stabilized by tween 80 (187). The pickering NEs containing  $\gamma$ CD (F2) displayed significantly higher  $G'$  value than its respective formulation containing HP $\gamma$ CD (F6). It indicated that the former formulation exhibited more elastic behavior and could enhance the emulsion stability.

## **12. Surface morphology of AmB NEs**

### **12.1. SEM analysis**

The SEM images of pickering NEs (F2, F6) and non-pickering NEs (F9, F11) are shown in Figure 24. The pickering NEs showed the spherical shaped droplet covered with the layer of solid particles. Whereas, the non-pickering NEs displayed the round and smooth surface appearance. This result was similar with the literature. The morphology of bupivacaine pickering emulsion stabilized by CD was characterized by rod-shaped structure coated with cubic crystals of oil/CD complexes (52) and curcumin nanoemulsion exhibited the smooth and circular-shaped droplets (188). In their study, oil/ $\alpha$ CD complexes were predominantly

observed as irregular rod-shaped microcrystals. During the sample preparation, the samples were collected in ethanol and this step led to the dehydration. It may affect the structure and size of the particles (131).

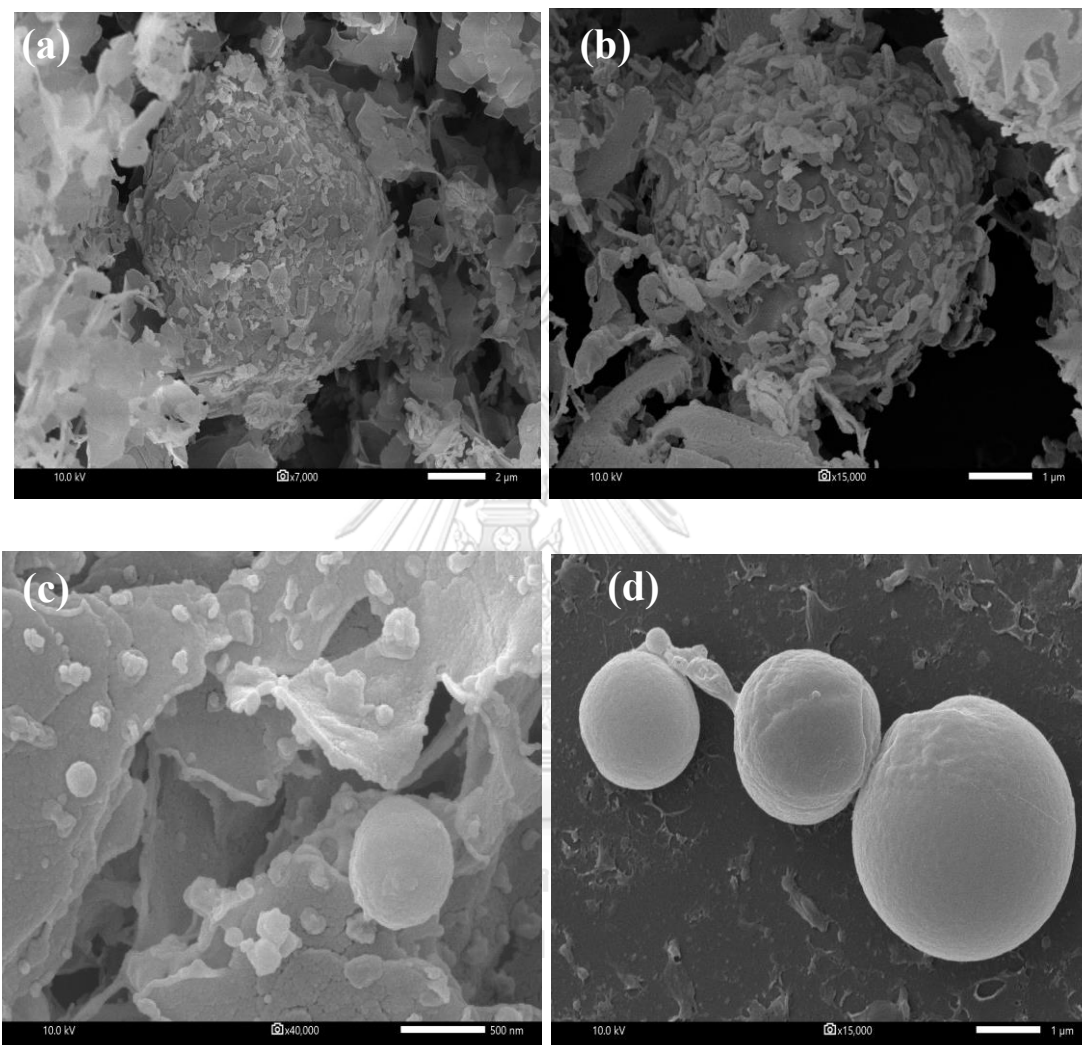


*Figure 24 SEM images of pickering NEs; F2 (a); F6 (b); and non-pickering NEs; F9 (c) and F11(d)*

## 12.2. AFM study

AFM is a type of scanning probe microscope which permits the particle detection for three-dimensional characterization (189). The AFM consists of a cantilever with a sharp tip (probe) that is used to scan



the specimen surface. When operating with non-contact mode, the tip will scan above the surface particles that adsorbed at liquid layer (190). Thus, only AmB pickering NEs could be assessed by the AFM method because the emulsion droplets were surrounded by the solid particles of MCT oil/ $\alpha$ CD complexes. Figure 25 exhibits the AFM micrographs of AmB pickering NEs i.e., F2 and F6. It was found that the solid particles were evenly distributed in both pickering NEs, but large number of precipitated solid MCT oil/CD complexes and some of particle agglomeration was observed in F2.  $\gamma$ CD has the tendency to form self-aggregation or drug/CD complexes aggregates which can be solid complexes around the emulsion droplets (120).

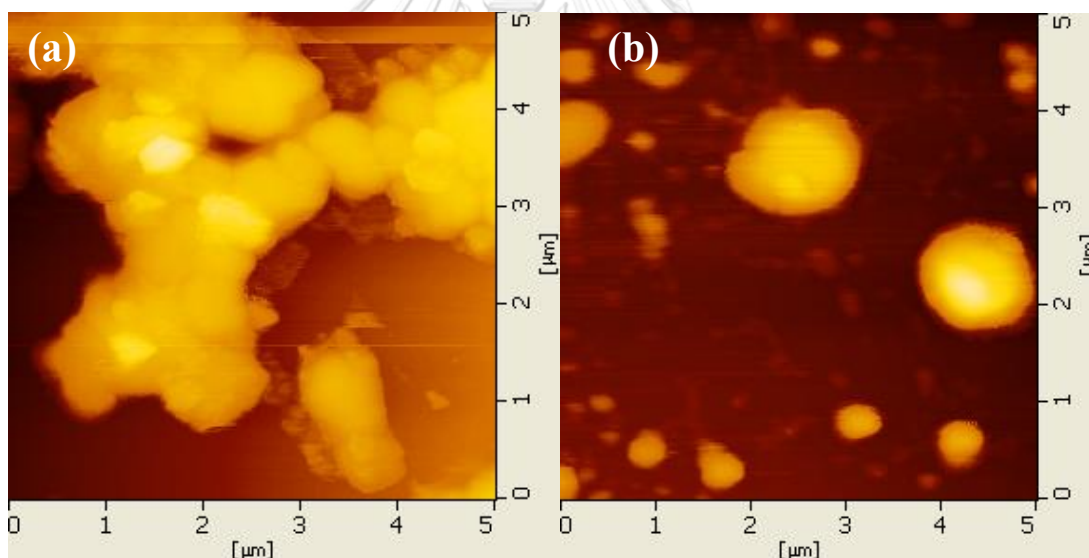


Figure 25 AFM images of pickering NEs; F2 (a) and F6 (b)

### 13. *In vitro* hemolytic study

The *in vitro* hemolytic study is an alternative method for the determination of the toxicity of AmB. The degree of hemolysis induced

by AmB in Amphotericin-B<sup>®</sup>, and the selected formulations is displayed in Figure 26.

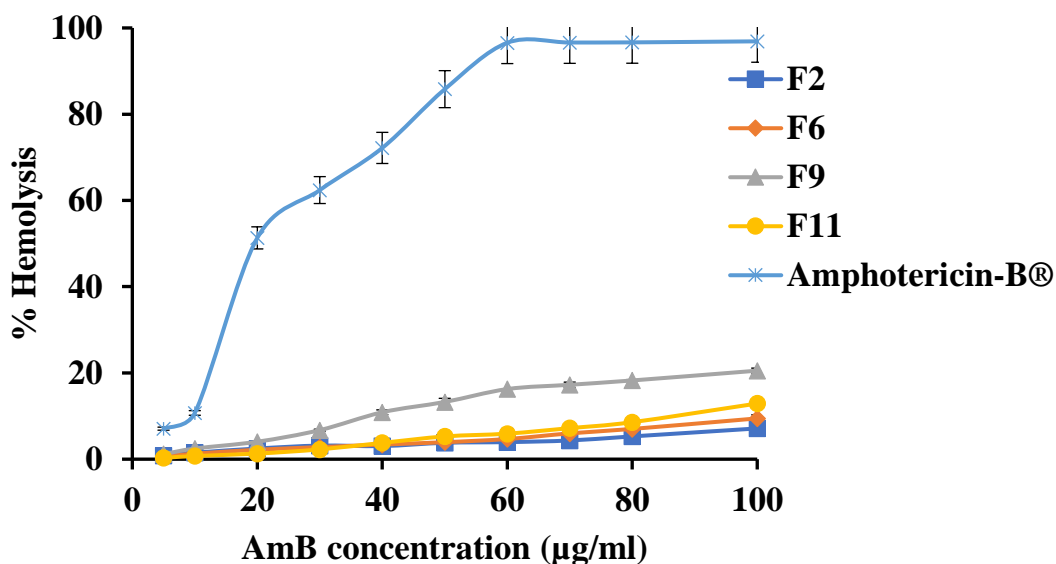


Figure 26 *In vitro* hemolytic study of sheep RBC at the various concentrations of AmB in formulations; F2 (■), F6 (◆), F9 (▲), F11 (●) and Amphotericin-B<sup>®</sup> (×), ( $n=3$ , Mean $\pm$ S.D.)

For Amphotericin-B<sup>®</sup>, the concentration of AmB that resulted in 50% of RBCs lysis ( $HC_{50}$ ) was 20  $\mu$ g/mL and  $HC_{100}$  was found to be at the concentration of about 60  $\mu$ g/mL. Due to its high degree of aggregation behavior and fast drug release characteristic (Table 11 and Figure 21), these led to the higher extent of hemolysis. Furthermore, because of the presence of surface active agent, sodium deoxycholate in Amphotericin-B<sup>®</sup>, it can cause the hemolysis in addition to AmB itself (191). In contrast, the developed AmB loaded formulations displayed only 7-20% of hemolysis even at the concentration of 100  $\mu$ g/mL because of their less aggregation state. Therefore, this result was relevant with the

study of aggregation behavior. The reduction of aggregation behavior and controlled release of AmB are definitely related with to the decreased activity of hemolysis (192). In our previous study, we also investigated that the drug-RBC interaction could be prevented by the shielding effect of CD and therefore, the less extent of hemolysis was attributed by the controlled drug release (153).

At the AmB concentration of 100  $\mu\text{g/mL}$ , the pickering NEs presented the significantly lower degree of hemolysis (F2 was 7% and F6 was 9%) than the non-pickering NEs (F9 was 20% and F11 was 12%) ( $p < 0.05$ ). According to the fact that the pickering NEs had higher drug entrapment and slower drug release than that of non-pickering NEs (Table 10 and Figure 21). These are crucial factors on the decreasing of hemolytic activity (115). As expected, the highest % hemolysis obtained from F9 because of its the least retarded release among the AmB NEs. However, in these NEs platforms, most of the drug were entrapped within CD cavities and/or incorporation into the internal oil phase resulting in diminished the toxicity. Various nanotechnological carriers were also reported to lower toxicity, i.e., chitosan nanoparticles, solid lipid nanoparticles and polymeric micelles (115, 193, 194).

#### **14. *In vitro* antifungal activity**

To evaluate the antifungal activity of AmB NEs, the MIC and MFC were determined against *C. albicans*, *A. flavus* and *F. solani* by using microdilution method. Table 12 shows the MIC and MFC values of pure AmB in DMSO, Amphotericin-B<sup>®</sup> and AmB NEs. The MIC and MFC of pure AmB in DMSO had the highest values against all fungal species among the tested samples. It indicated that Amphotericin-B<sup>®</sup> and

the developed AmB NEs established the superior formulations to AmB itself.

However, the MIC and MFC values of Amphotericin-B<sup>®</sup> were lower than those of selected AmB NEs formulations for filamentous fungi. This obtained data possible explained by most of drug entrapped in CD cavities and deposited in the inner core of NEs. Consequently, the slowly drug release from this platform affected to the fungistatic and fungicidal activity. Wang et al. (2016) reported the relationship between the controlled drug release profile and antifungal activity. It was concluded that the more sustained release formulations, the higher MIC and MFC values were required for antifungal effects (192). The drug release of AmB NEs was significantly slower when compared to Amphotericin-B<sup>®</sup> (Figure 21). Therefore, NEs required more concentrations to achieve the MIC and MFC values for antifungal activity. However, the developed AmB NEs equally inhibited as Amphotericin-B<sup>®</sup> for the growth of *C. albican*. This may be due to the production of extracellular phospholipase enzymes by *C. albican*, that caused the hydrolysis of lipid component in NEs and lead to the release of AmB (195). Inversely, the filamentous fungi of (*A. flavus* and *F. solani*), the extracellular protease enzymes were mainly produced (196, 197). It has been reported that AmB lipid complex exhibited the same antifungal activity for *C. albican* as the commercial product whereas it inferior to *A. flavus*.

Table 12 *In vitro* antifungal activities of AmB loaded formulations against various species of fungi (n=3, Mean±S.D.)

Formulations	<i>C. albican</i>		<i>A. flavus</i>		<i>F. solani</i>	
	MIC <sup>a</sup>	MFC <sup>b</sup>	MIC <sup>a</sup>	MFC <sup>b</sup>	MIC <sup>a</sup>	MFC <sup>b</sup>
AmB	0.31	2.5	>20	>20	>20	>20
Amphotericin-B <sup>®</sup>	0.09	0.18	0.78	0.78	0.78	0.78
F2	0.09	0.36	>12*	>12*	6.00*	6.00*
F6	0.09	0.36	>12*	>12*	6.00*	6.00*
F9	0.09	0.36	>12*	>12*	3.00*	3.00*
F11	0.09	0.36	>12*	>12*	6.00*	6.00*

<sup>a</sup>µg/mL, <sup>b</sup> µg/mL and \*significant higher values of MIC and MFC when more than two dilution compared to Amphotericin-B<sup>®</sup>

## 15. Physical and chemical stability studies of AmB NEs

### 15.1. Freeze-Thaw stability study

The freeze-thaw stability of the AmB pickering NEs and the AmB non-pickering NEs was evaluated by freezing at -20 °C for 24 h and then thawing at 30 °C for 6 h. Figure 27 displays the visual appearance of AmB NEs after storage zero to three freeze-thaw cycles. Both AmB pickering NEs were stable against the physical instability i.e., creaming, phase separation and the coalescence after freeze-thaw three cycles. This possible explained by the surrounding of MCT oil/αCD microcrystals at oil/water interface and forming the protective layer. These layers in the continuous phase had the ability to reduce the rate of coalescence (54). Whereas, the phase separation was occurred in AmB non-pickering NEs after the second and the third cycles. The pH values of all formulations were not significantly changed throughout the study period. The droplet

size and size distribution of the pickering NEs were slightly higher and broader from zero to three cycles, respectively. In case of the AmB non-pickering NEs, the mean particle size was markedly increased to micrometer range after two cycles. This might be due to the coalescence of emulsion droplets in the non-pickering NEs. Moreover, the zeta potential of non-pickering NEs was also significantly decreased at 2 and 3 cycles. This might be the reduction of repulsive force that also led to coalescence. The visual observation of AmB NEs instability was also confirmed by microscopic image (Figure 28). These observations distinctly indicated that the pickering NEs stabilized by  $\alpha$ CD (F2 and F6) exhibited the greater stability than the non-pickering NEs (F9 and F11). These findings are in agreement with the previous reports, pickering emulsions displayed the physical stability against the coalescence and Ostwald ripening while the inverse result was observed to the conventional emulsions (49, 50).

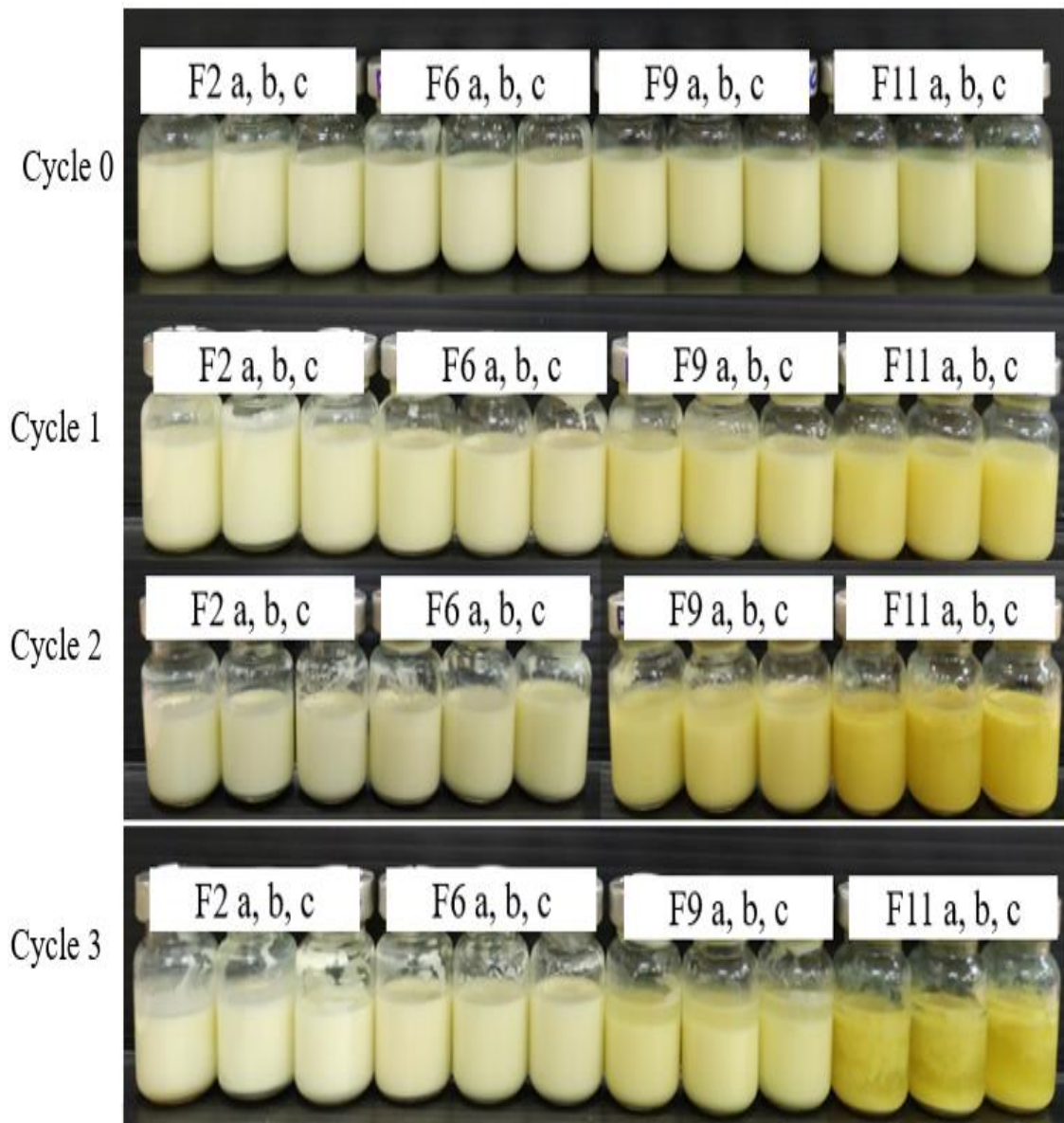


*Figure 27 The appearance of AmB NEs after storage zero to three freeze-thaw cycles*

*Table 13 pH values, average particle size (PS), size distribution (PDI) and zeta potential values of AmB NEs after storage zero to three freeze-thaw cycles (n=3, Mean±S.D.)*

Time (days)	AmB NEs			
	F2	F6	F9	F11
<i>pH</i>				
Day 0	4.56±0.02	4.42±0.03	4.71±0.15	4.56±0.07
Day 1	4.59±0.01	4.40±0.04	4.70±0.06	4.55±0.01
Day 2	4.52±0.02	4.31±0.01	4.57±0.02	4.50±0.01
Day 3	4.39±0.05	4.26±0.07	4.24±0.02	4.24±0.31
<i>PS (nm)</i>				
Day 0	221.86±2.80	224.10±2.36	153.47±0.61	223.73±2.89
Day 1	225.80±1.99	225.30±1.66	173.93±1.25	206.23±5.41
Day 2	263.20±6.32	250.13±12.02	2779.67±12.34	2906.33±48.88
Day 3	293.43±1.91	285.50±4.70	3171.33±140.99	3769.00±20.66
<i>PDI</i>				
Day 0	0.48±0.03	0.47±0.05	0.49±0.02	0.48±0.03
Day 1	0.57±0.07	0.62±0.04	0.49±0.05	0.64±0.01
Day 2	0.62±0.01	0.62±0.01	0.63±0.02	0.67±0.02
Day 3	0.63±0.04	0.68±0.09	0.76±0.02	0.68±0.06
<i>ZP (mV)</i>				
Day 0	+34.37±2.45	+33.83±1.59	+34.40±1.66	+35.27±0.29
Day 1	+34.03±1.42	+33.33±1.58	+33.23±0.58	+34.50±0.66
Day 2	+33.27±0.32	+31.30±1.77	+18.87±0.45	+25.97±2.22
Day 3	+31.27±0.55	+30.04±1.05	+15.97±0.98	+22.50±1.18



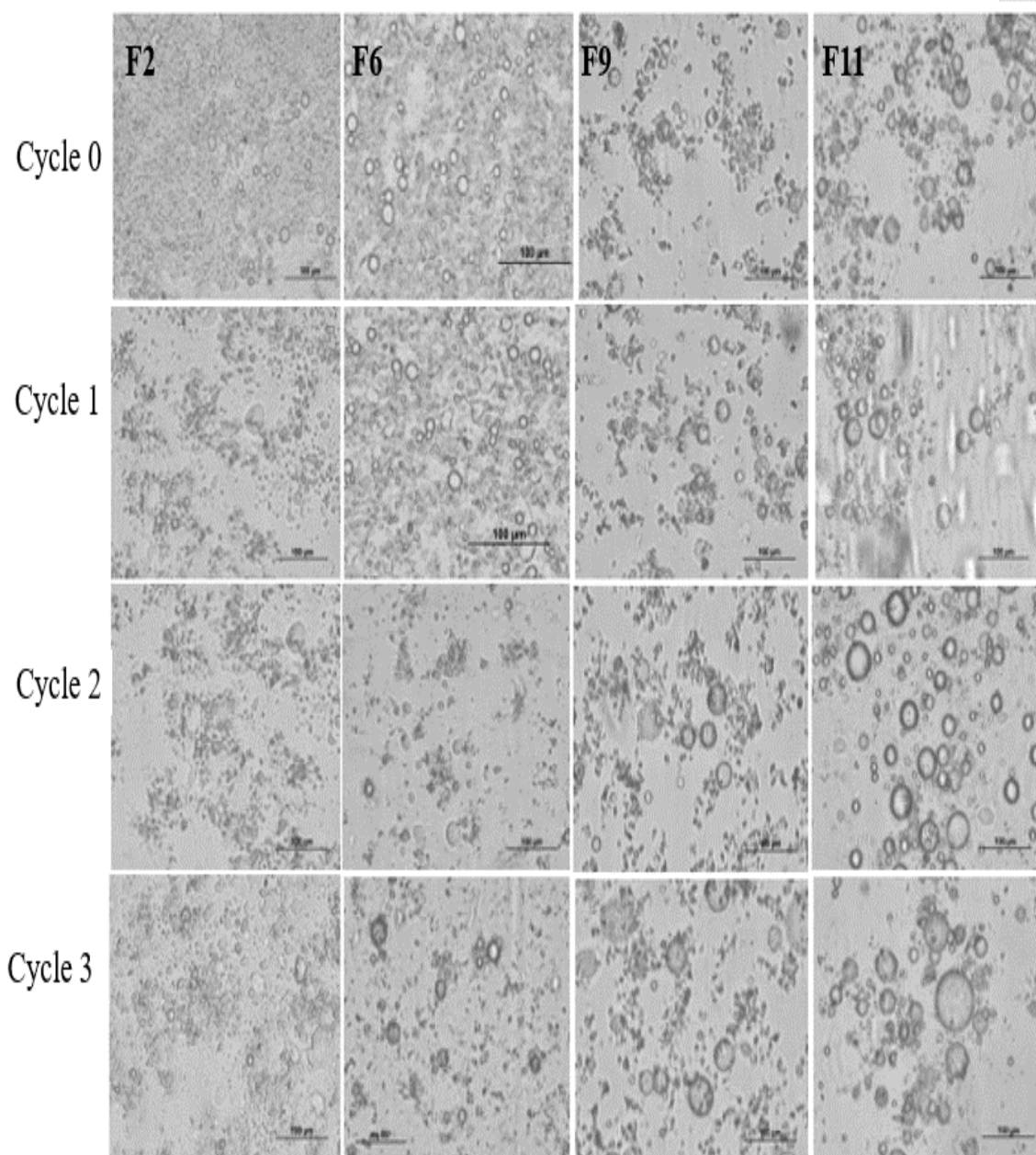


*Figure 28 Optical micrographs of AmB NEs after storage zero to three freeze-thaw cycles*

### **15.2. The stability study**

The physical stability of AmB NEs after storage at long-term ( $30\pm 2$  °C,  $75\pm 5\%$  RH) and accelerated ( $40\pm 2$  °C,  $75\pm 5\%$  RH) conditions at various time interval are shown in Tables 14 and 15, respectively.

Based on the result, pickering NEs (F2 and F6) showed the good stability throughout the study period for both conditions. After the storage of 6 months, the pH values and zeta potential of pickering NEs (F2 and F6) were slightly decreased. The particle size and size distribution of were significantly increased but these values still be within the acceptable range (i.e., the mean particle size  $< 5\mu\text{m}$  and  $\text{PDI} < 0.7$ ). As expected, the larger difference of these parameters was obtained in the accelerated condition than those of long-term condition. In case of non-pickering NEs, the pH value was significantly decreased at 3<sup>rd</sup> month storage. The particle size and size distribution were significantly increased, which values were out of specification. The zeta potential is an important parameter for the determination of physical stability. The zeta potential was significantly decreased at 3<sup>rd</sup> month storage. This may be due to the changes in the repulsion at the boundary of emulsion droplets and resulted in stronger tendency for coalescence lead to the instability.

The chemical stability of AmB NEs is shown in Table 16. The AmB stability in long-term condition was better than in accelerated condition. The drug content and %EE of pickering NEs were slightly decreased throughout 6-months storage whereas, the non-pickering NEs exhibited significant decreasing of drug content and %EE at 3<sup>rd</sup> and 6<sup>th</sup> month storage. The reduction of %EE affected to the decreasing of total drug content because AmB leaked into the continuous phase and led to the degradation of AmB. For the comparison of  $\gamma\text{CD}$  (F2) or  $\text{HP}\gamma\text{CD}$  (F6) contained pickering NEs, total drug content and %EE of F6 were slightly lower than that of F2. According to all stability studies, pickering NEs revealed the good stability than non-pickering NEs. Furthermore,  $\gamma\text{CD}$ -based pickering NEs showed the best stability followed by  $\text{HP}\gamma\text{CD}$ -based

ones. The literature also reported that chitosan-based pickering emulsions showed the higher stability index than the conventional emulsion without chitosan (198).

*Table 14 pH values, average particle size (PS), size distribution (PDI) and zeta potential, AmB NEs storage at accelerated stability condition for 0, 1, 3 and 6 months (n=3, Mean±S.D.)*

Time (months)	AmB NEs			
	F2	F6	F9	F11
<i>pH</i>				
0 Month	4.86±0.04	4.56±0.02	4.87±0.04	4.65±0.14
1 Month	4.65±0.11	4.43±0.05	4.53±0.05	4.03±0.16
3 Month	4.60±0.03	4.39±0.02	3.93±0.03	3.65±0.04
6 Month	4.59±0.04	4.35±0.11	3.65±0.07	3.49±0.09
<i>PS (nm)</i>				
0 Month	255.67±4.60	230.17±1.71	168.17±2.46	198.27±2.81
1 Month	287.57±9.92	264.03±5.90	234.37±6.74	280.70±8.09
3 Month	360.02±14.25	367.10±4.10	516.90±7.99	555.20±24.98
6 Month	373.40±1.04	391.1±15.94	691.17±7.93	651.17±8.08
<i>PDI</i>				
0 Month	0.41±0.02	0.52±0.01	0.49±0.01	0.44±0.01
1 Month	0.51±0.02	0.58±0.01	0.55±0.01	0.53±0.01
3 Month	0.59±0.01	0.65±0.02	0.69±0.04	0.66±0.07
6 Month	0.64±0.02	0.67±0.02	0.75±0.07	0.76±0.09
<i>ZP (mV)</i>				
0 Month	+32.53±0.60	+31.27±0.78	+34.50±0.61	+31.37±0.51
1 Month	+30.27±0.42	+30.03±2.90	+31.40±0.56	+27.87±0.21
3 Month	+29.83±0.25	+28.47±0.40	+19.83±2.12	+17.67±1.20
6 Month	+28.57±0.42	+28.23±0.65	+14.57±0.42	+13.67±1.21

*Table 15 pH values, average particle size (PS), size distribution (PDI) and zeta potential, of AmB NEs storage at long-term stability condition for 0, 1, 3 and 6 months (n=3, Mean±S.D.)*

Time (months)	AmB NEs			
	F2	F6	F9	F11
<i>pH</i>				
0 Month	4.86±0.04	4.56±0.02	4.87±0.04	4.65±0.14
1 Month	4.71±0.13	4.45±0.04	4.62±0.02	4.15±0.05
3 Month	4.65±0.02	4.40±0.04	4.11±0.04	3.71±0.03
6 Month	4.61±0.03	4.36±0.10	3.85±0.07	3.59±0.03
<i>PS (nm)</i>				
0 Month	255.67±4.60	230.17±1.71	168.17±2.46	198.27±2.81
1 Month	287.20±3.97	262.00±4.90	215.53±7.76	234.43±4.91
3 Month	338.87±16.06	359.37±4.39	472.36±9.93	437.50±7.10
6 Month	367.87±2.37	390.30±3.83	686.47±4.52	620.07±3.344
<i>PDI</i>				
0 Month	0.41±0.02	0.52±0.01	0.49±0.01	0.44±0.01
1 Month	0.51±0.01	0.58±0.01	0.54±0.01	0.53±0.01
3 Month	0.58±0.01	0.61±0.01	0.69±0.01	0.64±0.01
6 Month	0.64±0.01	0.65±0.02	0.74±0.03	0.72±0.01
<i>ZP (mV)</i>				
0 Month	+32.53±0.60	+31.27±0.78	+34.50±0.61	+31.37±0.51
1 Month	+30.57±1.45	+30.67±0.06	+32.43±0.61	+29.73±1.47
3 Month	+30.13±0.49	+29.77±1.15	+21.43±1.53	+19.63±1.36
6 Month	+29.73±0.15	+28.67±0.68	+16.63±1.15	+15.43±1.10

*Table 16 Total AmB content (%) and %EE of AmB NEs storage at accelerated and long-term stability conditions for 0, 1, 3 and 6 months (n=3, Mean±S.D.)*

Time (months)	AmB NEs			
	F2	F6	F9	F11
<i>Accelerated stability (40±2 °C, 75±5% RH)</i>				
<i>Total AmB content (%)</i>				
0 Month	99.71±0.78	98.86±1.44	98.82±0.68	99.23±0.83
1 Month	96.20±1.31	96.17±0.68	90.52±4.02	88.12±1.60
3 Month	94.27±1.28	93.17±3.70	68.12±2.23	52.91±2.19
6 Month	91.59±2.03	90.69±1.08	50.28±3.20	40.44±3.52
<i>%EE</i>				
0 Month	92.81±1.19	90.94±1.10	78.68±0.39	80.64±0.98
1 Month	90.87±0.20	87.57±1.14	61.08±1.28	62.61±1.33
3 Month	85.43±1.26	83.75±1.92	49.88±12.87	40.20±8.62
6 Month	82.86±4.21	80.08±3.61	41.16±1.43	20.31±3.36
<i>Long-term stability (30±2 °C, 75±5% RH)</i>				
<i>Total AmB content (%)</i>				
0 Month	99.71±0.78	98.86±1.44	98.82±0.68	99.23±0.83
1 Month	97.62±2.24	96.27±3.37	92.55±2.12	89.44±1.42
3 Month	95.51±4.32	94.02±3.30	78.36±3.35	60.54±2.92
6 Month	94.51±1.01	92.35±1.82	71.80±3.83	43.87±1.10
<i>%EE</i>				
0 Month	92.81±1.19	90.94±1.10	78.68±0.39	80.64±0.98
1 Month	91.02±0.53	89.32±0.28	63.88±1.12	67.31±2.95
3 Month	87.97±0.91	85.71±0.52	51.74±0.38	50.73±1.08
6 Month	86.22±2.72	83.04±0.69	45.31±2.22	23.81±4.39

## CHAPTER V

### CONCLUSIONS

Amphotericin B (AmB) is poorly water-soluble compound at the physiological pH. The solubility of AmB was increased by the formation of inclusion complex with cyclodextrin (CD) through the heating method (sonication at 60 °C for 30 min). Among the tested CDs,  $\gamma$ CD and HP $\gamma$ CD displayed the highest complexation efficiency according to  $A_P$ -type phase-solubility profiles. Prior to develop the pickering nanoemulsions (NEs) containing AmB, type and concentrations of oil and surfactant were selected based on the solubility study. MCT oil and phosphatidylcholine (lecithin) were chosen due to their highest solubilization of AmB. It had been also investigated the surface activity of various CDs. MCT oil/ $\alpha$ CD inclusion complexes showed the lowest interfacial tension at oil-water (o/w) interface among the tested MCT oil/CD inclusion complexes. Furthermore, the inclusion complexes of MCT oil/  $\alpha$ CD was characterized by FT-IR and  $^1\text{H-NMR}$ , and the morphology was observed by optical microscopic and SEM studies. It was found that MCT oil encapsulated with  $\alpha$ CD and there some interactions between MCT oils and  $\alpha$ CD were detected. Therefore, MCT oil/ $\alpha$ CD microcrystals was chosen as solid particles for the development of pickering NEs. According to the solution-state ( $^1\text{H-NMR}$ ) and solid-state (FT-TR, PXRD and DSC) characterizations, AmB was inserted into  $\gamma$ CD or HP $\gamma$ CD cavities as 1:1 and 1:2 complexes. Some interactions were observed between the components. This result supported the data obtained from phase-solubility studies.

AmB loaded  $\alpha$ CD-stabilized pickering NEs and lecithin-stabilized non-pickering NEs were developed. The pH values and osmolality of all formulations were within the acceptable range for the eye drops. The particle size in all formulation were in the nanometer range. However, the mean particle size of some formulations containing high  $\gamma$ CD or HP $\gamma$ CD and lecithin were significantly high consequently, lower stability index. The surface tension of  $\alpha$ CD containing pickering NEs was lower than that of respective non-pickering NEs. The entrapment efficiency (%EE) of pickering NEs was higher than non-pickering NEs, especially the formulations composed of high  $\gamma$ CD or HP $\gamma$ CD. This indicated that the increase in %EE resulted in more controlled drug release. For the evaluation of toxicity of AmB, the degree of aggregation behavior and hemolytic activity of developed formulations were performed. These results indicated that the AmB NEs showed lower degree of aggregation and hemolysis than Amphotericin-B<sup>®</sup>. It was found that the developed AmB loaded NEs formulations were safer than the commercial product, Amphotericin-B<sup>®</sup>. The susceptibility against pathogenic fungi was conducted and found that both pickering and non-pickering AmB NEs were superior to the AmB itself and equally effective to *C. albicans*. However, due to the slow release of AmB from the nanotechnology platform they were lower antifungal activity against filamentous fungi when compare to Amphotericin-B<sup>®</sup>. The selected AmB formulations were evaluated the physical and chemical stability studies i.e, freeze-thaw stability, long-term stability and accelerated stability studies. The CD-stabilized AmB pickering NEs showed better stability status than non-pickering NEs especially the formulation stabilized by

$\gamma$ CD. Therefore,  $\gamma$ CD-based pickering NEs containing AmB were potential candidate for further studies.





**APPENDIX A**  
**PHYSICAL STABILITY**

*Table 17 The pH values of AmB NEs storage at accelerated stability condition for 0, 1, 3 and 6 months*

Formulations	n1	n2	n3	Mean	S.D.
<b>0 Month</b>					
F2	4.82	4.88	4.89	4.86	0.04
F6	4.54	4.57	4.56	4.56	0.02
F9	4.91	4.86	4.84	4.87	0.04
F11	4.51	4.67	4.78	4.65	0.14
<b>1 Month</b>					
F2	4.75	4.65	4.54	4.65	0.11
F6	4.38	4.47	4.45	4.43	0.05
F9	4.58	4.51	4.49	4.53	0.05
F11	3.98	4.21	3.91	4.03	0.16
<b>3 Month</b>					
F2	4.63	4.59	4.58	4.60	0.03
F6	4.41	4.37	4.38	4.39	0.02
F9	3.94	3.95	3.89	3.93	0.03
F11	3.61	3.68	3.66	3.65	0.04
<b>6 Month</b>					
F2	4.63	4.55	4.58	4.59	0.04
F6	4.23	4.38	4.45	4.35	0.11
F9	3.66	3.58	3.71	3.65	0.07
F11	3.48	3.42	3.59	3.49	0.09

*Table 18 The pH values of AmB NEs storage at long-term stability condition for 0, 1, 3 and 6 months*

Formulations	n1	n2	n3	Mean	S.D.
<b>0 Month</b>					
F2	4.82	4.88	4.89	4.86	0.04
F6	4.54	4.57	4.56	4.56	0.02
F9	4.91	4.86	4.84	4.87	0.04
F11	4.51	4.67	4.78	4.65	0.14
<b>1 Month</b>					
F2	4.79	4.77	4.56	4.71	0.13
F6	4.41	4.48	4.46	4.45	0.04
F9	4.64	4.60	4.61	4.62	0.02
F11	4.10	4.20	4.15	4.15	0.05
<b>3 Month</b>					
F2	4.65	4.67	4.64	4.65	0.02
F6	4.36	4.43	4.41	4.40	0.04
F9	4.07	4.15	4.12	4.11	0.04
F11	3.68	3.73	3.73	3.71	0.03
<b>6 Month</b>					
F2	4.63	4.62	4.58	4.61	0.03
F6	4.26	4.38	4.45	4.36	0.10
F9	3.86	3.92	3.78	3.85	0.07
F11	3.56	3.61	3.59	3.59	0.03

*Table 19 The average particle size (nm) of AmB NEs storage at accelerated stability condition for 0, 1, 3 and 6 months*

Formulations	n1	n2	n3	Mean	S.D.
<b>0 Month</b>					
F2	260.6	251.5	254.9	255.67	4.60
F6	229.5	232.1	228.9	230.17	1.71
F9	170.5	165.6	168.4	168.17	2.46
F11	200.9	198.6	195.3	198.27	2.81
<b>1 Month</b>					
F2	298.6	284.7	279.4	287.57	9.92
F6	270.7	261.9	259.5	264.03	5.90
F9	241.5	233.5	228.1	234.37	6.74
F11	271.5	286.7	283.9	280.70	8.09
<b>3 Month</b>					
F2	359.7	345.9	374.4	360.02	14.25
F6	369.0	362.4	369.9	367.10	4.10
F9	520.9	507.7	522.1	516.90	7.99
F11	570.9	568.3	526.4	555.20	24.98
<b>6 Month</b>					
F2	372.7	372.9	374.6	373.40	1.04
F6	402.8	397.7	373.0	391.17	15.94
F9	697.4	682.7	695.2	691.67	7.93
F11	658.1	653.1	642.3	651.17	8.08

*Table 20 The average particle size (nm) of AmB NEs storage at long-term stability condition for 0, 1, 3 and 6 months*

Formulations	n1	n2	n3	Mean	S.D.
<b>0 Month</b>					
F2	260.6	251.5	254.9	255.67	4.60
F6	229.5	232.1	228.9	230.17	1.71
F9	170.5	165.6	168.4	168.17	2.46
F11	200.9	198.6	195.3	198.27	2.81
<b>1 Month</b>					
F2	291.6	286.1	283.9	287.20	3.97
F6	267.5	258.1	260.4	262.00	4.90
F9	224.1	212.6	209.3	215.33	7.76
F11	234.1	239.5	229.7	234.43	4.91
<b>3 Month</b>					
F2	321	343.5	352.1	338.87	16.06
F6	357.4	356.3	364.4	359.37	4.39
F9	471.5	482.7	462.9	472.36	9.93
F11	445.3	431.4	435.8	437.50	7.10
<b>6 Month</b>					
F2	367.5	365.7	370.4	367.87	2.37
F6	386.1	393.6	391.2	390.30	3.83
F9	682.2	686	691.2	686.47	4.52
F11	622.8	616.2	621.2	620.07	3.44

*Table 21 The PDI values of AmB NEs storage at accelerated stability condition for 0, 1, 3 and 6 months*

Formulations	n1	n2	n3	Mean	S.D.
<b>0 Month</b>					
F2	0.39	0.43	0.41	0.41	0.02
F6	0.51	0.53	0.52	0.52	0.01
F9	0.50	0.49	0.48	0.49	0.01
F11	0.45	0.44	0.44	0.44	0.01
<b>1 Month</b>					
F2	0.51	0.52	0.51	0.51	0.02
F6	0.58	0.58	0.58	0.58	0.01
F9	0.55	0.55	0.54	0.55	0.01
F11	0.53	0.54	0.52	0.53	0.01
<b>3 Month</b>					
F2	0.59	0.60	0.59	0.59	0.01
F6	0.63	0.67	0.63	0.65	0.02
F9	0.65	0.69	0.73	0.69	0.04
F11	0.61	0.73	0.63	0.66	0.07
<b>6 Month</b>					
F2	0.66	0.63	0.64	0.64	0.02
F6	0.68	0.68	0.66	0.67	0.02
F9	0.79	0.79	0.67	0.75	0.07
F11	0.75	0.77	0.76	0.76	0.09

*Table 22 The PDI values of AmB NEs storage at long-term stability condition for 0, 1, 3 and 6 months*

Formulations	n1	n2	n3	Mean	S.D.
<b>0 Month</b>					
F2	0.39	0.43	0.41	0.41	0.02
F6	0.51	0.53	0.52	0.52	0.01
F9	0.50	0.49	0.48	0.49	0.01
F11	0.45	0.44	0.44	0.44	0.01
<b>1 Month</b>					
F2	0.50	0.51	0.52	0.51	0.01
F6	0.57	0.58	0.58	0.58	0.01
F9	0.55	0.54	0.53	0.54	0.01
F11	0.53	0.53	0.54	0.53	0.01
<b>3 Month</b>					
F2	0.59	0.57	0.59	0.58	0.01
F6	0.62	0.61	0.61	0.61	0.01
F9	0.69	0.69	0.69	0.69	0.01
F11	0.65	0.64	0.64	0.64	0.01
<b>6 Month</b>					
F2	0.65	0.63	0.64	0.64	0.01
F6	0.65	0.65	0.65	0.65	0.02
F9	0.74	0.74	0.74	0.74	0.03
F11	0.73	0.72	0.70	0.72	0.01

*Table 23 The zeta potential values (mV) of AmB NEs storage at accelerated stability condition for 0, 1, 3 and 6 months (n=3, Mean±S.D.)*

Formulations	n1	n2	n3	Mean	S.D.
<b>0 Month</b>					
F2	+33.1	+32.6	+31.9	+32.53	0.60
F6	+31.5	+31.9	+30.4	+31.27	0.78
F9	+35.1	+34.5	+33.9	+34.50	0.60
F11	+31.8	+30.8	+31.5	+31.37	0.51
<b>1 Month</b>					
F2	+30.6	+29.8	+30.4	+30.27	0.42
F6	+27.2	+29.9	+33.0	+30.03	2.90
F9	+31.5	+31.9	+30.8	+31.40	0.56
F11	+27.8	+28.1	+27.7	+27.87	0.21
<b>3 Month</b>					
F2	+30.1	+29.6	+29.8	+29.83	0.25
F6	+28.9	+28.4	+28.1	+28.47	0.40
F9	+17.9	+22.1	+19.5	+19.83	2.12
F11	+16.5	+18.9	+17.6	+17.67	1.20
<b>6 Month</b>					
F2	+28.9	+28.7	+28.1	+28.57	0.42
F6	+28.9	+28.2	+27.6	+28.23	0.65
F9	+14.1	+14.7	+14.9	+14.57	0.42
F11	+12.5	+13.6	+14.9	+13.67	1.21

*Table 24 The zeta potential values (mV) of AmB NEs storage at long-term stability condition for 0, 1, 3 and 6 months*

Formulations	n1	n2	n3	Mean	S.D.
<b>0 Month</b>					
F2	+33.1	+32.6	+31.9	+32.53	0.60
F6	+31.5	+31.9	+30.4	+31.27	0.78
F9	+35.1	+34.5	+33.9	+34.50	0.61
F11	+31.8	+30.8	+31.5	+31.37	0.51
<b>1 Month</b>					
F2	+32.0	+29.1	+30.6	+30.57	1.45
F6	+30.6	+30.7	+30.7	+30.67	0.06
F9	+33.1	+31.9	+32.3	+32.43	0.61
F11	+29.2	+31.4	+28.6	+29.73	1.47
<b>3 Month</b>					
F2	+30.7	+29.9	+29.8	+30.13	0.49
F6	+29.8	+28.6	+30.9	+29.77	1.15
F9	+23.1	+21.1	+20.1	+21.43	1.53
F11	+20.9	+19.8	+18.2	+19.63	1.36
<b>6 Month</b>					
F2	+29.9	+29.7	+29.6	+29.73	0.15
F6	+28.9	+29.2	+27.9	+28.67	0.68
F9	+15.5	+16.6	+17.8	+16.63	1.15
F11	+15.8	+14.2	+16.3	+15.43	1.10



**APPENDIX B**  
**CHEMICAL STABILITY**

*Table 25 The total AmB content (%) of AmB NEs storage at accelerated stability condition for 0, 1, 3 and 6 months*

Formulations	n1	n2	n3	Mean	S.D.
<b>0 Month</b>					
F2	98.89	100.44	99.80	99.71	0.78
F6	99.75	99.64	97.23	98.86	1.44
F9	98.81	98.14	99.50	98.82	0.68
F11	98.88	98.70	100.19	99.23	0.83
<b>1 Month</b>					
F2	95.79	97.95	95.58	96.20	1.31
F6	96.11	95.52	96.88	96.17	0.68
F9	90.37	94.69	86.67	90.52	4.02
F11	90.07	87.53	87.11	88.12	1.60
<b>3 Month</b>					
F2	93.24	95.69	95.08	94.27	1.28
F6	88.91	95.05	95.55	93.17	3.70
F9	66.62	69.51	65.11	68.12	2.23
F11	49.17	53.53	51.02	52.91	2.19
<b>6 Month</b>					
F2	92.39	93.10	89.28	91.59	2.03
F6	91.16	89.45	91.45	90.69	1.08
F9	46.79	53.08	50.96	50.28	3.20
F11	36.42	42.97	41.92	40.44	3.52

*Table 26 The total AmB content (%) of AmB NEs storage at long-term stability condition for 0, 1, 3 and 6 months*

Formulations	n1	n2	n3	Mean	S.D.
<b>0 Month</b>					
F2	98.89	100.44	99.80	99.71	0.78
F6	99.75	99.64	97.23	98.86	1.44
F9	98.81	98.14	99.50	98.82	0.68
F11	98.88	98.70	100.19	99.23	0.83
<b>1 Month</b>					
F2	97.27	95.58	100.02	97.62	2.24
F6	93.15	95.82	99.85	96.27	3.37
F9	90.96	91.73	94.96	92.55	2.12
F11	88.89	88.71	91.26	89.44	1.42
<b>3 Month</b>					
F2	98.94	90.58	96.62	95.51	4.32
F6	95.96	95.55	90.04	94.02	3.30
F9	81.73	75.14	79.47	78.36	3.35
F11	56.82	61.72	62.02	60.54	2.92
<b>6 Month</b>					
F2	95.33	97.21	96.92	94.51	1.01
F6	91.16	94.45	91.45	92.35	1.82
F9	69.12	70.56	76.35	71.80	3.83
F11	43.85	45.03	42.83	43.87	1.10

*Table 27 %EE of AmB NEs storage at accelerated stability condition for 0, 1, 3 and 6 months*

Formulations	n1	n2	n3	Mean	S.D.
<b>0 Month</b>					
F2	94.19	92.01	92.24	92.81	1.19
F6	91.32	91.80	89.69	90.94	1.10
F9	78.53	79.12	78.39	78.68	0.39
F11	81.48	79.56	80.89	80.64	0.98
<b>1 Month</b>					
F2	90.92	90.79	90.54	90.87	0.20
F6	87.12	86.72	88.87	87.57	1.14
F9	60.92	59.88	62.43	61.08	1.28
F11	62.14	61.57	64.11	62.61	1.33
<b>3 Month</b>					
F2	86.88	87.64	85.19	85.43	1.26
F6	82.24	85.89	85.12	83.75	1.92
F9	53.16	60.80	35.69	49.88	12.87
F11	38.48	50.86	34.29	40.20	8.62
<b>6 Month</b>					
F2	84.68	85.85	78.05	82.86	4.21
F6	82.21	78.12	82.90	80.08	3.61
F9	40.91	39.86	42.69	41.16	1.43
F11	23.35	23.15	17.44	21.31	3.36

*Table 28 %EE of AmB NEs storage at long-term stability condition for 0, 1, 3 and 6 months*

Formulations	n1	n2	n3	Mean	S.D.
<b>0 Month</b>					
F2	94.19	92.01	92.24	92.81	1.19
F6	91.32	91.80	89.69	90.94	1.10
F9	78.53	79.12	78.39	78.68	0.39
F11	81.48	79.56	80.89	80.64	0.98
<b>1 Month</b>					
F2	91.67	90.89	91.90	91.02	0.53
F6	89.14	89.49	89.69	89.32	0.28
F9	65.12	62.95	63.57	63.88	1.12
F11	70.16	67.49	64.27	67.31	2.95
<b>3 Month</b>					
F2	88.78	86.98	88.17	87.97	0.91
F6	85.74	85.90	84.94	85.71	0.52
F9	51.33	51.72	52.10	51.74	0.38
F11	50.98	51.44	49.39	50.73	1.08
<b>6 Month</b>					
F2	88.76	89.07	84.20	86.22	2.72
F6	85.53	85.71	84.43	83.04	0.69
F9	46.47	44.15	48.58	45.31	2.22
F11	20.58	28.62	21.54	23.81	4.39

## REFERENCES



จุฬาลงกรณ์มหาวิทยาลัย  
**CHULALONGKORN UNIVERSITY**

1. Mravičić I, Dekaris I, Gabrić N, Romac I, Glavota V, Mlinarić-Missoni E. An overview of fungal keratitis and case report on trichophyton keratitis. *Keratitis: InTechOpen*; 2012:1-14.
2. Ansari Z, Miller D, Galor A. Current thoughts in fungal keratitis: diagnosis and treatment. *Current Fungal Infection Reports*. 2013;7(3):209-18.
3. Bharathi MJ, Ramakrishnan R, Meenakshi R, Padmavathy S, Shivakumar C, Srinivasan M. Microbial keratitis in South India: influence of risk factors, climate, and geographical variation. *Ophthalmic Epidemiology*. 2007;14(2):61-9.
4. Leck A, Thomas P, Hagan M, Kaliamurthy J, Ackuaku E, John M, Newman MJ, Codjoe FS, Opintan JA, Kalavathy CM, Essuman V. Aetiology of suppurative corneal ulcers in Ghana and South India, and epidemiology of fungal keratitis. *British Journal of Ophthalmology*. 2002;86(11):1211-5.
5. Tabatabaee A, Mohajernejhadfard Z, Daneshgar F, Mansouri M. Keratomycosis after incidental spillage of vegetative material into the eye: Report of two cases. *Oman Journal of Ophthalmology*. 2013;6(2):122-6.
6. Wong T-Y, Ng T-P, Fong K-S, Tan D. Risk factors and clinical outcomes between fungal and bacterial keratitis: a comparative study. *The CLAO journal: Official Publication of the Contact Lens Association of Ophthalmologists, Inc*. 1997;23(4):275-81.
7. Foster C. Fungal keratitis. *Infectious Disease Clinics of North America*. 1992;6(4):851-7.
8. Sirikul T, Prabriputaloong T, Smathivat A, Chuck RS, Vongthongsri A. Predisposing factors and etiologic diagnosis of ulcerative keratitis. *Cornea*. 2008;27(3):283-7.
9. Słowik M, Biernat MM, Urbaniak-Kujda D, Kapelko-Słowik K, Misiuk-Hojło M. Mycotic infections of the eye. *Advances in Clinical and Experimental Medicine: Official Organ Wroclaw Medical University*. 2015;24(6):1113-7.
10. Srinivasan M, Gonzales CA, George C, Cevallos V, Mascarenhas JM, Asokan B, Wilkins J, Smolin G, Whitcher JP. Epidemiology and aetiological diagnosis of corneal ulceration in Madurai, South India. *British Journal of Ophthalmology*. 1997;81(11):965-71.
11. Keay LJ, Gower EW, Iovieno A, Oechsler RA, Alfonso EC, Matoba A, Colby K, Tuli SS, Hammersmith K, Cavanagh D, Lee SM. Clinical and microbiological characteristics of fungal keratitis in the United States, 2001–2007: a multicenter study. *Ophthalmology*. 2011;118(5):920-6.

12. Acharya Y, Acharya B, Karki P. Fungal keratitis: study of increasing trend and common determinants. *Nepal Journal of Epidemiology*. 2017;7(2):685-93.
13. Nielsen SE, Nielsen E, Julian HO, Lindegaard J, Hojgaard K, Ivarsen A, Hjortdal J, Heegaard S. Incidence and clinical characteristics of fungal keratitis in a Danish population from 2000 to 2013. *ACTA Ophthalmologica*. 2015;93(1):54-8.
14. Sun RL, Jones DB, Wilhelmus KR. Clinical characteristics and outcome of *Candida* keratitis. *American Journal of Ophthalmology*. 2007;143(6):1043-5.
15. Gupta N, Tandon R. Investigative modalities in infectious keratitis. *Indian Journal of Ophthalmology*. 2008;56(3):209-13.
16. Nada W, Borai A, Alsawad M. Different modalities of antifungal agents in the treatment of fungal keratitis: a retrospective study. *Journal of Clinical and Experimental Ophthalmology*. 2017;8(1):1-4.
17. Anya M. Supramolecular lipid drug delivery systems: from laboratory to clinic: a review of the recently introduced commercial liposomal and lipid based formulations of amphotericin B. *Advanced Drug Delivery Reviews*. 1997;24(2-):345-63.
18. Hartsel S, Bolard J. Amphotericin B: new life for an old drug. *Trends in Pharmacological Sciences*. 1996;17(12):445-9.
19. Muller GG, Kara-Jose N, De Castro RS. Antifungals in eye infections: drugs and routes of administration. *Revista Brasileira de Oftalmologia*. 2013; 72 (2):132-41.
20. Bolard J. Mechanism of action of an anti-*Candida* drug: amphotericin B and its derivatives. *Candida Albicans: Cellular and Molecular Biology*. 1991.214-38.
21. Silva AE, Barratt G, Chéron M, Egito EST. Development of oil-in-water microemulsions for the oral delivery of amphotericin B. *International Journal of Pharmaceutics*. 2013;454(2):641-8.
22. Silberberg M. Cyclodextrin as a drug carrier increasing drug solubility. *The Science Journal of the Lander College of Arts and Sciences*. 2017;11(1):28-35.
23. Loftsson T, Brewster ME. Cyclodextrins as functional excipients: methods to enhance complexation efficiency. *Journal of Pharmaceutical Sciences*. 2012;101(9):3019-32.
24. Jansook P, Moya-Ortega MD, Loftsson T. Effect of self-aggregation of  $\gamma$ -cyclodextrin on drug solubilization. *Journal of Inclusion Phenomena and Macrocyclic Chemistry*. 2010;68(1):229-36.

25. Loftsson T, Brewster ME. Pharmaceutical applications of cyclodextrins. 1. drug solubilization and stabilization. *Journal of Pharmaceutical Sciences*. 1996;85(10):1017-25.
26. Rajewski RA, Stella VJ. Pharmaceutical applications of cyclodextrins. 2. *In vivo* drug delivery. *Journal of Pharmaceutical Sciences*. 1996;85(11):1142-69.
27. Tollemar J, Klingspor L, Ringden O. Liposomal amphotericin B (AmBisome) for fungal infections in immunocompromised adults and children. *Clinical Microbiology and Infection*. 2001;(7)68-79.
28. Chhonker YS, Prasad YD, Chandasana H, Vishvkarma A, Mitra K, Shukla PK, Bhatta RS. Amphotericin-B entrapped lecithin/chitosan nanoparticles for prolonged ocular application. *International Journal of Biological Macromolecules*. 2015;72:1451-8.
29. Zu Y, Sun W, Zhao X, Wang W, Li Y, Ge Y, Liu Y, Wang K. Preparation and characterization of amorphous amphotericin B nanoparticles for oral administration through liquid antisolvent precipitation. *European Journal of Pharmaceutical Sciences*. 2014;53:109-17.
30. Goldblum D, Frueh BE, Zimmerli S, Böhnke M. Treatment of postkeratitis fusarium endophthalmitis with amphotericin B lipid complex. *Cornea*. 2000;19(6):853-6.
31. Green WR, Bennett JE, Goos RD. Ocular penetration of amphotericin B: a report of laboratory studies and a case report of postsurgical cephalosporium endophthalmitis. *Archives of Ophthalmology*. 1965;73(6):769-75.
32. Kaur IP, Rana C, Singh H. Development of effective ocular preparations of antifungal agents. *Journal of Ocular Pharmacology and Therapeutics*. 2008;24(5):481-94.
33. O'Day DM, Head WS, Robinson RD, Stern WH, Freeman JM. Intraocular penetration of systemically administered antifungal agents. *Current Eye Research*. 1985;4(2):131-4.
34. O'Day DM. Selection of appropriate antifungal therapy. *Cornea*. 1987;6(4):238-45.
35. O'Day DM, Ray WA, Robinson RD, Head WS, Williams TE. Differences in response in vivo to amphotericin B among *Candida albicans* strains. *Investigative Ophthalmology and Visual Science*. 1991;32(5):1569-72.
36. Schwartz SD, Harrison SA, Engstrom Jr RE, Bawdon RE, Lee DA, Mondino BJ. Collagen shield delivery of amphotericin B. *American Journal of Ophthalmology*. 1990;109(6):701-4.



37. Kaushik S, Ram J, Brar GS, Jain AK, Chakraborti A, Gupta A. Intracameral amphotericin B: initial experience in severe keratomycosis. *Cornea*. 2001;20(7):715-9.
38. Kuriakose T, Kothari M, Paul P, Jacob P, Thomas R. Intracameral amphotericin B injection in the management of deep keratomycosis. *Cornea*. 2002;21(7):653-6.
39. Yilmaz S, Ture M, Maden A. Efficacy of intracameral amphotericin B injection in the management of refractory keratomycosis and endophthalmitis. *Cornea*. 2007;26(4):398-402.
40. Qu L, Li L, Xie H. Corneal and aqueous humor concentrations of amphotericin B using three different routes of administration in a rabbit model. *Ophthalmic Research*. 2010;43(3):153-8.
41. Pleyer U, Grammer J, Pleyer J, Kosmidis P, Friess D, Schmidt K, Thiel HJ. Amphotericin B-bioavailability in the cornea. Studies with local administration of liposome incorporated amphotericin B. *Der Ophthalmologe: Zeitschrift der Deutschen Ophthalmologischen Gesellschaft*. 1995;92(4):469-75.
42. O'day DM, Head WS, Robinson RD, Clanton JA. Corneal penetration of topical amphotericin B and natamycin. *Current Eye Research*. 1986;5(11):877-82.
43. O'day DM, Ray WA, Head WS, Robinson RD. Influence of the corneal epithelium on the efficacy of topical antifungal agents. *Investigative Ophthalmology and Visual Science*. 1984;25(7):855-9.
44. Glavas-Dodov M, Fredro-Kumbaradzi E, Goracinova K, Simonoska M, Calis S, Trajkovic-Jolevska S, Hincal AA. The effects of lyophilization on the stability of liposomes containing 5-FU. *International Journal of Pharmaceutics*. 2005;291(1-2):79-86.
45. Sarbolouki M, Toliat T. Storage stability of stabilized MLV and REV liposomes containing sodium methotrexate (aqueous and lyophilized). *PDA Journal of Pharmaceutical Science and Technology*. 1998;52(1):23-7.
46. Brandl M. Liposomes as drug carriers: a technological approach. *Biotechnology Annual Review*. 2001;7:59-85.
47. Marquez R, Forgiarini AM, Langevin D, Salager J-L. Instability of emulsions made with surfactant-oil-water systems at optimum formulation with ultralow interfacial tension. *Langmuir*. 2018;34(31):9252-63.
48. Li X, Li H, Xiao Q, Wang L, Wang M, Lu X, York P, Shi S, Zhang J. Two-way effects of surfactants on pickering emulsions stabilized by the self-assembled microcrystals of  $\alpha$ -cyclodextrin and oil. *Physical Chemistry Chemical Physics*. 2014;16(27):144059-69.

49. Aveyard R, Binks BP, Clint JH. Emulsions stabilised solely by colloidal particles. *Advances in Colloid and Interface Science*. 2003;100:503-46.
50. Binks BP. Particles as surfactants-similarities and differences. *Current Opinion in Colloid and Interface Science*. 2002;7(1-2):21-41.
51. Marku D, Wahlgren M, Rayner M, Sjöö M, Tingren A. Characterization of starch pickering emulsions for potential applications in topical formulations. *International Journal of Pharmaceutics*. 2012;428(1-2):1-7.
52. Hu JW, Yen MW, Wang AJ, Chu IM. Effect of oil structure on cyclodextrin-based pickering emulsions for bupivacaine topical application. *Colloids and Surfaces B: Biointerfaces*. 2018;161:51-8.
53. Du Sorbier QM, Aimable A, Pagnoux C. Influence of the electrostatic interactions in a pickering emulsion polymerization for the synthesis of silica-polystyrene hybrid nanoparticles. *Journal of Colloid and Interface Science*. 2015;448:306-14.
54. Mathapa BG, Paunov VN. Cyclodextrin stabilised emulsions and cyclodextrinosomes. *Physical Chemistry Chemical Physics*. 2013;15(41):17903-14.
55. Inoue M, Hashizaki K, Taguchi H, Saito Y. Preparation and characterization of n-alkane/water emulsion stabilized by cyclodextrin. *Journal of Oleo Science*. 2009;58(2):85-90.
56. Davarpanah L, Vahabzadeh F. Formation of oil-in-water (o/w) pickering emulsions via complexation between  $\beta$ -cyclodextrin and selected organic solvents. *Starch-Stärke*. 2012;64(11):898-913.
57. Hashizaki K, Kageyama T, Inoue M, Taguchi H, Saito Y. Preparation and characterization of cycloalkanol/water emulsion using  $\alpha$ -cyclodextrin as an emulsifier. *Journal of Dispersion Science and Technology*. 2009;30(6):852-6.
58. Hashizaki K, Kageyama T, Inoue M, Taguchi H, Ueda H, Saito Y. Study on preparation and formation mechanism of n-alkanol/water emulsion using  $\alpha$ -cyclodextrin. *Chemical and Pharmaceutical Bulletin*. 2007;55(11):1620-5.
59. Cheong AM, Tan KW, Tan CP, Nyam KL. Kenaf (*Hibiscus cannabinus* L.) seed oil-in-water pickering nanoemulsions stabilised by mixture of sodium caseinate, tween 20 and  $\beta$ -cyclodextrin. *Food Hydrocolloids*. 2016;52:934-41.
60. Mathapa BG, Paunov VN. Self-assembly of cyclodextrin-oil inclusion complexes at the oil-water interface: a route to surfactant-free emulsions. *Journal of Materials Chemistry A*. 2013;1(36):10836-46.

61. Shimada KA, Kawano KI, Ishii JU, Nakamura TA. Structure of inclusion complexes of cyclodextrins with triglyceride at vegetable oil/water interface. *Journal of Food Science*. 1992;57(3):655-6.
62. Yang F, Liu S, Xu J, Lan Q, Wei F, Sun D. Pickering emulsions stabilized solely by layered double hydroxides particles: the effect of salt on emulsion formation and stability. *Journal of Colloid and Interface Science*. 2006;302(1):159-69.
63. Rai M, Grupenmacher A, Ingle AP, Paralikar P, Gupta I, Alves M. Evolving nanotechnological trends in the management of mycotic keratitis. *IET Nanobiotechnology*. 2019;13(5):464-70.
64. Shukla P, Kumar M, Keshava G. Mycotic keratitis: an overview of diagnosis and therapy. *Mycoses*. 2008;51(3):183-99.
65. Keay L, Edwards K, Naduvilath T, Taylor HR, Snibson GR, Forde K, Stapleton F. Microbial keratitis: predisposing factors and morbidity. *Ophthalmology*. 2006;113(1):109-16.
66. Agrawal P, Lal B, Shukla P, Khan Z, Srivastava O. Clinical and experimental keratitis due to *Curvularia lunata* (Wakker) Boedijn var. *aeria* (Batista, Lima and Vasconcelos) Ellis. *Sabouraudia*. 1982;20(3):225-32.
67. Shukla P, Khan Z, Lal B, Agrawal P, Srivastava O. Clinical and experimental keratitis caused by the *Colletotrichum* state of *Glomerella cingulata* and *Acrophialophora fuispora*. *Sabouraudia*. 1983;21(2):137-47.
68. Mahmoudi S, Masoomi A, Ahmadikia K, Tabatabaei SA, Soleimani M, Rezaie S, Ghahvechian H, Banafsheafshan A. Fungal keratitis: an overview of clinical and laboratory aspects. *Mycoses*. 2018;61(12):916-30.
69. Caffrey P, Lynch S, Flood E, Finnan S, Oliynyk M. Amphotericin biosynthesis in *Streptomyces nodosus*: deductions from analysis of polyketide synthase and late genes. *Chemistry and Biology*. 2001;8(7):713-23.
70. Ellis D. Amphotericin B: spectrum and resistance. *Journal of Antimicrobial Chemotherapy*. 2002;49(1):7-10.
71. Mesa-Arango AC, Scorzoni L, Zaragoza O. It only takes one to do many jobs: Amphotericin B as antifungal and immunomodulatory drug. *Frontiers in Microbiology*. 2012;3(286): 1-10.
72. Diaz AA, Tripp MC, Zertuche MF, Romero JD, Montejo FE, Buitimea AL, Nava RM, Martinez LO, Blake IO, Esparza JA, Frangoso MD, inventors. Amphotericin analogous compounds and pharmaceutical compositions containing them. United States Patent Application. 2014:1-28.

73. Brajtburg J, Powderly WG, Kobayashi GS, Medoff G. Amphotericin B: current understanding of mechanisms of action. *Antimicrobial Agents and Chemotherapy*. 1990;34(2):183-8.
74. Pitkanen L, Ranta VP, Moilanen H, Urtti A. Permeability of retinal pigment epithelium: effects of permeant molecular weight and lipophilicity. *Investigative Ophthalmology and Visual Science*. 2005;46(2):641-6.
75. Klyce SD, Crosson CE. Transport processes across the rabbit corneal epithelium: a review. *Current Eye Research*. 1985;4(4):323-31.
76. McLaughlin BJ, Caldwell RB, Sasaki Y, Wood TO. Freeze-fracture quantitative comparison of rabbit corneal epithelial and endothelial membranes. *Current Eye Research*. 1985;4(9):951-61.
77. Barar J, Javadzadeh AR, Omid Y. Ocular novel drug delivery: impacts of membranes and barriers. *Expert Opinion on Drug Delivery*. 2008;5(5):567-81.
78. Sunkara G, Kompella U. Membrane transport processes in the eye. *In Ophthalmic Drug Delivery Systems*: CRC Press. 2003: 34-79.
79. Saha P, Kim KJ, Lee VH. A primary culture model of rabbit conjunctival epithelial cells exhibiting tight barrier properties. *Current Eye Research*. 1996;15(12):1163-9.
80. Alvarez-Trabado J, Diebold Y, Sanchez A. Designing lipid nanoparticles for topical ocular drug delivery. *International Journal of Pharmaceutics*. 2017;532(1):204-17.
81. Urtti A, Salminen L. Minimizing systemic absorption of topically administered ophthalmic drugs. *Survey of Ophthalmology*. 1993;37(6):435-56.
82. Loftsson T, Stefánsson E. Effect of cyclodextrins on topical drug delivery to the eye. *Drug Development and Industrial Pharmacy*. 2008;23(5):473-81.
83. Loftsson T, Stefánsson E. Cyclodextrins and topical drug delivery to the anterior and posterior segments of the eye. *International Journal of Pharmaceutics*. 2017;531(2):413-23.
84. Loftsson T, Duchêne D. Cyclodextrins and their pharmaceutical applications. *International Journal of Pharmaceutics*. 2007;329(1):1-11.
85. Loftsson T, Jarho P, Masson M, Jarvinen T. Cyclodextrins in drug delivery. *Expert Opinion on Drug Delivery*. 2005;2(2):335-51.
86. Saokham P, Muankaew C, Jansook P, Loftsson T. Solubility of cyclodextrins and drug/cyclodextrin complexes. *Molecules*. 2018;23(5):1-15.
87. Frank DW, Gray JE, Weaver RN. Cyclodextrin nephrosis in the rat. *The American Journal of Pathology*. 1976;83(2):367-82.

88. Welliver M, McDonough J. Anesthetic related advances with cyclodextrins. *The Scientific World Journal*. 2007;83(7):364-71.
89. Connors K, Higuchi T. Phase solubility techniques. *Advances in Analytical Chemistry and Instrumentation*. 1965;4(2):117-212.
90. Brewster M, Loftsson T. Complexation-use of cyclodextrins to improve pharmaceutical properties of intramuscular formulations. *Injectable Drug Development Techniques to Reduce Pain and Irritation* Interpharm Press, Denver, CO. 1999:307-36.
91. Brewster ME, Loftsson T. Cyclodextrins as pharmaceutical solubilizers. *Advanced Drug Delivery Reviews*. 2007;59(7):645-66.
92. Loftsson T, Hreinsdóttir D, Másson M. The complexation efficiency. *Journal of Inclusion Phenomena and Macrocyclic Chemistry*. 2007;57(1-4):545-52.
93. Keipert S, Fedder J, Böhm A, Hanke B. Interactions between cyclodextrins and pilocarpine as an example of a hydrophilic drug. *International Journal of Pharmaceutics*. 1996;142(2):153-62.
94. Schuette JM, Warner IM. Structural considerations and fluorescence spectral definition of cyclodextrin/perylene complexes in the presence of 1-pentanol. *Talanta*. 1994;41(5):647-9.
95. Yousef F, Zughul M, Badwan A. The modes of complexation of benzimidazole with aqueous  $\beta$ -cyclodextrin explored by phase solubility, potentiometric titration,  $^1\text{H-NMR}$  and molecular modeling studies. *Journal of Inclusion Phenomena and Macrocyclic Chemistry*. 2007;57(1-4):519-23.
96. Mura P. Analytical techniques for characterization of cyclodextrin complexes in aqueous solution: a review. *Journal of Pharmaceutical and Biomedical Analysis*. 2014;101:238-50.
97. Loftsson T, Másson M, Sigurdsson HH. Cyclodextrins and drug permeability through semi-permeable cellophane membranes. *International Journal of Pharmaceutics*. 2002;232(1-2):35-43.
98. Anand S, Braga VML. Cyclodextrins in ocular drug delivery. *Nano-Biomaterials For Ophthalmic Drug Delivery*. 2016:243-52.
99. Reer O, Bock TK, Muller BW. In vitro corneal permeability of diclofenac sodium in formulations containing cyclodextrins compared to the commercial product voltaren ophtha. *Journal of Pharmaceutical Sciences*. 1994;83(9):1345-9.
100. Suhonen P, Järvinen T, Lehmuusaari K, Reunamäki T, Urtti A. Ocular absorption and irritation of pilocarpine prodrug is modified with buffer, polymer, and cyclodextrin in the eyedrop. *Pharmaceutical Research*. 1995;12(4):529-33.

101. Loftsson T, Brewster ME. Pharmaceutical applications of cyclodextrins: effects on drug permeation through biological membranes. *The Journal of Pharmacy and Pharmacology*. 2011;63(9):1119-35.
102. Uekama K, Adachi H, Irie T, Yano T, Saita M, Noda K. Improved transdermal delivery of prostaglandin E1 through hairless mouse skin: combined use of carboxymethyl-ethyl-beta-cyclodextrin and penetration enhancers. *The Journal of Pharmacy and Pharmacology*. 1992;44(2):119-21.
104. Loftsson T, Jansook P, Stefánsson E. Topical drug delivery to the eye: Dorzolamide. *ACTA Ophthalmologica*. 2012;90(7):603-608.
105. McClements DJ. Advances in fabrication of emulsions with enhanced functionality using structural design principles. *Current Opinion in Colloid and Interface Science*. 2012;17(5):235-45.
106. Pickering SU. CXCVI.-Emulsions. *Journal of the Chemical Society, Transactions*. 1907;91(0):2001-21.
107. Chevalier Y, Bolzinger MA. Emulsions stabilized with solid nanoparticles: Pickering emulsions. *Colloids and Surfaces A: Physicochemical and Engineering Aspects*. 2013;439:23-34.
108. Yang Y, Fang Z, Chen X, Zhang W, Xie Y, Chen Y, Liu Z, Yuan W. An overview of pickering emulsions: solid-particle materials, classification, morphology, and applications. *Frontiers in Pharmacology*. 2017;287(8):1-20.
109. Monegier du Sorbier Q, Aimable A, Pagnoux C. Influence of the electrostatic interactions in a pickering emulsion polymerization for the synthesis of silica-polystyrene hybrid nanoparticles. *Journal of Colloid and Interface Science*. 2015;448:306-14.
110. Miller R, Fainerman VB, Kovalchuk VI, Grigoriev DO, Leser ME, Michel M. Composite interfacial layers containing micro-size and nano-size particles. *Advances in Colloid and Interface Science*. 2006;(128-130):17-26.
111. Leclercq L, Nardello-Rataj V. Pickering emulsions based on cyclodextrins: a smart solution for antifungal azole derivatives topical delivery. *European Journal of Pharmaceutical Sciences*. 2016;82:126-37.
112. Loftsson T, Hreinsdóttir D, Másson M. Evaluation of cyclodextrin solubilization of drugs. *International Journal of Pharmaceutics*. 2005;302(1-2):18-28.
113. Jansook P, Fulop Z, Ritthidej GC. Amphotericin B loaded solid lipid nanoparticles (SLNs) and nanostructured lipid carrier (NLCs): physicochemical and solid-solution state characterizations. *Drug Development and Industrial Pharmacy*. 2019;45(4):560-7.

114. Bai L, Huan S, Xiang W, Rojas O. Pickering emulsions by combining cellulose nanofibrils and nanocrystals: Phase behavior and depletion stabilization. *Green Chemistry*. 2018;20(7):1571-82.
115. Jansook P, Pichayakorn W, Ritthidej GC. Amphotericin B-loaded solid lipid nanoparticles (SLNs) and nanostructured lipid carrier (NLCs): effect of drug loading and biopharmaceutical characterizations. *Drug Development and Industrial Pharmacy*. 2018;44(10):1693-700.
116. Zhu XF, Zhang N, Lin WF, Tang CH. Freeze-thaw stability of pickering emulsions stabilized by soy and whey protein particles. *Food Hydrocolloids*. 2017;69:173-84.
117. Guideline IHT. Stability testing of new drug substances and products. Q1A (R2), Current Step. 2003;4:1-24.
118. Lemke A, Kiderlen AF, Kayser O. Amphotericin B. *Applied Microbiology and Biotechnology*. 2005;68(2):151-62.
119. Rajagopalan N, Chen SC, Chow W-S. A study of the inclusion complex of amphotericin B with  $\gamma$ -cyclodextrin. *International Journal of Pharmaceutics*. 1986;29(2):161-8.
120. Jansook P, Kurkov SV, Loftsson T. Cyclodextrins as solubilizers: formation of complex aggregates. *Journal of Pharmaceutical Sciences*. 2010;99(2):719-29.
121. Jambhekar SS, Breen P. Cyclodextrins in pharmaceutical formulations I: structure and physicochemical properties, formation of complexes, and types of complex. *Drug Discovery Today*. 2016;21(2):356-62.
122. Cannon JB, Shi Y, Gupta P. Emulsions, microemulsions, and lipid-based drug delivery systems for drug solubilization and delivery-Part I: parenteral applications. *Water-Insoluble Drug Formulation: CRC Press*; 2018. 211-45.
123. Land LM, Li P, Bummer PM. The influence of water content of triglyceride oils on the solubility of steroids. *Pharmaceutical Research*. 2005;22(5):784-8.
124. Li P, Hynes SR, Haefele TF, Pudipeddi M, Royce AE, Serajuddin AT. Development of clinical dosage forms for a poorly water-soluble drug II: formulation and characterization of a novel solid microemulsion preconcentrate system for oral delivery of a poorly water-soluble drug. *Journal of Pharmaceutical Sciences*. 2009;98(5):1750-64.
125. Prajapati H, Patel D, Patel N, Dalrymple D, Serajuddin A. Effect of difference in fatty acid chain lengths of medium-chain lipids on lipid/surfactant/water phase diagrams and drug solubility. *Journal of Excipients and Food Chemicals*. 2011;2(3):73-88.

126. Lo JT, Lee TM, Chen BH. Nonionic microemulsions as solubilizers of hydrophobic drugs: solubilization of paclitaxel. *Materials*. 2016;761(9):1-13.
127. Patton JS, Stone B, Papa C, Abramowitz R, Yalkowsky SH. Solubility of fatty acids and other hydrophobic molecules in liquid trioleoylglycerol. *Journal of Lipid Research*. 1984;25(2):189-97.
128. Ibrahim SS. The role of surface active agents in ophthalmic drug delivery: a comprehensive review. *Journal of Pharmaceutical Sciences*. 2019;108(6):1923-33.
129. Mobasheri M, Attar H, Rezayat Sorkhabadi SM, Khamesipour A, Jaafari MR. Solubilization behavior of polyene antibiotics in nanomicellar system: insights from molecular dynamics simulation of the amphotericin B and nystatin interactions with polysorbate 80. *Molecules*. 2015;21(1):1-6.
130. Matsuoka S, Matsumori N, Murata M. Amphotericin B-phospholipid covalent conjugates: dependence of membrane-permeabilizing activity on acyl-chain length. *Organic and Biomolecular Chemistry*. 2003;1(22):3882-4.
131. Adamski Z, Rybska E, Błoszyk J. Pros and cons of scanning electron microscopy as a research method in acarology. *Current Microscopy Contributions to Advances in Science and Technology*. 2012:215-21.
132. Forfang K, Zimmermann B, Kosa G, Kohler A, Shapaval V. FTIR spectroscopy for evaluation and monitoring of lipid extraction efficiency for oleaginous Fungi. *PloS One*. 2017;12(1):e0170611.
133. Lahiani-Skiba M, Boulet Y, Youm I, Bounoure F, Vérité P, Arnaud P, Skiba M. Interaction between hydrophilic drug and  $\alpha$ -cyclodextrins: physicochemical aspects. *Journal of Inclusion Phenomena and Macrocyclic Chemistry*. 2007;57(1):211-7.
134. Rakmai J, Cheirsilp B, Cid A, Torrado Agrasar A, Mejuto J, Simal-Gandara J. Encapsulation of essential oils by cyclodextrins: Characterization and Evaluation. *Cyclodextrin: A Versatile Ingredient*. 2018:263-282.
135. Terekhova IV, Kumeev RS, Alper GA. Inclusion complex formation of  $\alpha$ -and  $\beta$ -cyclodextrins with aminobenzoic acids in aqueous solution studied by  $^1\text{H}$  NMR. *Journal of Inclusion Phenomena and Macrocyclic Chemistry*. 2007;59(3-4):301-6.
136. Anaya-Castro MA, Ayala-Zavala JF, Muñoz-Castellanos L, Hernández-Ochoa L, Peydecastaing J, Durrieu V.  $\beta$ -Cyclodextrin inclusion complexes containing clove (*Eugenia caryophyllata*) and Mexican oregano (*Lippia berlandieri*) essential oils: preparation,



physicochemical and antimicrobial characterization. *Food Packaging and Shelf Life*. 2017;14:96-101.

137. Kim YT, Shin BK, Garripelli VK, Kim JK, Davaa E, Jo S, Park JS. A thermosensitive vaginal gel formulation with HPgammaCD for the pH dependent release and solubilization of amphotericin B. *European Journal of Pharmaceutical Sciences*. 2010;41(2):399-406.

138. Angra PK, Oettinger C, Balakrishna Pai S, D'Souza MJ. Amphotericin B microspheres: a therapeutic approach to minimize toxicity while maintaining antifungal efficacy. *Journal of Microencapsulation*. 2009;26(7):580-7.

139. Ruiz HK, Serrano DR, Dea-Ayuela MA, Bilbao-Ramos PE, Bolas-Fernandez F, Torrado JJ, Molero G. New amphotericin B-gamma cyclodextrin formulation for topical use with synergistic activity against diverse fungal species and *Leishmania* spp. *International Journal of Pharmaceutics*. 2014;473(1-2):148-57.

140. Chhonker YS, Prasad YD, Chandasana H, Vishvkarma A, Mitra K, Shukla PK, Bhatta RS. Amphotericin-B entrapped lecithin/chitosan nanoparticles for prolonged ocular application. *International Journal of Biological Macromolecules*. 2015;72:1451-8.

141. Schwartzman G, Asher I, Folen V, Brannon W, Taylor J. Ambiguities in IR and X-Ray characterization of amphotericin B. *Journal of Pharmaceutical Sciences*. 1978;67(3):398-400.

142. Jansook P, Ritthidej GC, Ueda H, Stefansson E, Loftsson T. yCD/HPyCD mixtures as solubilizer: solid-state characterization and sample dexamethasone eye drop suspension. *Journal of Pharmacy and Pharmaceutical Sciences*. 2010;13(3):336-50.

143. Li S, Yuan L, Chen Y, Zhou W, Wang X. Studies on the inclusion complexes of daidzein with  $\beta$ -cyclodextrin and derivatives. *Molecules*. 2017;22(12):1-11.

144. Choi KC, Bang JY, Kim PI, Kim C, Song CE. Amphotericin B-incorporated polymeric micelles composed of poly(d,l-lactide-co-glycolide)/dextran graft copolymer. *International Journal of Pharmaceutics*. 2008;355(1-2):224-30.

145. Jansook P, Kulsirachote P, Loftsson T. Cyclodextrin solubilization of celecoxib: solid and solution state characterization. *Journal of Inclusion Phenomena and Macrocyclic Chemistry*. 2018;90(1):75-88.

146. Inoue Y, Hirano A, Murata I, Kobata K, Kanamoto I. Assessment of the physical properties of inclusion complexes of forchlorfenuron and gamma-cyclodextrin derivatives and their promotion of plant growth. *American Chemical Society Omega*. 2018;3(10):13160-9.

147. Nagarsenker MS, Joshi MS. Celecoxib-cyclodextrin systems: characterization and evaluation of *in vitro* and *in vivo* advantage. *Drug Development and Industrial Pharmacy*. 2005;31(2):169-78.
148. Wu L, Liao Z, Liu M, Yin X, Li X, Wang M, Lu X, Lv N, Singh V, He Z, Li H. Fabrication of non-spherical pickering emulsion droplets by cyclodextrins mediated molecular self-assembly. *Colloids and Surfaces A: Physicochemical and Engineering Aspects*. 2016;490:163-72.
149. Ibrahim MM, Abd-Elgawad A-EH, Soliman OA-E, Jablonski MM. Natural bioadhesive biodegradable nanoparticle-based topical ophthalmic formulations for management of glaucoma. *Translational Vision Science and Technology*. 2015;4(3):1-13.
150. World Health Organization. WHO model prescribing information: drugs used in HIV-related infections. Geneva: World Health Organization; 1999.
151. Ravikumar P. InSitu ophthalmic gel forming solution of moxifloxacin hydrochloride for sustained ocular delivery. *International Journal of Pharmaceutical Sciences and Research*. 2016;7(3):192-205.
152. Frisch D, Eyring H, Kincaid JF. Pressure and temperature effects on the viscosity of liquids. *Journal of Applied Physics*. 1940;11(1):75-80.
153. Jansook P, Pichayakorn W, Muankaew C, Loftsson T. Cyclodextrin-poloxamer aggregates as nanocarriers in eye drop formulations: dexamethasone and amphotericin B. *Drug Development and Industrial Pharmacy*. 2016;42(9):1446-54.
154. Harada A, Hashidzume A, Yamaguchi H, Takashima Y. Polymeric rotaxanes. *Chemical Reviews*. 2009;109(11):5974-6023.
155. Kramer I, Haber M, Duis A. Formulation requirements for the ophthalmic use of antiseptics. *Development in Ophthalmology*. 2002;33:85-116.
156. Fathalla ZM, Khaled KA, Hussein AK, Alany RG, Vangala A. Formulation and corneal permeation of ketorolac tromethamine-loaded chitosan nanoparticles. *Drug Development and Industrial Pharmacy*. 2016;42(4):514-24.
157. Finkle P, Draper HD, Hildebrand JH. The theory of emulsification1. *Journal of the American Chemical Society*. 1923;45(12):2780-8.
158. Schulman JH, Leja J. Control of contact angles at the oil-water-solid interfaces. Emulsions stabilized by solid particles ( $\text{BaSO}_4$ ). *Transactions of the Faraday Society*. 1954;50:598-605.
159. Lee MN, Chan HK, Mohraz A. Characteristics of pickering emulsion gels formed by droplet bridging. *Langmuir*. 2011;28(6):3085-91.

160. Moriyama H, Saito Y, Bagchi D. Characterization of cyclodextrin nanoparticles as emulsifiers. *Bio-Nanotechnology: A Revolution in Food, Biomedical and Health Sciences*. 2013;476-86.
161. Cheong AM, Nyam KL. Improvement of physical stability of kenaf seed oil-in-water nanoemulsions by addition of  $\beta$ -cyclodextrin to primary emulsion containing sodium caseinate and tween 20. *Journal of Food Engineering*. 2016;183:24-31.
162. Song X, Pei Y, Qiao M, Ma F, Ren H, Zhao Q. Preparation and characterizations of pickering emulsions stabilized by hydrophobic starch particles. *Food Hydrocolloids*. 2015;45:256-63.
163. Wang S, He Y, Zou Y. Study of Pickering emulsions stabilized by mixed particles of silica and calcite. *Particuology*. 2010;8(4):390-3.
164. Danaei M, Dehghankhold M, Ataei S, Hasanzadeh Davarani F, Javanmard R, Dokhani A, Khorasani S, Mozafari MR. Impact of particle size and polydispersity index on the clinical applications of lipidic nanocarrier systems. *Pharmaceutics*. 2018;10(2):1-17.
165. Tavernier I, Patel AR, Van der Meeren P, Dewettinck K. Emulsion-templated liquid oil structuring with soy protein and soy protein:  $\kappa$ -carrageenan complexes. *Food Hydrocolloids*. 2017;65:107-20.
166. Schuh R, Bruxel F, Teixeira H. Physicochemical properties of lecithin-based nanoemulsions obtained by spontaneous emulsification or high-pressure homogenization. *Química Nova*. 2014;37(7):1193-8.
167. Dhakar RC. From formulation variables to drug entrapment efficiency of microspheres: a technical review. *Journal of Drug Delivery and Therapeutics*. 2012;2:128-33.
168. Thakkar H, Sharma RK, Mishra AK, Chuttani K, Murthy RR. Albumin microspheres as carriers for the antiarthritic drug celecoxib. *The American Association of Pharmaceutical Scientists*. 2005;6(1):E65-73.
169. Iyer V, Cayatte C, Guzman B, Schneider-Ohrum K, Matuszak R, Snell A, Rajani GM, McCarthy MP, Muralidhara B. Impact of formulation and particle size on stability and immunogenicity of oil-in-water emulsion adjuvants. *Human Vaccines and Immunotherapeutics*. 2015;11(7):1853-64.
170. Wang CH, Wang WT, Hsiue GH. Development of polyion complex micelles for encapsulating and delivering amphotericin B. *Biomaterials*. 2009;30(19):3352-8.
171. Boudet G, Bolard J. Interaction of the polyene antibiotic amphotericin B with phospholipid bilayer membranes: a circular dichroism study. *Biochemical and Biophysical Research Communications*. 1979;88(3):998-1002.

172. Espuelas MS, Legrand P, Cheron M, Barratt G, Puisieux F, Devissaguet JP, Irache JM. Interaction of amphotericin B with polymeric colloids: A spectroscopic study. *Colloids and Surfaces B: Biointerfaces*. 1998;11(3):141-51.
173. Charvalos E, Tzatzarakis MN, Van Bambeke F, Tulkens PM, Tsatsakis AM, Tzanakakis GN, Mingeot-Leclercq MP. Water-soluble amphotericin B-polyvinylpyrrolidone complexes with maintained antifungal activity against *Candida* spp. and *Aspergillus* spp. and reduced haemolytic and cytotoxic effects. *Journal of Antimicrobial Chemotherapy*. 2005;57(2):236-44.
174. Hemenger R, Kaplan T, Gray L. Structure of amphotericin B aggregates based on calculations of optical spectra. *Biopolymers: Original Research on Biomolecules*. 1983;22(3):911-8.
175. Kajtar M, Vikmon M, Morlin E, Szejtli J. Aggregation of amphotericin B in the presence of gamma-cyclodextrin. *Biopolymers*. 1989;28(9):1585-96.
176. Zielińska J, Wieczór M, Baczek T, Gruszecki M, Czub J. Thermodynamics and kinetics of amphotericin B self-association in aqueous solution characterized in molecular detail. *Scientific Reports*. 2016;10109(6):1-11.
177. Larabi M, Gulik A, Dedieu JP, Legrand P, Barratt G, Cheron M. New lipid formulation of amphotericin B: spectral and microscopic analysis. *Biochimica et Biophysica ACTA (BBA)-Biomembranes*. 2004;1664(2):172-81.
178. Frelichowska J, Bolzinger MA, Valour JP, Mouaziz H, Pelletier J, Chevalier Y. Pickering w/o emulsions: Drug release and topical delivery. *International Journal of Pharmaceutics*. 2009;368(1):7-15.
179. Ye F, Miao M, Cui S, Jiang B, Jin Z, Li X. Characterisations of oil-in-water pickering emulsion stabilized hydrophobic phyto-glycogen nanoparticles. *Food Hydrocolloids*. 2017;(76):78-87.
180. Dickinson E. Food emulsions and foams: stabilization by particles. *Current Opinion in Colloid and Interface Science*. 2010;15(1-2):40-9.
181. Amiri A, Øye G, Sjöblom J. Influence of pH, high salinity and particle concentration on stability and rheological properties of aqueous suspensions of fumed silica. *Colloids and Surfaces A: Physicochemical and Engineering Aspects*. 2009;349(1-3):43-54.
182. Ruiz-Rodriguez PE, Meshulam D, Lesmes U. Characterization of pickering o/w emulsions stabilized by silica nanoparticles and their responsiveness to *in vitro* digestion conditions. *Food Biophysics*. 2014;9(4):406-15.

183. Johannsdottir S, Jansook P, Stefansson E, Loftsson T. Development of a cyclodextrin-based aqueous cyclosporin A eye drop formulations. *International Journal of Pharmaceutics*. 2015;493(1-2):86-95.
184. Bortnowska G, Balejko J, Tokarczyk G, Romanowska-Osuch A, Krzemińska N. Effects of pregelatinized waxy maize starch on the physicochemical properties and stability of model low-fat oil-in-water food emulsions. *Food Hydrocolloids*. 2014;36:229-37.
185. Junqueira LA, Amaral TN, Leite Oliveira N, Prado MET, de Resende JV. Rheological behavior and stability of emulsions obtained from *Pereskia aculeata* Miller via different drying methods. *International Journal of Food Properties*. 2018;21(1):21-35.
186. Hoffmann H, Reger M. Emulsions with unique properties from proteins as emulsifiers. *Advances in Colloid and Interface Science*. 2014;205:94-104.
187. Eslami P, Davarpanah L, Vahabzadeh F. Encapsulating role of  $\beta$ -cyclodextrin in formation of pickering water-in-oil-in-water (W1/O/W2) double emulsions containing *Lactobacillus dellbrueckii*. *Food Hydrocolloids*. 2016;64:133-48.
188. Ahmad N, Ahmad R, Al-Qudaihi A, Alaseel S, Fita I, Khalid M, Pottoo FH. Preparation of a novel curcumin nanoemulsion by ultrasonication and its comparative effects in wound healing and the treatment of inflammation. *Royal Society of Chemistry Advances*. 2019;9(35):20192-206.
189. Singer A, Barakat Z, Mohapatra S, Mohapatra SS. Chapter 13 - Nanoscale drug-delivery systems: *in vitro* and *in vivo* characterization. *Nanocarriers for Drug Delivery*. 2019:395-419.
190. Mierke CT. Cell-cell and cell-matrix adhesion strength, local cell stiffness and forces. In: *Physics of Cancer* [Internet]. IOP Publishing; [4-1-4-49]. Available from: <http://dx.doi.org/10.1088/978-0-7503-1134-24>. 2015.
191. Radwan MA, AlQuadeib BT, Siller L, Wright MC, Horrocks B. Oral administration of amphotericin B nanoparticles: antifungal activity, bioavailability and toxicity in rats. *Drug Delivery*. 2017;24(1):40-50.
192. Wang Y, Ke X, Voo ZX, Yap SSL, Yang C, Gao S, Liu S, Venkataraman S, Obuobi SA, Khara JS, Yang YY. Biodegradable functional polycarbonate micelles for controlled release of amphotericin B. *ACTA Biomaterialia*. 2016;46:211-20.
193. Tiyaboonthai W, Limpeanchob N. Formulation and characterization of amphotericin B-chitosan-dextran sulfate nanoparticles. *International Journal of Pharmaceutics*. 2007;329(1-2):142-9.

194. Bang JY, Song CE, Kim C, Park WD, Cho KR, Kim PI, Lee Sr, Chung WT, Choi KC. Cytotoxicity of amphotericin B-incorporated polymeric micelles composed of poly(DL-lactide-co-glycolide)/dextran graft copolymer. *Archives of Pharmacal Research*. 2008;31(11):1463-9.
195. Swenson CE, Perkins WR, Roberts P, Ahmad I, Stevens R, Stevens DA, Janoff AS. *In vitro* and *in vivo* antifungal activity of amphotericin B lipid complex: are phospholipases important? *Antimicrobial Agents and Chemotherapy*. 1998;42(4):767-71.
196. Gopinathan U, Ramakrishna T, Willcox M, Rao CM, Balasubramanian D, Kulkarni A, Vemuganti GK, Rao GN. Enzymatic, clinical and histologic evaluation of corneal tissues in experimental fungal keratitis in rabbits. *Experimental Eye Research*. 2001;72(4):433-42.
197. Mythili A, Singh YRB, Priya R, Hassan AS, Manikandan P, Panneerselvam K, Narendran V, Shobana CS. *In vitro* and comparative study on the extracellular enzyme activity of molds isolated from keratomycosis and soil. *International Journal of Ophthalmology*. 2014;7(5):778.
198. Wang XY, Heuzey MC. Chitosan-based conventional and pickering emulsions with long-term stability. *Langmuir*. 2016;32(4):929-36.

## VITA

**NAME** Phyo Darli Maw  
**DATE OF BIRTH** 10 March 1994  
**PLACE OF BIRTH** Mandalay, Myanmar  
**INSTITUTIONS ATTENDED** University of Pharmacy, Mandalay  
**HOME ADDRESS** 70 Suwanna Apartment, Rama 1 Road, Pathuwan, Bangkok  
**AWARD RECEIVED** CU ASEAN Scholarship



จุฬาลงกรณ์มหาวิทยาลัย  
CHULALONGKORN UNIVERSITY